JHEP

Published for SISSA by Springer

Received: January 10, 2022
Accepted: March 22, 2022
Published: April 13, 2022

Top-pair production at the LHC with MiNNLO$_{\rm PS}$

Javier Mazzitelli,[a] **Pier Francesco Monni,**[b] **Paolo Nason,**[c] **Emanuele Re,**[c,d] **Marius Wiesemann**[a] **and Giulia Zanderighi**[a,e]

[a] *Max-Planck-Institut für Physik, Föhringer Ring 6, 80805 München, Germany*
[b] *CERN, Theoretical Physics Department, CH-1211 Geneva 23, Switzerland*
[c] *Università di Milano-Bicocca and INFN, Sezione di Milano-Bicocca, Piazza della Scienza 3, 20126 Milano, Italy*
[d] *LAPTh, Université Grenoble Alpes, Université Savoie Mont Blanc, CNRS, 74940 Annecy, France*
[e] *Physik-Department, Technische Universität München, James-Franck-Strasse 1, 85748 Garching, Germany*

E-mail: jmazzi@mpp.mpg.de, pier.monni@cern.ch, paolo.nason@mib.infn.it, emanuele.re@mib.infn.it, marius.wiesemann@mpp.mpg.de, zanderi@mpp.mpg.de

Abstract: We consider the production of a pair of heavy quarks and illustrate the derivation of the MiNNLO$_{\rm PS}$ method to match next-to-next-to-leading order calculations with parton showers (NNLO+PS) for this class of processes. As a first application, we construct an event generator for the fully differential simulation of hadronic top-quark pair production at NNLO+PS and discuss all details of its implementation in a parton shower Monte Carlo framework. We present new phenomenological results for the Large Hadron Collider obtained by including the tree-level decays of the top quarks, while accounting for spin-correlation effects. A comprehensive comparison to LHC measurements shows an excellent description of experimental data across multiple hadronic and leptonic particle-level observables. The computer code is available for download within the Powheg-Box.

Keywords: Higher-Order Perturbative Calculations, Parton Shower, Top Quark

ArXiv ePrint: 2112.12135

https://doi.org/10.1007/JHEP04(2022)079

JHEP04(2022)079

Contents

1 Introduction **1**

2 From POWHEG to MiNNLOPS: the colour singlet case **4**

3 The MiNNLOPS method for heavy-quark pair production **7**
- 3.1 Structure of heavy-quark pair production at small p_{T} 7
- 3.2 The MiNNLOPS master formulae for heavy-quark pair production 13

4 Computational aspects **16**
- 4.1 Renormalisation and factorisation scale dependence 16
- 4.2 Resummation scale dependence 18
- 4.3 Profiled logarithms and scale setting at large p_{T} 19
- 4.4 Top-quark decays and spin correlations 21

5 Phenomenological results **22**
- 5.1 Input parameters and fiducial cuts 23
- 5.2 Comparison to data extrapolated to the inclusive $t\bar{t}$ phase space 24
- 5.3 Comparison to data in the fully leptonic top-decay mode 26
- 5.4 Comparison to data in the semi-leptonic top-decay mode 29
- 5.5 Comparison to data in the fully hadronic top-decay mode 31

6 Summary **33**

A Resummation ingredients **35**

B Generation of virtualities in top-quark decays **37**

C Additional comparisons to data **39**
- C.1 Fully leptonic top-decay mode including τ decays to electrons/muons 40
- C.2 Fully leptonic top-decay mode excluding τ decays to electrons/muons 41
- C.3 Semi-leptonic top-quark decay mode 43
- C.4 Fully hadronic top-quark decay mode 44

1 Introduction

The experimental precision reached by present and future LHC experiments demands theoretical simulations with an accuracy at the edge of (or beyond) what can be achieved with current technology. The data-theory comparisons used in the precise studies of the SM and the extraction of SM parameters directly profit from smaller experimental and theoretical uncertainties. Furthermore, high-precision predictions and measurements play a fundamental role in the quest for new-physics phenomena at the LHC when searching for

JHEP04(2022)079

small deviations from the SM picture. Theoretical predictions for the LHC are commonly computed as a perturbative expansion in the coupling constants, with corrections in the strong coupling of QCD being the most important ones at a hadron collider. For typical LHC production processes the computation of next-to-next-to-leading order (NNLO) QCD corrections (or even beyond in some cases) on the theoretical side are crucial to keep up with the experimental precision. Moreover, the matching of such fixed-order calculations at NNLO QCD with increasingly accurate parton-shower generators, which can provide a description of full-fledged hadronic LHC events, is indispensable to fully exploit the vast potential of data taken at the LHC.

The matching to a QCD parton-shower simulation becomes crucial not only for a direct comparison at hadron level between theoretical predictions and experimental measurements, but also to guarantee physical predictions in corners of phase space where fixed-order QCD calculations become unreliable. The latter generally fail to provide physical results for observables sensitive to soft/collinear QCD radiation due to a hierarchy between two or more scales that lead to large logarithms of their ratios. The inclusion of soft/collinear QCD emissions to all orders in perturbation theory, as provided for instance by a parton shower, effectively resums the large logarithmic corrections, leading to a physical description. The recent progress in this field has been remarkable, both on the matching technology to combine higher-order QCD corrections with parton shower Monte Carlo generators [1–13], as well as on the development of parton-shower algorithms whose logarithmic accuracy can be formally established and systematically improved for a wide class of observables (see e.g. refs. [14–21]).

The problem of matching NNLO QCD corrections to (leading logarithmic) parton showers (NNLO+PS) has been addressed with different approaches: reweighting of MiNLO′ generators [5, 6], Geneva [7–9], Unnlops [10], MiNNLO$_{\rm PS}$ [11, 12], and Sector Showers matching [13]. All processes involving only two massless coloured legs (either in the initial or final state) at the Born level can be described with NNLO+PS accuracy by now, and many results have been already obtained [6, 8–12, 22–40]. On the other hand, hadronic reactions with final-state coloured particles cannot be straightforwardly simulated with the same theoretical accuracy.

Recently, the MiNNLO$_{\rm PS}$ method was extended to more complicated collider reactions containing colour charges in both the initial and the final state already at the Born level, and specifically to the NNLO+PS simulation of top-quark pair production at hadron colliders [41]. Besides being an important background in Higgs-physics measurements and new-physics searches (see e.g. refs. [42–44]), this process is used for high-precision studies of the properties of the top quark, which have by now been performed at the level of both inclusive and multi-differential observables [45–54]. These investigations have led to the precise extraction of fundamental parameters of the Standard Model, such as α_s, parton density functions (PDFs), and the top-quark mass (see e.g. refs. [55–59]).

The crucial role of top-quark pair production for the precision physics programme of the LHC has motivated a significant progress in the associated theoretical calculations. Specifically, fixed-order computations of the perturbative expansion in the strong coupling constant α_s are known up to NNLO [60–68] (also including the top-quark decays in the

JHEP04(2022)079

narrow-width approximation [69, 70]), full off-shell effects have been studied extensively at the NLO order [71–74], and electroweak (EW) corrections have been computed up to next-to-leading order (NLO) [75–79]. In certain kinematic regimes, a reliable perturbative description requires the all-order resummation of large logarithmic corrections [80–87]. Some of the above calculations have been consistently combined to obtain state-of-the-art perturbative predictions for top-quark pair production at the LHC [88]. Moreover, NLO+PS predictions for top-quark pair production have been achieved in a number of event generators [89–97]. The striking accuracy of experimental measurements of the top-quark mass requires pushing theoretical calculations to the edge of what can be achieved with perturbative methods (for recent reviews see refs. [98, 99]), and motivates new studies of non-perturbative aspects of top-quark physics (see e.g. refs. [100–103]).

In this article, we present a detailed derivation of the method presented in ref. [41] and describe all necessary steps to build an event generator with NNLO+PS accuracy for top-quark pair production. In particular, besides the construction of the event generator, we discuss the implementation of dynamical perturbative (i.e. renormalisation, factorisation and resummation) scales in the simulation, which we use to provide a robust estimate of the associated theoretical errors. Moreover, we describe how the top-quark decays and spin correlations are included. We exploit the newly developed event generator to carry out an extensive phenomenological study of several differential observables, for which we present a comparison to recent LHC experimental measurements, both for inclusive observables extrapolated to the $t\bar{t}$ phase space and in the fiducial phase space of all relevant top-decay modes (i.e. leptonic, semi-leptonic and hadronic). Overall, we find a remarkable agreement with data within the substantially reduced uncertainties compared to lower-order Monte-Carlo predictions. The computer code is publicly released with the article in the POWHEG-BOX-V2 framework.[1]

The paper is organised as follows: section 2 presents an introduction to the MiNNLO$_{\text{PS}}$ method for colour-singlet production at hadron colliders, and in section 3 we derive its extension to the production of two heavy quarks (specifically a top-quark pair). In section 4 several computational aspects are discussed, including the scale dependence of the MiNNLO$_{\text{PS}}$ formulae and the inclusion of the top-quark decays and spin correlations at tree-level. Phenomenological results are presented in section 5 and a detailed comparison of the MiNNLO$_{\text{PS}}$ predictions to experimental data from the LHC experiments is performed, for on-shell top quarks as well as leptonic, semi-leptonic, and hadronic decays of the two top quarks. Section 6 contains our summary and conclusions. In appendix A we provide technical details on the additional resummation ingredients necessary to implement the MiNNLO$_{\text{PS}}$ method for top-quark pair production. In appendix B we give some details on how off-shell effects can be approximately included in our prescription used for the top-quark decays. In appendix C we show further observables comparing MiNNLO$_{\text{PS}}$ predictions with data that were not discussed in the main text for fully leptonic top-decays including (C.1) and excluding (C.2) τ decays to electrons and muons, and for the semi-leptonic (C.3) and fully-hadronic (C.4) decay mode.

[1] Instructions to download the code can be found on the webpage http://powhegbox.mib.infn.it/.

JHEP04(2022)079

2 From POWHEG to MiNNLO$_{\rm PS}$: the colour singlet case

In this section we summarise in a schematic way the main features of the MiNNLO$_{\rm PS}$ method. We consider the production of a colour-singlet final state F with transverse momentum $p_{\rm T}$. For sake of illustration we assume F to be a Higgs boson produced in gluon fusion. To define the goals of the method developed in this article, we start by stating what the requirements of a NNLO+PS prediction are:

- to reach NNLO accuracy for observables that are inclusive over QCD radiation (possibly without introducing any extra resolution/slicing scales);
- to reach NLO(LO) accuracy for the production of F in association with one (two) final-state hard jets, possibly with a scale setting that is appropriate to the treatment of each kinematic regime;
- to preserve the (leading-logarithmic) accuracy of common parton-shower generators in the relevant kinematic regions.[2]

Our starting point for the construction of an event generator with NNLO+PS accuracy is a POWHEG [2, 105, 106] calculation for the production of a general colour-singlet system in association with a light jet (FJ) at NLO QCD matched to parton showers (NLO+PS). The POWHEG formula for FJ production can be schematically written as

$$\mathrm{d}\sigma = \mathrm{d}\Phi_{\rm FJ}\ \bar{B}(\Phi_{\rm FJ})\left\{\Delta_{\rm pwg}(\Lambda_{\rm pwg}) + \mathrm{d}\Phi_{\rm rad}\Delta_{\rm pwg}(p_{\rm T,rad})\frac{R(\Phi_{\rm FJ},\Phi_{\rm rad})}{B(\Phi_{\rm FJ})}\right\}, \tag{2.1}$$

which describes the production of F in association with either one or two real partons. In eq. (2.1), $\Phi_{\rm FJ}$ refers to the phase space of the FJ final state, while $\Delta_{\rm pwg}(\mu)$ denotes the POWHEG Sudakov form factor [2], representing the no-emission probability for the real radiation down to a transverse-momentum scale μ, and the scale $\Lambda_{\rm pwg}$ represents an infrared cutoff chosen to avoid the Landau singularity in the QCD coupling. We have also defined

$$\bar{B}(\Phi_{\rm FJ}) = \int \mathrm{d}\Phi_{\rm rad}\tilde{B}(\Phi_{\rm FJ},\Phi_{\rm rad}), \quad \tilde{B}(\Phi_{\rm FJ},\Phi_{\rm rad}) \equiv B(\Phi_{\rm FJ}) + V(\Phi_{\rm FJ}) + R(\Phi_{\rm FJ},\Phi_{\rm rad}), \tag{2.2}$$

where $B(\Phi_{\rm FJ})$, $V(\Phi_{\rm FJ})$ and $R(\Phi_{\rm FJ},\Phi_{\rm rad})$ denote the Born, virtual and real corrections, respectively. The real and virtual corrections include local counter-terms [105] such that the $\bar{B}(\Phi_{\rm FJ})$ function is finite and can be evaluated numerically. The radiation phase space $\mathrm{d}\Phi_{\rm rad}$ is normalised such that $\int \mathrm{d}\Phi_{\rm rad} = 1$, and the corresponding Jacobian factor is included in $R(\Phi_{\rm FJ},\Phi_{\rm rad})$. Eq. (2.1) is used to generate events with either one or two real partons, which are then fed into a parton shower that completes them with the addition of soft and collinear radiation at all perturbative orders, with the requirement that the radiation from the parton shower is softer than that generated by eq. (2.1). The original POWHEG formulation is restricted to the generation of the colour-singlet system F with a relatively hard associated

[2] These commonly include also next-to-leading logarithmic (NLL) corrections of type $\alpha_s^2 L^2$ to the Sudakov form factor captured by the CMW scheme [104], which should be preserved as well. Note that many current parton showers achieve LL accuracy only at leading colour.

JHEP04(2022)079

jet and has NLO accuracy for the production of the FJ final state. In the following we denote this accuracy by NLO$^{(1)}$, where the superscript (1) refers to the jet multiplicity.[3] The POWHEG generator based upon eq. (2.1) contains parts of the NNLO corrections to the inclusive production of the system F, i.e. the double-real and real-virtual corrections of relative order α_s^2 above a resolution scale set by the hardness of the resolved jet. In particular, if we introduce any transverse-momentum cut on the jet, the POWHEG generator based upon eq. (2.1) has the same perturbative accuracy as a NNLO+PS generator for F above the cut, while it is divergent below the cut. Therefore, the missing ingredients to achieve NNLO accuracy for the production of the system F are given by the contributions with F kinematics $\Phi_{\rm F}$ (i.e Born, one- and two-loop virtual corrections for F production) as well as a calculation of the FJ and FJJ contributions below the cut.

The MINLO procedure [107] is a modification of eq. (2.2) such that the corresponding POWHEG generator gives meaningful results also below the transverse-momentum cut. This is achieved by multiplying the $\tilde{B}$-function by an appropriate Sudakov form factor that acts as a regulator of the infrared singularity in the limit of a vanishing transverse momentum cut and applying appropriate (transverse-momentum dependent) scale choices. For common (leading-logarithmic) parton showers, such Sudakov form factor can be extracted from the transverse-momentum resummation for the system F. The inclusion of this correction in eq. (2.2) must be accompanied by a suitable compensating term in order to avoid double counting. With this prescription, one also achieves LO accuracy, i.e. LO$^{(0)}$, for observables defined on the phase space of F (inclusive over radiation).

In ref. [5] it was shown that the Sudakov form factor can be corrected in such a way that observables inclusive over radiation acquire $\mathcal{O}(\alpha_s)$ accuracy relative to the Born process of F production, i.e. NLO$^{(0)}$ accuracy, and the corresponding method was dubbed MINLO$'$. This work also pointed out that NNLO$^{(0)}$ accuracy for the inclusive production of F can be achieved using an *a-posteriori* reweighing of the MINLO$'$ events differential in the F kinematics $\Phi_{\rm F}$. This procedure was applied to several processes [6, 22, 24–27]. However, for complex processes this approach becomes prohibitively intensive from a computational viewpoint.

In refs. [11, 12] an alternative approach was introduced to achieve NNLO$^{(0)}$ accuracy by including the appropriate higher-order terms directly during the generation of events, circumventing the issues of the previous approach based on reweighting. The precise expression of these terms can be extracted from the following formula for the differential cross section

$$\frac{\mathrm{d}\sigma}{\mathrm{d}p_{\rm T}\mathrm{d}\Phi_{\rm F}} = \frac{\mathrm{d}}{\mathrm{d}p_{\rm T}}\Big\{\mathcal{L}(\Phi_{\rm F},p_{\rm T})\exp[-\tilde{S}(\Phi_{\rm F},p_{\rm T})]\Big\} + R_{\rm finite}(p_{\rm T})\,. \tag{2.3}$$

The right-hand side of eq. (2.3) can be derived from the resummation of the transverse momentum of F at next-to-next-to-NLL (N^{3}LL) matched to fixed-order. Here $\mathcal{L}(\Phi_{\rm F},p_{\rm T})$ denotes a *luminosity* factor that includes the PDFs, the hard-virtual corrections and the collinear coefficient functions for the production of the system F expanded in powers of $\alpha_s(p_{\rm T})$ up to two loops. The factor $\exp[-\tilde{S}(p_{\rm T})]$ denotes the Sudakov form factor for the

[3] We use the notation ((N)N)LO$^{(j)}$ to denote ((N)N)LO accuracy for observables defined for the production of the system F in association with j hard jets.

JHEP04(2022)079

resummation of logarithms $\ln(Q/p_{\mathrm{T}})$ (with Q being a scale of the order of the invariant mass of F), and $R_{\mathrm{finite}}(p_{\mathrm{T}})$ denotes the regular part of the differential cross section, also expanded in powers of $\alpha_s(p_{\mathrm{T}})$. To obtain eq. (2.3), we have simplified the original N^{3}LL transverse-momentum resummation formula to retain only terms that are relevant up to $\mathcal{O}(\alpha_s^2)$ relative to F production at LO, while preserving the LL accuracy (including also the $\alpha_s^2 \ln^2(Q/p_{\mathrm{T}})$ CMW corrections to the Sudakov radiator $\tilde{S}(p_{\mathrm{T}})$, which are accounted for in common parton showers we will match onto). In its present form, the integral of eq. (2.3) over p_{T} up to any perturbative value is NNLO$^{(0)}$ accurate.

In order to include NNLO$^{(0)}$ accuracy in eq. (2.1) we need to modify the expression for $\tilde{B}(\Phi_{\mathrm{FJ}}, \Phi_{\mathrm{rad}})$ in eq. (2.2) in the following way [11, 12]:

$$\tilde{B}(\Phi_{\mathrm{FJ}}, \Phi_{\mathrm{rad}}) = \exp[-\tilde{S}(\Phi_{\mathrm{F}}, p_{\mathrm{T}})]\Bigg[B(\Phi_{\mathrm{FJ}})\left(1 + \frac{\alpha_s(p_{\mathrm{T}})}{2\pi}[\tilde{S}(\Phi_{\mathrm{F}}, p_{\mathrm{T}})]^{(1)}\right) + V(\Phi_{\mathrm{FJ}}) + R(\Phi_{\mathrm{FJ}}, \Phi_{\mathrm{rad}}) + D^{(\geq 3)}(\Phi_{\mathrm{F}}, p_{\mathrm{T}}) F^{\mathrm{corr}}(\Phi_{\mathrm{FJ}})\Bigg], \tag{2.4}$$

where we have defined

$$D^{(\geq 3)}(\Phi_{\mathrm{F}}, p_{\mathrm{T}}) = D(\Phi_{\mathrm{F}}, p_{\mathrm{T}}) - \frac{\alpha_s(p_{\mathrm{T}})}{2\pi}[D(\Phi_{\mathrm{F}}, p_{\mathrm{T}})]^{(1)} - \left(\frac{\alpha_s(p_{\mathrm{T}})}{2\pi}\right)^2 [D(\Phi_{\mathrm{F}}, p_{\mathrm{T}})]^{(2)},$$
$$D(\Phi_{\mathrm{F}}, p_{\mathrm{T}}) = -\frac{\mathrm{d}\tilde{S}(\Phi_{\mathrm{F}}, p_{\mathrm{T}})}{\mathrm{d}p_{\mathrm{T}}}\mathcal{L}(\Phi_{\mathrm{F}}, p_{\mathrm{T}}) + \frac{\mathrm{d}\mathcal{L}(\Phi_{\mathrm{F}}, p_{\mathrm{T}})}{\mathrm{d}p_{\mathrm{T}}}. \tag{2.5}$$

In the above equations we use the notation $[X]^{(k)}$ to denote the coefficient of the expansion $X = \sum_k (\frac{\alpha_s}{2\pi}(p_{\mathrm{T}}))^k [X]^{(k)}$. We note that the term $[\tilde{S}(\Phi_{\mathrm{F}}, p_{\mathrm{T}})]^{(1)}$ in eq. (2.4) cancels the corresponding $\mathcal{O}(\alpha_s)$ term arising from the expansion of the Sudakov form factor, which is required to avoid double counting and to preserve NLO$^{(1)}$ accuracy. Although for simplicity in eq. (2.4) we have factorised the Sudakov form factor, p_{T} is actually evaluated in the Φ_{FJ} configuration for all terms except $R(\Phi_{\mathrm{FJ}}, \Phi_{\mathrm{rad}})$, for which it is taken equal to the transverse momentum of the system F in the full Φ_{FJJ} phase space. Without the last term, eq. (2.4) corresponds exactly to the MiNLO′ formula, yielding both NLO$^{(0)}$ and NLO$^{(1)}$ accuracy.

The quantity $D^{(\geq 3)}(\Phi_{\mathrm{F}}, p_{\mathrm{T}})$ guarantees that the integral of $\tilde{B}$ at fixed Φ_{F} matches the expansion of eq. (2.3), up to the accuracy that we require, namely NNLO$^{(0)}$. This quantity depends on Φ_{F} and p_{T}. On the other hand, $\tilde{B}(\Phi_{\mathrm{FJ}}, \Phi_{\mathrm{rad}})$ depends on the full Φ_{FJ}. Thus, we must spread the $D^{(\geq 3)}(\Phi_{\mathrm{F}}, p_{\mathrm{T}})$ term in the Φ_{FJ} phase space. This is done by the function $F^{\mathrm{corr}}(\Phi_{\mathrm{FJ}})$, which is defined such that its integral at fixed Φ_{F} and p_{T} equals one (see ref. [11] for a precise definition).

We note that the correction term $D^{(\geq 3)}(\Phi_{\mathrm{F}}, p_{\mathrm{T}})$, starting formally at order $\alpha_s^3(p_{\mathrm{T}})$, after integration over p_{T} at fixed Φ_{F} contributes starting at relative order $\alpha_s^2(Q)$. This is because $D^{(\geq 3)}(\Phi_{\mathrm{F}}, p_{\mathrm{T}})$ contains logarithmic singularities that are regulated by the Sudakov form factor. When integrated over p_{T}, their product gives rise to a Gaussian integral of the form

$$\int_0^\infty \mathrm{d}L \exp[-\alpha_s L^2] \alpha_s^m L^n \propto \alpha_s^{m-\frac{n+1}{2}}, \tag{2.6}$$

where we schematically defined $L = \ln(Q/p_{\mathrm{T}})$ and ignored the running of α_s (cf. appendix C of ref. [5] for a detailed discussion on this point). Therefore, to reach NNLO$^{(0)}$ accuracy

JHEP04(2022)079

one must ensure that the perturbative truncation error is of relative order $\alpha_s^3(Q)$, which in turn requires including all singular terms at least up to $m = 3$ and $n = 0$.[4] However, we also stress that the definition of the function $D^{(\geq 3)}(\Phi_{\rm F}, p_{\rm T})$ does not require any actual computation at order $\mathcal{O}(\alpha_s^3)$. The higher-order terms beyond $\alpha_s^2(p_{\rm T})$ in $\tilde{B}(\Phi_{\rm FJ}, \Phi_{\rm rad})$ are simply generated by taking the total derivative in eq. (2.3), leading to eq. (2.5).

In refs. [11, 12, 35–39] the MiNNLO$_{\rm PS}$ formalism was applied to several processes where the system F is a colour singlet. Strictly speaking, eq. (2.3) holds in this form only in this case. The production of a colour-charged heavy system involves additional conceptual complications related to the fact that the final state will exchange soft gluons within itself and with the initial state. This leads to a more complicated structure of the transverse-momentum resummation formula, which now involves colour matrices (see e.g. [80–83]). Thus, in order to deal with heavy-quark pair production one must first generalize the procedure adopted in the colour singlet case by finding the appropriate extension of eq. (2.3). This will be discussed in the next section.

3 The MiNNLO$_{\rm PS}$ method for heavy-quark pair production

In this section we present an extension of the MiNNLO$_{\rm PS}$ method to the production of a pair of heavy quarks in hadronic collisions, having in mind the concrete application to top-quark pair production. Our goal is to achieve NNLO$^{(0)}$ accuracy for all observables defined in the phase space of the pair of heavy quarks, and inclusive in the additional QCD radiation. At the same time, we will retain NLO$^{(1)}$ (LO$^{(2)}$) accuracy for observables which require one (two) resolved hard jet(s). We also demand that our matching procedure preserves the leading logarithmic (LL) accuracy (plus the simple NLL corrections to the Sudakov form factor captured by the CMW scheme [104]) of the parton shower the calculation is matched onto, which in this case is assumed to be ordered in a transverse-momentum variable. Specifically, we will consider the dipole shower Pythia8 [108] in all phenomenological applications presented in this article.[5] The above accuracy goals will be taken into account when performing some of the approximations necessary in the extension of the MiNNLO$_{\rm PS}$ method.

3.1 Structure of heavy-quark pair production at small $p_{\rm T}$

We consider the production of a pair of heavy quarks, F $\equiv Q\bar{Q}$ from now on, differential in the phase space of the pair $\mathrm{d}\Phi_{Q\bar{Q}} \equiv \mathrm{d}\bar{x}_1\mathrm{d}\bar{x}_2[\mathrm{d}\Phi_2]$. Here $\bar{x}_{1,2} = m_{Q\bar{Q}}/\sqrt{s}\, e^{\pm y_{Q\bar{Q}}}$, with $y_{Q\bar{Q}}$ being the rapidity of the $Q\bar{Q}$ system, $m_{Q\bar{Q}}$ its invariant mass, $[\mathrm{d}\Phi_2]$ denotes the Lorentz-invariant two-body phase space and $\sqrt{s}$ is the collider centre-of-mass energy. Our starting point is the well-known formula for transverse-momentum resummation for a $Q\bar{Q}$

[4] We stress that the function $D(\Phi_{\rm F}, p_{\rm T})$ contains at most single logarithmic terms (i.e. only $n = 1$ and $n = 0$) as a consequence of the fact that the coupling and the PDFs are evaluated at scales of order $p_{\rm T}$.

[5] For different ordering variables, preserving the accuracy of the shower is more subtle. A common procedure is to resort to truncated showers [2, 109] to compensate for missing collinear and soft radiation. Failing to do so spoils the shower accuracy at leading-logarithmic level (in fact, at the double-logarithmic level).

JHEP04(2022)079

pair, which reads [80–83] (we denote $b_0 = 2\,e^{-\gamma_E}$, $b = |\vec{b}|$)

$$\frac{\mathrm{d}\sigma}{\mathrm{d}^2\vec{p}_{\mathrm{T}}\,\mathrm{d}\Phi_{Q\bar{Q}}} = \sum_{c=q,\bar{q},g} \frac{|M_{c\bar{c}}^{(0)}|^2}{2m_{Q\bar{Q}}^2} \int \frac{\mathrm{d}^2\vec{b}}{(2\pi)^2} e^{i\vec{b}\cdot\vec{p}_{\mathrm{T}}} e^{-S_{c\bar{c}}\left(\frac{b_0}{b}\right)} \sum_{i,j} \mathrm{Tr}(\mathbf{H}_{c\bar{c}}\boldsymbol{\Delta})\ (C_{ci}\otimes f_i)\,(C_{\bar{c}j}\otimes f_j)\,. \tag{3.1}$$

The first sum in eq. (3.1) runs over all possible flavour configurations of the incoming partons p_1 of flavour c and p_2 of flavour $\bar{c}$. In the above equation, the quantity $S_{c\bar{c}}$ represents the Sudakov radiator,

$$S_{c\bar{c}}\left(\frac{b_0}{b}\right) \equiv \int_{\frac{b_0^2}{b^2}}^{m_{Q\bar{Q}}^2} \frac{\mathrm{d}q^2}{q^2}\left[A_{c\bar{c}}(\alpha_s(q))\ln\frac{m_{Q\bar{Q}}^2}{q^2} + B_{c\bar{c}}(\alpha_s(q))\right], \tag{3.2}$$

which encodes the resummation of logarithms of the impact parameter b (and thus p_{T} of the heavy-quark pair) of collinear and soft-collinear origin (i.e. double and single logarithms), that originate entirely from initial-state radiation.

The coefficient functions $C_{ij} \equiv C_{ij}(z, p_1, p_2, \vec{b}; \alpha_s(b_0/b))$ encode constant contributions to the factorisation theorem that originate from initial-state collinear radiation. The symbol $\otimes$ denotes the usual convolution,

$$(f\otimes g)(z) = \int_z^1 \frac{\mathrm{d}x}{x} f(x) g\left(\tfrac{z}{x}\right)\,. \tag{3.3}$$

Both $S_{c\bar{c}}$ and C_{ij} are universal, and are identical to the ones featuring in the resummation formula describing the low transverse momentum behaviour of a heavy colorless final state.

In eq. (3.1) and throughout the paper, operators in colour space are denoted in bold face. The colour-space operator $\boldsymbol{\Delta}$ encodes the resummation of single-logarithmic corrections that arise from soft radiation exchanged with large angles between the final state heavy-quark legs and between the initial and final state (we refer the reader to ref. [82] for a more thorough discussion).

The trace $\mathrm{Tr}(\mathbf{H}_{c\bar{c}}\boldsymbol{\Delta})$ runs over the colour indices and encodes the difference between the factorisation formula (3.1) and the corresponding one for colour-singlet production. It can be given an explicit representation by using the colour space formalism of ref. [110]. In order to do so, we will denote by $|M_{c\bar{c}}\rangle$ the all-orders *infrared-subtracted* amplitude for the production of the heavy-quark pair from the incoming partons p_1 of flavour c and p_2 of flavour $\bar{c}$. All amplitudes here are considered to be renormalised, specifically in the $\overline{\mathrm{MS}}$ scheme. The object $|M_{c\bar{c}}\rangle$ represents a vector in colour space, and can be obtained from the un-subtracted (IR divergent) scattering amplitude $|M_{c\bar{c}}^{\text{IR-div.}}\rangle$ by applying an appropriate subtraction operator [82]

$$|M_{c\bar{c}}\rangle = (\mathbb{1} - \mathbf{I}_{c\bar{c}})\,|M_{c\bar{c}}^{\text{IR-div.}}\rangle\,. \tag{3.4}$$

In terms of $|M_{c\bar{c}}\rangle$, the operator $\mathbf{H}_{c\bar{c}}$ can be written as $\mathbf{H}_{c\bar{c}} = |M_{c\bar{c}}\rangle\langle M_{c\bar{c}}|/|M_{c\bar{c}}^{(0)}|^2$, and therefore we have [82]

$$\mathrm{Tr}(\mathbf{H}_{c\bar{c}}\boldsymbol{\Delta})(C_{ci}\otimes f_i)\,(C_{\bar{c}j}\otimes f_j) \equiv \frac{\langle M_{c\bar{c}}|\boldsymbol{\Delta}|M_{c\bar{c}}\rangle}{|M_{c\bar{c}}^{(0)}|^2}(C_{ci}\otimes f_i)\,(C_{\bar{c}j}\otimes f_j)\,, \tag{3.5}$$

JHEP04(2022)079

where a sum over the colours (and spins) of the external legs is understood. The symbolic object $\mathrm{Tr}(\mathbf{H}_{c\bar{c}}\boldsymbol{\Delta})\,(C_{ci}\otimes f_i)\,(C_{\bar{c}j}\otimes f_j)$ takes a different form in the $q\bar{q}$ and gg channels. In particular, while eq. (3.5) is strictly valid for $q\bar{q}$ annihilation, in the gluon-initiated gg channel this factor has a rich Lorentz structure. Firstly, the object $(C_{ci}\otimes f_i)\,(C_{\bar{c}j}\otimes f_j)$ now contains the contribution from additional coefficient functions that encode azimuthal correlations of collinear origin (commonly denoted with G_{ij} [111]). Furthermore, eq. (3.5) should be now understood as a tensor contraction between $\mathrm{Tr}(\mathbf{H}_{c\bar{c}}\boldsymbol{\Delta})$ and $(C_{ci}\otimes f_i)\,(C_{\bar{c}j}\otimes f_j)$. This leads to additional azimuthal correlations of soft nature that, for simplicity, are kept implicit in eq. (3.1). For more details, we refer the reader to eq. (13) of ref. [82], and subsequent discussions. We note that in the case in which the produced final state is a colour singlet, we have $\boldsymbol{\Delta}=\mathbb{1}$ and eq. (3.5) simply reduces to $\mathrm{Tr}(\mathbf{H}_{c\bar{c}})=H_{c\bar{c}}$, where $H_{c\bar{c}}$ is the usual process-dependent hard-virtual coefficient.

It is worth pointing out that while the pole structure of the subtraction operator $\mathbf{I}_{c\bar{c}}$ is uniquely defined, its finite $\mathcal{O}(\epsilon^0)$ piece is, in principle, arbitrary. Its exact definition is tied to the choice of the resummation scheme. In the current work we adopt the resummation scheme of ref. [82] (which in the colour-singlet case reduces to the so-called hard scheme [112]). The corresponding finite terms can only be obtained by means of an explicit calculation of the expansion coefficients $\mathbf{I}^{(i)}_{c\bar{c}}$, defined by the perturbative series

$$\mathbf{I}_{c\bar{c}}=\sum_i\left(\frac{\alpha_s(\mu)}{2\pi}\right)^i\mathbf{I}^{(i)}_{c\bar{c}}\,. \tag{3.6}$$

The expression for $\mathbf{I}^{(1)}_{c\bar{c}}$ can be found in ref. [82], while the NNLO operator $\mathbf{I}^{(2)}_{c\bar{c}}$ has been taken from ref. [113], which has been used in the context of q_T-subtraction [114] for heavy-quark production [66, 67, 115].

As already mentioned, the operator $\boldsymbol{\Delta}$ encodes the main source of difference between the colour-singlet and the $Q\bar{Q}$ final states. It can be written as $\boldsymbol{\Delta}=\mathbf{V}^\dagger\mathbf{D}\mathbf{V}$, where the operator $\mathbf{V}$ is obtained by exponentiating the soft anomalous dimension matrix for heavy-quark pair production $\boldsymbol{\Gamma}_t(\Phi_{Q\bar{Q}};\alpha_s(q))$, i.e. [82]

$$\mathbf{V}=\mathcal{P}\exp\left\{-\int_{b_0^2/b^2}^{m^2_{Q\bar{Q}}}\frac{\mathrm{d}q^2}{q^2}\boldsymbol{\Gamma}_t(\Phi_{Q\bar{Q}};\alpha_s(q))\right\}\,. \tag{3.7}$$

In the above equation, the symbol $\mathcal{P}$ denotes the path ordering (with increasing scales from left to right) of the exponential matrix with respect to the integration variable q^2. The operator $\mathbf{D}\equiv\mathbf{D}(\Phi_{Q\bar{Q}},\vec{b};\alpha_s(b_0/b))$, on the other hand, encodes the azimuthal correlations of the produced $Q\bar{Q}$ system in the low-p_{T} limit due to soft radiation at large angles. It is normalised in such a way that $[\mathbf{D}]_\phi=\mathbb{1}$, where $[\cdots]_\phi$ denotes the average over the azimuthal angle ϕ of $\vec{p}_{\mathrm{T}}$. As mentioned above, additional sources of azimuthal correlations, this time of collinear origin, are present in the coefficient functions C_{ij} corresponding to the gluon-initiated channels (the two are combined in the contraction of eq. (3.5) to produce non-trivial correlations that are typical of the process under consideration). We note that $\mathbf{V}$ and $\mathbf{D}$ are also resummation-scheme dependent quantities. In the adopted resummation scheme all the dependence on the azimuthal angle is absorbed in $\mathbf{D}$ and absent from $\mathbf{H}_{c\bar{c}}$ and $\mathbf{V}$, but other schemes could be defined in which this is not the case [82].

JHEP04(2022)079

Having introduced the main features of the resummation formula (3.1), we focus now on its connection to the derivation of a NNLO+PS generator for $Q\bar{Q}$ production. In the colour-singlet case [11, 12], the resummation formula (in particular its formulation in direct space [116, 117]) is the basis to constructing eq. (2.3). The low-q_T structure of the $Q\bar{Q}$ cross section is, however, clearly more involved. In particular, writing the equivalent to eq. (2.3) starting from eq. (3.1) is not straightforward due to the colour interference effects present in $\mathbf{\Delta}$ and due to the non-trivial azimuthal correlations in eq. (3.5). However, as in the colour singlet case, we are not seeking a formula that is N^{3}LL accurate for the transverse-momentum distribution of the $Q\bar{Q}$ pair (which through matching to the shower reduces to its accuracy regardless), but instead we only need to ensure that its integral at fixed $\Phi_{Q\bar{Q}}$ is accurate at the NNLO level, while preserving the logarithmic accuracy of the shower algorithms we match to. This allows us to perform several approximations in eq. (3.1), which are described in what follows, with the goal of transforming it into a NNLO-accurate expression which resembles the (considerably simpler) structure of the colour-singlet case.

We start by defining the perturbative expansion of the different ingredients entering eq. (3.1),

$$\begin{aligned} Z(\{x\};\alpha_s(\mu)) &= \sum_i \left(\frac{\alpha_s(\mu)}{2\pi}\right)^i Z^{(i)}(\{x\}) \,, \\ |M_{c\bar{c}}\rangle &= \sum_i \left(\frac{\alpha_s(m_{Q\bar{Q}})}{2\pi}\right)^i |M_{c\bar{c}}^{(i)}\rangle \,, \end{aligned} \tag{3.8}$$

where Z represents any of the quantities $Z \equiv \{A_{c\bar{c}}, B_{c\bar{c}}, C_{ij}, \mathbf{H}_{c\bar{c}}, \mathbf{D}, \mathbf{\Gamma}_t\}$, and $\{x\}$ stands for any additional set of arguments. The scale μ at which the expansion is performed is the one explicitly indicated in the corresponding function Z. Explicit results for the coefficients $Z^{(i)}$ up to two loops can be extracted from the results presented in refs. [67, 81, 82, 111, 113, 118–128]. We note that $\mathbf{D}^{(2)}$ is still unknown at present, however due to the property $[\mathbf{D}]_\phi = \mathbb{1}$ its contribution for azimuthally-averaged observables exactly vanishes at NNLO (this is not the case for $\mathbf{D}^{(1)}$, as discussed in the following). In the case of $|M_{c\bar{c}}\rangle$, as stated in eq. (3.8), the expansion is performed in powers of $\alpha_s(m_{Q\bar{Q}})$. The additional power of α_s present already at LO is included in the definition of $|M_{c\bar{c}}^{(i)}\rangle$, and is evaluated at a hard scale $\mu_{\rm R}^{(0)} \sim m_{Q\bar{Q}}$. The evaluation of $|M_{c\bar{c}}^{(i)}\rangle$ up to NNLO requires the knowledge of the complete two-loop virtual corrections for $p_1p_2 \to Q\bar{Q}$, which we take from the numerical implementation in ref. [123], as well as the corresponding subtraction operator $\mathbf{I}_{c\bar{c}}^{(2)}$ [113].

Let us now consider the matrix exponential in $\mathbf{V}$. Up to N^{3}LL accuracy, we can expand the $\mathbf{\Gamma}_t^{(2)}$ term inside the path ordering sign in the following way,

$$\mathbf{V} = \mathcal{P}\left[\exp\left\{-\int_{b_0^2/b^2}^{m_{Q\bar{Q}}^2}\frac{\mathrm{d}q^2}{q^2}\frac{\alpha_s(q)}{2\pi}\mathbf{\Gamma}_t^{(1)}\right\}\times\left(1-\int_{b_0^2/b^2}^{m_{Q\bar{Q}}^2}\frac{\mathrm{d}q^2}{q^2}\frac{\alpha_s^2(q)}{(2\pi)^2}\mathbf{\Gamma}_t^{(2)}\right)\right] + \mathcal{O}(\mathrm{N^3LL})\,. \tag{3.9}$$

The path ordered expression must be now evaluated exactly to retain next-to-NLL (NNLL) accuracy. However, we recall that our goal is to achieve NNLO$^{(0)}$ and we do not necessarily need to preserve the full logarithmic accuracy of the resummation formula, which allows us to

JHEP04(2022)079

make the following approximation. Without spoiling the NNLO$^{(0)}$ accuracy of the expression, we can take the $\mathbf{\Gamma}_t^{(2)}$ contribution out of the path-ordering symbol in eq. (3.9). This is because $\mathbf{\Gamma}_t^{(2)}$ enters at relative order $\mathcal{O}(\alpha_s^2)$ and therefore the action of the path-ordering would only start at $\mathcal{O}(\alpha_s^3)$. Then we have

$$\mathbf{V} = \mathbf{V}_{\rm NLL} \times \left(1 - \int_{b_0^2/b^2}^{m_{Q\bar{Q}}^2} \frac{\mathrm{d}q^2}{q^2} \frac{\alpha_s^2(q)}{(2\pi)^2} \mathbf{\Gamma}_t^{(2)}\right) + \mathcal{O}(\alpha_s^3)\,, \tag{3.10}$$

where we have defined the object $\mathbf{V}_{\rm NLL}$ entering q_T-resummation at NLL accuracy,

$$\mathbf{V}_{\rm NLL} = \mathcal{P}\left[\exp\left\{-\int_{b_0^2/b^2}^{m_{Q\bar{Q}}^2} \frac{\mathrm{d}q^2}{q^2} \frac{\alpha_s(q)}{2\pi} \mathbf{\Gamma}_t^{(1)}\right\}\right]. \tag{3.11}$$

We focus now on the contribution to eq. (3.1) proportional to $\mathbf{\Gamma}_t^{(2)}$. Firstly, we observe that said contribution is no longer in an exponential form, due to the approximations made in eq. (3.10). Furthermore, it is accompanied by an α_s^2 suppression. This implies that it contributes to the trace $\mathrm{Tr}(\mathbf{H}_{c\bar{c}}\mathbf{\Delta})$ with the following NNLO term

$$\mathrm{Tr}(\mathbf{H}_{c\bar{c}}\mathbf{\Delta}) \supset -\frac{\langle M_{c\bar{c}}^{(0)}|\mathbf{\Gamma}_t^{(2)\,\dagger} + \mathbf{\Gamma}_t^{(2)}|M_{c\bar{c}}^{(0)}\rangle}{|M_{c\bar{c}}^{(0)}|^2} \int_{b_0^2/b^2}^{m_{Q\bar{Q}}^2} \frac{\mathrm{d}q^2}{q^2} \frac{\alpha_s^2(q)}{(2\pi)^2}\,, \tag{3.12}$$

where, to simplify the discussion, the notation $A \supset B$ indicates that A contains the summand B in its perturbative expansion. We now note that this contribution has the functional (single-logarithmic) form of the $\mathcal{O}(\alpha_s^2)$ term stemming from the $B^{(2)}$ coefficient in the Sudakov radiator,

$$e^{-S_{c\bar{c}}\left(\frac{b_0}{b}\right)} \supset -B_{c\bar{c}}^{(2)} \int_{b_0^2/b^2}^{m_{Q\bar{Q}}^2} \frac{\mathrm{d}q^2}{q^2} \frac{\alpha_s^2(q)}{(2\pi)^2}\,. \tag{3.13}$$

This implies that the $\mathbf{\Gamma}_t^{(2)}$ contribution can be completely absorbed into the $B_{c\bar{c}}^{(2)}$ coefficient at the desired accuracy by performing the replacement

$$B_{c\bar{c}}^{(2)} \to B_{c\bar{c}}^{(2)} + \frac{\langle M_{c\bar{c}}^{(0)}|\mathbf{\Gamma}_t^{(2)\,\dagger} + \mathbf{\Gamma}_t^{(2)}|M_{c\bar{c}}^{(0)}\rangle}{|M_{c\bar{c}}^{(0)}|^2}\,. \tag{3.14}$$

We turn now to the term coming from $\mathbf{V}_{\rm NLL}$, which appears in the combination $\mathbf{V}_{\rm NLL}^\dagger \mathbf{D}\, \mathbf{V}_{\rm NLL}$. As stated before, the function $\mathbf{D}$ depends upon the azimuthal angle ϕ of $\vec{p}_{\rm T}$ and it is an important source of azimuthal correlations. However, due to the fact that $\mathbf{\Gamma}_t^{(1)}$ does not depend on ϕ, the $\mathcal{O}(\alpha_s^2)$ contribution proportional to $\mathbf{\Gamma}_t^{(1)}\mathbf{D}^{(1)}$ present in the product $\mathbf{V}_{\rm NLL}^\dagger \mathbf{D}\, \mathbf{V}_{\rm NLL}$ vanishes upon taking the azimuthal average since $[\mathbf{D}]_\phi = \mathbb{1}$. We can therefore perform the approximation

$$\frac{\langle M_{c\bar{c}}|\mathbf{V}_{\rm NLL}^\dagger \mathbf{D}\, \mathbf{V}_{\rm NLL}|M_{c\bar{c}}\rangle}{|M_{c\bar{c}}^{(0)}|^2} = \frac{\langle M_{c\bar{c}}|\mathbf{V}_{\rm NLL}^\dagger \mathbf{V}_{\rm NLL}|M_{c\bar{c}}\rangle}{|M_{c\bar{c}}^{(0)}|^2}\, \mathrm{Tr}(\mathbf{H}_{c\bar{c}}\mathbf{D}) + E_{c\bar{c}}(\Phi_{Q\bar{Q}}, \vec{b}) + \mathcal{O}(\alpha_s^3)\,, \tag{3.15}$$

where the remainder term $E_{c\bar{c}}(\Phi_{Q\bar{Q}}, \vec{b})$ contributes at order $\alpha_s^2 \ln(m_{Q\bar{Q}}\, b)$, but for the reasons just discussed vanishes upon azimuthal integration and therefore can be safely ignored. We

JHEP04(2022)079

now focus on the object $\langle M_{c\bar{c}}|\mathbf{V}_{\rm NLL}^{\dagger}\mathbf{V}_{\rm NLL}|M_{c\bar{c}}\rangle$, and deal with the NNLO contribution from the function $\mathbf{D}$ afterwards.

In order to obtain a colour-singlet-like resummation formula, we would like to factorize the loop corrections in the following way,

$$\frac{\langle M_{c\bar{c}}|\mathbf{V}_{\rm NLL}^{\dagger}\mathbf{V}_{\rm NLL}|M_{c\bar{c}}\rangle}{|M_{c\bar{c}}^{(0)}|^2} \to \frac{\langle M_{c\bar{c}}^{(0)}|\mathbf{V}_{\rm NLL}^{\dagger}\mathbf{V}_{\rm NLL}|M_{c\bar{c}}^{(0)}\rangle}{|M_{c\bar{c}}^{(0)}|^2}\frac{\langle M_{c\bar{c}}|M_{c\bar{c}}\rangle}{|M_{c\bar{c}}^{(0)}|^2}\,, \tag{3.16}$$

however, the replacement in eq. (3.16) is not NNLO accurate due to the colour structure of the operator $\mathbf{V}_{\rm NLL}$ and the amplitude $|M_{c\bar{c}}\rangle$. We can however subtract the incorrect $\mathcal{O}(\alpha_s^2)$ term that is induced by such replacement, and add back the correct one in order to match the l.h.s. of eq. (3.16) up to NNLO accuracy. This yields:

$$\begin{aligned}\frac{\langle M_{c\bar{c}}|\mathbf{V}_{\rm NLL}^{\dagger}\mathbf{V}_{\rm NLL}|M_{c\bar{c}}\rangle}{|M_{c\bar{c}}^{(0)}|^2} &\to \frac{\langle M_{c\bar{c}}^{(0)}|\mathbf{V}_{\rm NLL}^{\dagger}\mathbf{V}_{\rm NLL}|M_{c\bar{c}}^{(0)}\rangle}{|M_{c\bar{c}}^{(0)}|^2}\frac{\langle M_{c\bar{c}}|M_{c\bar{c}}\rangle}{|M_{c\bar{c}}^{(0)}|^2} \\ &+ 2\Re\left[\frac{\langle M_{c\bar{c}}^{(1)}|M_{c\bar{c}}^{(0)}\rangle}{|M_{c\bar{c}}^{(0)}|^2}\right]\frac{\langle M_{c\bar{c}}^{(0)}|\mathbf{\Gamma}_t^{(1)\,\dagger}+\mathbf{\Gamma}_t^{(1)}|M_{c\bar{c}}^{(0)}\rangle}{|M_{c\bar{c}}^{(0)}|^2}\frac{\alpha_s(m_{Q\bar{Q}})}{2\pi}\int_{b_0^2/b^2}^{m_{Q\bar{Q}}^2}\frac{\mathrm{d}q^2}{q^2}\frac{\alpha_s(q)}{2\pi} \\ &- 2\,\Re\left[\frac{\langle M_{c\bar{c}}^{(1)}|\mathbf{\Gamma}_t^{(1)\,\dagger}+\mathbf{\Gamma}_t^{(1)}|M_{c\bar{c}}^{(0)}\rangle}{|M_{c\bar{c}}^{(0)}|^2}\right]\frac{\alpha_s(m_{Q\bar{Q}})}{2\pi}\int_{b_0^2/b^2}^{m_{Q\bar{Q}}^2}\frac{\mathrm{d}q^2}{q^2}\frac{\alpha_s(q)}{2\pi}+\mathcal{O}(\alpha_s^3)\,.\end{aligned} \tag{3.17}$$

If in addition we replace $\alpha_s(m_{Q\bar{Q}}) = \alpha_s(q) + \mathcal{O}(\alpha_s^2)$ in the above equation, which does not affect the NNLO accuracy of the expression, we can notice that the additional terms in the second and third line of eq. (3.17) have again the same structure as those generated by $B_{c\bar{c}}^{(2)}$ in eq. (3.13). Therefore, we can perform the simplification in eq. (3.16) accompanied by the further replacement, in addition to that in eq. (3.14),

$$\begin{aligned}B_{c\bar{c}}^{(2)} \to B_{c\bar{c}}^{(2)} &- 2\Re\left[\frac{\langle M_{c\bar{c}}^{(1)}|M_{c\bar{c}}^{(0)}\rangle}{|M_{c\bar{c}}^{(0)}|^2}\right]\frac{\langle M_{c\bar{c}}^{(0)}|\mathbf{\Gamma}_t^{(1)\,\dagger}+\mathbf{\Gamma}_t^{(1)}|M_{c\bar{c}}^{(0)}\rangle}{|M_{c\bar{c}}^{(0)}|^2} \\ &+ 2\,\Re\left[\frac{\langle M_{c\bar{c}}^{(1)}|\mathbf{\Gamma}_t^{(1)\,\dagger}+\mathbf{\Gamma}_t^{(1)}|M_{c\bar{c}}^{(0)}\rangle}{|M_{c\bar{c}}^{(0)}|^2}\right]\,.\end{aligned} \tag{3.18}$$

The exponential factor present in $\langle M_{c\bar{c}}^{(0)}|\mathbf{V}_{\rm NLL}^{\dagger}\mathbf{V}_{\rm NLL}|M_{c\bar{c}}^{(0)}\rangle$ can now be evaluated explicitly by performing a rotation in colour space into a basis in which $\mathbf{\Gamma}_t^{(1)}$ is diagonal. Explicit expressions for the corresponding colour matrices can be found in ref. [129] and are reported in appendix A.

After performing the approximations described above, we arrive to the following expression:

$$\begin{aligned}\frac{\mathrm{d}\sigma}{\mathrm{d}^2\vec{p}_{\rm T}\,\mathrm{d}\Phi_{Q\bar{Q}}} = \frac{1}{2m_{Q\bar{Q}}^2}\sum_{c=q,\bar{q},g}\int\frac{\mathrm{d}^2\vec{b}}{(2\pi)^2}e^{i\vec{b}\cdot\vec{p}_{\rm T}}e^{-\hat{S}_{c\bar{c}}\left(\frac{b_0}{b}\right)}\langle M_{c\bar{c}}^{(0)}|\left(\mathbf{V}_{\rm NLL}\right)^{\dagger}\mathbf{V}_{\rm NLL}|M_{c\bar{c}}^{(0)}\rangle \\ \times\sum_{i,j}\left[\mathrm{Tr}(\mathbf{H}_{c\bar{c}}\mathbf{D})\,\left(C_{ci}\otimes f_i\right)\left(C_{\bar{c}j}\otimes f_j\right)\right]+\mathcal{O}(\alpha_s^5)\,,\end{aligned} \tag{3.19}$$

JHEP04(2022)079

where the effective Sudakov radiator $\hat{S}_{c\bar{c}}$ is obtained from the usual colour-singlet case by replacing $B^{(2)}_{c\bar{c}} \to \hat{B}^{(2)}_{c\bar{c}}$, with

$$\begin{aligned}\hat{B}^{(2)}_{c\bar{c}} = B^{(2)}_{c\bar{c}} &+ \frac{\langle M^{(0)}_{c\bar{c}}|\mathbf{\Gamma}^{(2)\,\dagger}_t + \mathbf{\Gamma}^{(2)}_t|M^{(0)}_{c\bar{c}}\rangle}{|M^{(0)}_{c\bar{c}}|^2} \\ &- 2\Re\left[\frac{\langle M^{(1)}_{c\bar{c}}|M^{(0)}_{c\bar{c}}\rangle}{|M^{(0)}_{c\bar{c}}|^2}\right]\frac{\langle M^{(0)}_{c\bar{c}}|\mathbf{\Gamma}^{(1)\,\dagger}_t + \mathbf{\Gamma}^{(1)}_t|M^{(0)}_{c\bar{c}}\rangle}{|M^{(0)}_{c\bar{c}}|^2} \\ &+ 2\,\Re\left[\frac{\langle M^{(1)}_{c\bar{c}}|\mathbf{\Gamma}^{(1)\,\dagger}_t + \mathbf{\Gamma}^{(1)}_t|M^{(0)}_{c\bar{c}}\rangle}{|M^{(0)}_{c\bar{c}}|^2}\right]. \end{aligned} \tag{3.20}$$

We finally need to address the contribution coming from the azimuthally-dependent operator $\mathbf{D}$. As mentioned before, due to the property $[\mathbf{D}]_\phi = \mathbb{1}$, the second-order coefficient $\mathbf{D}^{(2)}$ gives a vanishing contribution to azimuthally-averaged observables at NNLO. On the other hand, in the case of $\mathbf{D}^{(1)}$ we still have an $\mathcal{O}(\alpha_s^2)$ contribution after averaging over ϕ, due to the interference between $\mathbf{D}^{(1)}$ and the collinear functions C_{ij} in eq. (3.1) (see ref. [82] for a detailed discussion). More specifically, this non-vanishing contribution arises only in the gluon-initiated channel, and it originates from the product of $\mathbf{D}^{(1)}$ with the polarization-dependent coefficient functions G_{ij} [111]. Therefore, the term in square brackets in eq. (3.19) can be written, upon azimuthal averaging, as

$$\begin{aligned}&[\mathrm{Tr}(\mathbf{H}_{c\bar{c}}\mathbf{D})\,(C_{ci}\otimes f_i)\,(C_{\bar{c}j}\otimes f_j)]_\phi \equiv [H_{c\bar{c}}\,(C_{ci}\otimes f_i)\,(C_{\bar{c}j}\otimes f_j)]_\phi \\ &+\left(\frac{\alpha_s(b_0/b)}{2\pi}\right)^2\left[\left(\frac{\langle M^{(0)}_{c\bar{c}}|\mathbf{D}^{(1)}|M^{(0)}_{c\bar{c}}\rangle}{|M^{(0)}_{c\bar{c}}|^2}\right)\Big((C^{(1)}_{ci}\otimes f_i)\,(f_{\bar{c}}) + (f_c)\,(C^{(1)}_{\bar{c}j}\otimes f_j)\Big)\right]_\phi + \mathcal{O}(\alpha_s^3)\,. \end{aligned} \tag{3.21}$$

The first term in the r.h.s. of eq. (3.21) is analogous to what features in colour-singlet production, where the quantity $H_{c\bar{c}}$ is defined as

$$H_{c\bar{c}} \equiv \frac{|M_{c\bar{c}}|^2}{|M^{(0)}_{c\bar{c}}|^2} = 1 + \frac{\alpha_s}{2\pi}H^{(1)}_{c\bar{c}} + \frac{\alpha_s^2}{(2\pi)^2}H^{(2)}_{c\bar{c}} + \mathcal{O}(\alpha_s^3)\,. \tag{3.22}$$

We recall, however, that the subtraction operator needed to compute the IR-subtracted amplitudes defining $H_{c\bar{c}}$ is not the same as in the colour-singlet case. The analytic result for the integrals over the azimuthal angle that are needed to compute the additional term in eq. (3.21) can be found in ref. [129], see e.g. eq. (4.85) of that reference.

3.2 The MiNNLO$_{\rm PS}$ master formulae for heavy-quark pair production

The result obtained in eq. (3.19) can be regarded as the starting point for the derivation of the MiNNLO$_{\rm PS}$ formalism for $Q\bar{Q}$ production. If we compare eq. (3.19) with the factorisation formula for colour-singlet production (obtained from eq. (3.1) by setting $\mathbf{\Delta} = \mathbb{1}$), we can see that the only difference, besides the extra term taken into account by eq. (3.21), is the replacement of the usual Sudakov radiator by the more complicated expression $\exp(-\hat{S}_{c\bar{c}})\langle M^{(0)}_{c\bar{c}}|\,(\mathbf{V}_{\rm NLL})^\dagger\,\mathbf{V}_{\rm NLL}|M^{(0)}_{c\bar{c}}\rangle$, where $\hat{S}_{c\bar{c}}$ is defined by eq. (3.2) with the replacement (3.20). In the colour basis in which $\mathbf{\Gamma}^{(1)}_t$ is diagonal, this expression reduces to a linear combination of complex exponential terms, whose coefficients are related to the

JHEP04(2022)079

rotation needed for the change of basis. More specifically, the structure of each of the terms in the sum is exactly that of a Sudakov radiator with a *complex* coefficient $\hat{B}^{(1)}_{c\bar{c}}$, obtained from the one in $\hat{S}_{c\bar{c}}$ by adding the contribution from the eigenvalues of the $\mathbf{\Gamma}^{(1)}_t$ operator. The details of the linear combination are given in appendix A.

We are now in a position to write an expression for the $p_{\rm T}$ distribution of the $Q\bar{Q}$ system, differential in the Born phase space $\Phi_{Q\bar{Q}}$, that is NNLO-accurate upon integration over $p_{\rm T}$ and LL accurate (plus the CMW corrections associated with the coefficient $A^{(2)}$ in the Sudakov captured by common parton showers) in the limit $p_{\rm T} \to 0$. Each summand of this formula will have the same structure as in the colour-singlet case discussed in eq. (2.3). Since the new starting point given in eq. (3.19) is a linear combination of colour-singlet-like terms, we can follow the same steps used for the colour-singlet MiNNLO$_{\rm PS}$ formulation that lead from the q_T-resummation formula to eq. (2.3) [11]. Specifically, the Fourier integral of eq. (3.19) can be performed as described in appendix E of ref. [11], leading to the result

$$\frac{\mathrm{d}\sigma}{\mathrm{d}p_{\rm T}\,\mathrm{d}\Phi_{Q\bar{Q}}} = \frac{\mathrm{d}}{\mathrm{d}p_{\rm T}}\Bigg\{\sum_c \frac{e^{-\tilde{S}_{c\bar{c}}(p_{\rm T})}}{2m^2_{Q\bar{Q}}}\,\langle M^{(0)}_{c\bar{c}}|\,(\mathbf{V}_{\rm NLL})^\dagger\,\mathbf{V}_{\rm NLL}|M^{(0)}_{c\bar{c}}\rangle \times \sum_{i,j}\Big[\mathrm{Tr}(\tilde{\mathbf{H}}_{c\bar{c}}\mathbf{D})\,(\tilde{C}_{ci}\otimes f_i)\,(\tilde{C}_{\bar{c}j}\otimes f_j)\Big]_\phi\Bigg\} + R_{\rm finite}(p_{\rm T}) + \mathcal{O}(\alpha_s^5)\,. \tag{3.23}$$

The quantities $\tilde{S}_{c\bar{c}}$, $\tilde{\mathbf{H}}_{c\bar{c}}$ and $\tilde{C}_{ij}$ in eq. (3.23) are now all evaluated at the scale $p_{\rm T}$, and can be obtained from the ones in eq. (3.19) by means of the following additional replacements [11]:

$$\hat{B}^{(2)}_{c\bar{c}} \to \tilde{B}^{(2)}_{c\bar{c}} \equiv \hat{B}^{(2)}_{c\bar{c}} + 2\zeta_3 (A^{(1)}_{c\bar{c}})^2 + 2\pi\beta_0\, H^{(1)}_{c\bar{c}}\,, \tag{3.24}$$

$$H^{(2)}_{c\bar{c}} \to \tilde{H}^{(2)}_{c\bar{c}} \equiv H^{(2)}_{c\bar{c}} - 2\zeta_3 A^{(1)}_{c\bar{c}} B^{(1)}_{c\bar{c}}\,, \tag{3.25}$$

$$C^{(2)}_{ci}(z) \to \tilde{C}^{(2)}_{ci}(z) \equiv C^{(2)}_{ci}(z) - 2\zeta_3 A^{(1)}_{c\bar{c}} \hat{P}^{(0)}_{ci}(z)\,, \tag{3.26}$$

where $H^{(2)}_{c\bar{c}}$ is the second-order term in the α_s expansion of $H_{c\bar{c}}$ defined in eq. (3.22) and $\hat{P}^{(0)}(z)$ is the tree-level regularised Altarelli-Parisi splitting function.

The final steps in the derivation of the MiNNLO$_{\rm PS}$ algorithm for $Q\bar{Q}$ production follow again the procedure described in refs. [11, 12] for the colour-singlet case. Thanks to the structure of eq. (3.23), being a sum of terms of the type (2.3), the derivation can be applied to each of the terms in the sum individually. The more technical details can therefore be found in refs. [11, 12], while the main features of the derivation have been already described in section 2. To connect with the results in section 2, we now write eq. (3.23) as

$$\frac{\mathrm{d}\sigma}{\mathrm{d}p_{\rm T}\,\mathrm{d}\Phi_{Q\bar{Q}}} = \frac{\mathrm{d}}{\mathrm{d}p_{\rm T}}\Bigg\{\sum_c \Bigg[\sum_{i=1}^{n_c} \mathcal{C}^{[\gamma_i]}_{c\bar{c}}(\Phi_{Q\bar{Q}})\, e^{-\tilde{S}^{[\gamma_i]}_{c\bar{c}}(p_{\rm T})}\Bigg]\mathcal{L}_{c\bar{c}}(\Phi_{\rm F}, p_{\rm T})\Bigg\} + R_{\rm finite}(p_{\rm T}) + \mathcal{O}(\alpha_s^5)\,, \tag{3.27}$$

where we have diagonalised the one-loop soft anomalous dimension in $\mathbf{V}_{\rm NLL}$ and used

$$e^{-\tilde{S}_{c\bar{c}}(p_{\rm T})}\langle M^{(0)}_{c\bar{c}}|\,(\mathbf{V}_{\rm NLL})^\dagger\,\mathbf{V}_{\rm NLL}|M^{(0)}_{c\bar{c}}\rangle = |M^{(0)}_{c\bar{c}}|^2 \sum_{i=1}^{n_c} \mathcal{C}^{[\gamma_i]}_{c\bar{c}}(\Phi_{Q\bar{Q}})\, e^{-\tilde{S}^{[\gamma_i]}_{c\bar{c}}(p_{\rm T})}\,. \tag{3.28}$$

JHEP04(2022)079

We defined $\tilde{S}^{[\gamma_i]}_{c\bar{c}}$ as the Sudakov obtained from eq. (3.23) via the replacement

$$B^{(1)}_{c\bar{c}} \to \tilde{B}^{(1)}_{c\bar{c}} \equiv B^{(1)}_{c\bar{c}} + \gamma_i(\Phi_{Q\bar{Q}})\,, \tag{3.29}$$

where the functions $\gamma_i \equiv \gamma_{c\bar{c},i}$ (we omit the $c\bar{c}$ subscript in the following) are obtained from the eigenvalues of the operator $\mathbf{\Gamma}^{(1)}_t$. Moreover, the coefficients $\mathcal{C}^{[\gamma_i]}_{c\bar{c}} \equiv \mathcal{C}^{[\gamma_i]}_{c\bar{c}}(\Phi_{Q\bar{Q}})$ define the linear combination in terms of the resulting complex exponentials, and obey the constraint

$$\sum_{i=1}^{n_c} \mathcal{C}^{[\gamma_i]}_{c\bar{c}}(\Phi_{Q\bar{Q}}) = 1\,. \tag{3.30}$$

The number of terms n_c in the sum depends on the SU(3) representation of a given flavour configuration of the initial state, and in particular one has $n_c = 4$ for $q\bar{q}$ channels and $n_c = 9$ for the gg channel. The expressions for the γ_i and $\mathcal{C}^{[\gamma_i]}_{c\bar{c}}$ coefficients is reported in appendix A. We also defined the luminosity factor in eq. (3.27) as

$$\mathcal{L}_{c\bar{c}}(\Phi_{\rm F}, p_{\rm T}) \equiv \frac{|M^{(0)}_{c\bar{c}}|^2}{2m^2_{Q\bar{Q}}} \sum_{i,j} \Big[\mathrm{Tr}(\tilde{\mathbf{H}}_{c\bar{c}}\mathbf{D})\ (\tilde{C}_{ci}\otimes f_i)\,(\tilde{C}_{\bar{c}j}\otimes f_j)\Big]_\phi\,. \tag{3.31}$$

We can now repeat the derivation of eq. (2.4) for each of the terms in the sum over i in eq. (3.27), and we obtain the following definition of the MiNNLO$_{\rm PS}$ $\tilde{B}$ function

$$\begin{aligned}
\tilde{B}_{Q\bar{Q}}(\Phi_{\rm FJ}, \Phi_{\rm rad}) \equiv \sum_{c_{\rm FJ}} \Bigg\{ & \sum_{i=1}^{n_{c_{\rm F}\leftarrow c_{\rm FJ}}} \mathcal{C}^{[\gamma_i]}_{c_{\rm F}\leftarrow c_{\rm FJ}}(\Phi_{\rm F}) \exp[-\tilde{S}^{[\gamma_i]}_{c_{\rm F}\leftarrow c_{\rm FJ}}(\Phi_{\rm F}, p_{\rm T})] \\
& \times \left[B_{c_{\rm FJ}}(\Phi_{\rm FJ}) \left(1 + \frac{\alpha_s(p_{\rm T})}{2\pi}[\tilde{S}^{[\gamma_i]}_{c_{\rm F}\leftarrow c_{\rm FJ}}(\Phi_{\rm F}, p_{\rm T})]^{(1)}\right) + V_{c_{\rm FJ}}(\Phi_{\rm FJ})\right]\Bigg\} \\
& + \sum_{c_{\rm FJJ}} \Bigg\{ \sum_{i=1}^{n_{c_{\rm F}\leftarrow c_{\rm FJJ}}} \mathcal{C}^{[\gamma_i]}_{c_{\rm F}\leftarrow c_{\rm FJJ}}(\Phi_{\rm F}) \exp[-\tilde{S}^{[\gamma_i]}_{c_{\rm F}\leftarrow c_{\rm FJJ}}(\Phi_{\rm F}, p_{\rm T})] \Bigg\} R_{c_{\rm FJJ}}(\Phi_{\rm FJ}, \Phi_{\rm rad}) \\
& + \sum_{c_{\rm FJ}} \Bigg\{ \sum_{c_{\rm F}} \sum_{i=1}^{n_{c_{\rm F}}} \mathcal{C}^{[\gamma_i]}_{c_{\rm F}}(\Phi_{\rm F}) \exp[-\tilde{S}^{[\gamma_i]}_{c_{\rm F}}(\Phi_{\rm F}, p_{\rm T})] D^{[\gamma_i],\,(\geq 3)}_{c_{\rm F}}(\Phi_{\rm F}, p_{\rm T}) \Bigg\} F^{\rm corr}_{c_{\rm FJ}}(\Phi_{\rm FJ})\,.
\end{aligned} \tag{3.32}$$

In the above equation, the phase space $\Phi_{\rm F}$ is obtained with an appropriate kinematic map from the $\Phi_{\rm FJ}$ phase space. The projection can be obtained, for example (see refs. [2, 105, 106]), with a longitudinal boost such that the F-system has zero rapidity, followed by a transverse boost such that the F-system has zero transverse momentum, and a final longitudinal boost equal and opposite to the first one. Analogously to eq. (2.4) (and with a little abuse of notation), the transverse momentum $p_{\rm T}$ in each term of eq. (3.32) is calculated in the corresponding kinematics (either $\Phi_{\rm FJ}$ or $\Phi_{\rm FJJ}$).

The sum over $c_{\rm FJ}$ in eq. (3.32) runs over all possible initial-state flavour compositions of the FJ process (in this case $c_{\rm FJ} = \{gg, gq, q\bar{q}\}$, and we omit for simplicity all conjugate configurations in our notation). The notation $c_{\rm F} \leftarrow c_{\rm FJ}$ denotes instead the flavour configuration of the final state F corresponding to the flavour projection of the FJ final state. Analogously, $c_{\rm F} \leftarrow c_{\rm FJJ}$ indicates a projection between the flavour configuration of

JHEP04(2022)079

FJJ and F, which is obtained by first deriving the flavour of FJ via the POWHEG flavour mapping and then applying the $c_{\rm F} \leftarrow c_{\rm FJ}$ projection. There are various ways to define such a projection, meaning that each summand might be unphysical and only the total combination (i.e. $\tilde{B}_{Q\bar{Q}}$) is physical. We define the projection using the following procedure:

- If $c_{\rm FJ} = \{gg, q\bar{q}\}$ then there is no ambiguity and we set $c_{\rm F} = c_{\rm FJ}$;
- If $c_{\rm FJ} = gq$ then we assign the flavour $c_{\rm F}$ as follows. In the partonic c.o.m. frame, we consider the rapidity η_ℓ of the light parton in the FJ final state and we split the event into two hemispheres at $\eta_\ell = 0$. If the parton shares the same hemisphere with an initial-state gluon, then we assign $c_{\rm F} = q\bar{q}$. Conversely, if the parton shares the same hemisphere with an initial-state quark (or anti-quark), then we assign $c_{\rm F} = gg$. This procedure guarantees that the flavour configuration is correctly assigned when the light parton is collinear to one of the initial-state legs (i.e. the collinear singularity is correctly reproduced by the Sudakov $\tilde{S}^{[\gamma_i]}_{c_{\rm F} \leftarrow c_{\rm FJ}}$).

The function $D^{[\gamma_i],\,(\geq 3)}_{c_{\rm F}}$ is defined by extending eq. (2.5) as

$$D^{[\gamma_i],\,(\geq 3)}_{c_{\rm F}}(\Phi_{\rm F}, p_{\rm T}) = D^{[\gamma_i]}_{c_{\rm F}}(\Phi_{\rm F}, p_{\rm T}) - \frac{\alpha_s(p_{\rm T})}{2\pi}[D^{[\gamma_i]}_{c_{\rm F}}(\Phi_{\rm F}, p_{\rm T})]^{(1)} - \left(\frac{\alpha_s(p_{\rm T})}{2\pi}\right)^2 [D^{[\gamma_i]}_{c_{\rm F}}(\Phi_{\rm F}, p_{\rm T})]^{(2)}\,,$$
$$D^{[\gamma_i]}_{c_{\rm F}}(\Phi_{\rm F}, p_{\rm T}) = -\frac{{\rm d}\tilde{S}^{[\gamma_i]}_{c_{\rm F}}(\Phi_{\rm F}, p_{\rm T})}{{\rm d}p_{\rm T}}\mathcal{L}_{c_{\rm F}}(\Phi_{\rm F}, p_{\rm T}) + \frac{{\rm d}\mathcal{L}_{c_{\rm F}}(\Phi_{\rm F}, p_{\rm T})}{{\rm d}p_{\rm T}}\,. \tag{3.33}$$

The explicit expressions of the expansion coefficients $[D^{[\gamma_i]}_{c_{\rm F}}(\Phi_{\rm F}, p_{\rm T})]^{(1)}$ and $[D^{[\gamma_i]}_{c_{\rm F}}(\Phi_{\rm F}, p_{\rm T})]^{(2)}$ directly follow from the colour-singlet formulae given in eqs. (27), (28) of ref. [12]. In eq. (3.32) we have explicitly indicated the dependence of the Sudakov $\tilde{S}$ and the luminosity factor $\mathcal{L}$ on the phase space $\Phi_{\rm F}$.

4 Computational aspects

In this section we discuss some computational aspects of the implementation of eq. (3.32). In particular, we derive the dependence of eq. (3.32) on the perturbative scales and introduce their settings, whose variation is used to estimate the size of subleading perturbative corrections. We further comment on the treatment of the Landau pole in the strong coupling constant that is encountered in the calculation of the Sudakov radiators $\tilde{S}^{[\gamma_i]}_{c\bar{c}}$. Finally, we also describe the implementation of the decay of the top quarks.

4.1 Renormalisation and factorisation scale dependence

The fixed-order elements of eq. (3.32) (i.e. $B_{c_{\rm FJ}}$,$V_{c_{\rm FJ}}$ and $R_{c_{\rm FJJ}}$) receive the customary dependence on the renormalisation- and factorisation-scale variations. For collider reactions that are mediated by strong interactions already at the Born level, such as the process considered here, the n_B powers of the strong coupling in the Born squared matrix element are evaluated at a scale $\mu^{(0)}_{\rm R}$ which is always of order $m_{Q\bar{Q}}$, and we would like to maintain its dependence explicit in the expressions that follow so that different choices for this scale can be made by the user. In particular, we will set this scale to a dynamical hard scale in

JHEP04(2022)079

the phenomenological study of this article. The remaining scales are defined with respect to the central value as $\mu_{\rm R} = K_{\rm R}\,\mu_0$, $\mu_{\rm F} = K_{\rm F}\,\mu_0$, with $\mu_0 \sim p_{\rm T}$ in the regime $p_{\rm T} \ll m_{Q\bar{Q}}$. For the time being we will consider $\mu_0 = p_{\rm T}$, but in section 4.3 this will be consistently modified by means of a prescription to turn off all resummation effects at large $p_{\rm T}$. The $K_{\rm R}$ and $K_{\rm F}$ dependence of the remaining terms in eq. (3.32) is obtained by following refs. [11, 12] and, for completeness, it is reported below.

We start from the Sudakov radiators $\tilde{S}^{[\gamma_i]}_{c\bar{c}}(p_{\rm T})$, which now become

$$\tilde{S}^{[\gamma_i]}_{c\bar{c}}\,(p_{\rm T}, K_{\rm R}) \equiv \int_{p_{\rm T}^2}^{m^2_{Q\bar{Q}}} \frac{{\rm d}q^2}{q^2} \left[A_{c\bar{c}}(\alpha_s(K_{\rm R}\,q), K_{\rm R}) \ln \frac{m^2_{Q\bar{Q}}}{q^2} + \tilde{B}_{c\bar{c}}(\alpha_s(K_{\rm R}\,q), K_{\rm R}) \right], \tag{4.1}$$

where the $K_{\rm R}$ dependent perturbative coefficients $A^{(i)}_{c\bar{c}}$ and $\tilde{B}^{(i)}_{c\bar{c}}$ are obtained from those given in eqs. (3.2), (3.20), (3.24), (3.29) by means of the relations [11]

$$\begin{aligned} A^{(2)}_{c\bar{c}}(K_{\rm R}) &\equiv A^{(2)}_{c\bar{c}} + (2\pi\beta_0) A^{(1)}_{c\bar{c}} \ln K^2_{\rm R}, \\ \tilde{B}^{(2)}_{c\bar{c}}(K_{\rm R}) &\equiv \tilde{B}^{(2)}_{c\bar{c}} + (2\pi\beta_0) \tilde{B}^{(1)}_{c\bar{c}} \ln K^2_{\rm R} + (2\pi\beta_0)^2\, n_B \ln \frac{(\mu^{(0)}_{\rm R})^2}{m^2_{Q\bar{Q}}}\,. \end{aligned} \tag{4.2}$$

The factor n_B (defined as the power of α_s of the Born squared amplitude) is induced by the presence of $H^{(1)}_{c\bar{c}}$ in the $\tilde{B}^{(2)}_{c\bar{c}}$ coefficient, which, in turn, originates from evaluating the hard virtual corrections $\tilde{\mathbf{H}}_{c\bar{c}}$ at $p_{\rm T}$ in the factor $\mathcal{L}_{c\bar{c}}$ defined in eq. (3.31), see also eq. (3.21). The integral in eq. (4.1) is evaluated exactly without additional approximations through a numerical integration using a quadrature method, which allows us to adopt the strong coupling constant used in the evolution of the parton densities, encoding the effect of heavy-quark thresholds as taken from the parton-densities provider.

We now continue with the scale dependence of the luminosity factor (3.31). All coupling constants are now evaluated at $\mu_{\rm R} = K_{\rm R}\,p_{\rm T}$ and the parton densities are calculated at $\mu_{\rm F} = K_{\rm F}\,p_{\rm T}$. The definition of the $[\dots]_\phi$ expectation value is given in eq. (3.21). The perturbative coefficients of the hard factor $H_{c\bar{c}}$ acquire the following $K_{\rm R}$ and $K_{\rm F}$ dependence [11]

$$H^{(1)}_{c\bar{c}}(K_{\rm R}) \equiv H^{(1)}_{c\bar{c}} + (2\pi\beta_0) n_B \ln \frac{(\mu^{(0)}_{\rm R})^2}{m^2_{Q\bar{Q}}}\,, \tag{4.3}$$

$$\begin{aligned} \tilde{H}^{(2)}_{c\bar{c}}(K_{\rm R}) \equiv \tilde{H}^{(2)}_{c\bar{c}} &- 2\,n_B(1-n_B)\pi^2\beta_0^2 \ln^2 \frac{(\mu^{(0)}_{\rm R})^2}{m^2_{Q\bar{Q}}} + 4\pi^2 n_B \ln \frac{(\mu^{(0)}_{\rm R})^2}{m^2_{Q\bar{Q}}} \left(\beta_1 + \beta_0^2 \ln K^2_{\rm R}\right) \\ &+ 2\pi\beta_0 \left(n_B \ln \frac{(\mu^{(0)}_{\rm R})^2}{m^2_{Q\bar{Q}}} + \ln K^2_{\rm R} \right) H^{(1)}_{c\bar{c}}\,. \end{aligned} \tag{4.4}$$

The coefficient functions C_{ij} receive the following scale dependence [11]:

$$C^{(1)}_{ij}(z, K_{\rm F}) \equiv C^{(1)}_{ij}(z) - \hat{P}^{(0)}_{ij}(z) \ln K^2_{\rm F}, \tag{4.5}$$

$$\begin{aligned} \tilde{C}^{(2)}_{ij}(z, K_{\rm F}, K_{\rm R}) \equiv \tilde{C}^{(2)}_{ij}(z) &+ \pi\beta_0 \hat{P}^{(0)}_{ij}(z) \left(\ln^2 K^2_{\rm F} - 2 \ln K^2_{\rm F} \ln K^2_{\rm R}\right) - \hat{P}^{(1)}_{ij}(z) \ln K^2_{\rm F} \\ &+ \frac{1}{2} (\hat{P}^{(0)} \otimes \hat{P}^{(0)})_{ij}(z) \ln^2 K^2_{\rm F} - (\hat{P}^{(0)} \otimes C^{(1)})_{ij}(z) \ln K^2_{\rm F} + 2\pi\beta_0 C^{(1)}_{ij}(z) \ln K^2_{\rm R}\,, \end{aligned}$$

JHEP04(2022)079

while the part of the coefficient functions G_{ij} as well as the second term in the r.h.s. of eq. (3.21), which together contain all sources of azimuthal and colour correlations, remain unchanged since they enter first at relative order $\mathcal{O}(\alpha_s^2)$.

We use the above coefficients in the evaluation of the MiNNLO$_{\rm PS}$ coefficient $D_{c\mathrm{F}}^{[\gamma_i],\,(\geq 3)}$ defined in eq. (3.33). In addition to the scale dependence of the coefficients above (which is understood in the following equations), the $[D_{c\bar{c}}^{[\gamma_i]}(\Phi_{\rm F}, p_{\rm T})]^{(1)}$ and $[D_{c\bar{c}}^{[\gamma_i]}(\Phi_{\rm F}, p_{\rm T})]^{(2)}$ terms acquire an additional explicit dependence on the scale factors $K_{\rm R}$ and $K_{\rm F}$ due to expanding the derivative of the luminosity in eq. (3.33) in powers of $\alpha_s(K_{\rm R}\, p_{\rm T})$. This reads

$$\begin{aligned}
&\left[D_{c\bar{c}}^{[\gamma_i]}(\Phi_{\rm F}, p_{\rm T})\right]^{(1)}(K_{\rm F}, K_{\rm R}) \equiv \left[D_{c\bar{c}}^{[\gamma_i]}(\Phi_{\rm F}, p_{\rm T})\right]^{(1)}\,, \\
&\left[D_{c\bar{c}}^{[\gamma_i]}(\Phi_{\rm F}, p_{\rm T})\right]^{(2)}(K_{\rm F}, K_{\rm R}) \equiv \left[D_{c\bar{c}}^{[\gamma_i]}(\Phi_{\rm F}, p_{\rm T})\right]^{(2)} - 2\beta_0\pi \left[\frac{\mathrm{d}\mathcal{L}_{c\bar{c}}(\Phi_{\rm F}, p_{\rm T})}{\mathrm{d}p_{\rm T}}\right]^{(1)} \ln\frac{K_{\rm F}^2}{K_{\rm R}^2}\,.
\end{aligned} \tag{4.6}$$

On the other hand, the scale dependence in the $D_{c\bar{c}}^{[\gamma_i],\,(\geq 3)}(\Phi_{\rm F}, p_{\rm T})$ originating from the luminosity factor $\mathcal{L}$ is retained implicitly by performing the derivative of $\mathcal{L}$ numerically.

4.2 Resummation scale dependence

We also introduce some flexibility in the scale at which one turns off the resummation effects in eq. (3.32) in phase space regions characterised by a large transverse momentum $p_{\rm T}$ of the heavy-quark pair.[6] This is done by means of a resummation scale $Q \sim m_{Q\bar{Q}}$, which is introduced in both the Sudakov radiators and the luminosity factor. At the level of the Sudakov, the resummation scale Q effectively replaces the upper bound of the integral, as we now show. We start by re-writing the Sudakov factors in eq. (4.1) as (we define $K_{\rm Q} \equiv Q/m_{Q\bar{Q}}$)

$$\begin{aligned}
\tilde{S}_{c\bar{c}}^{[\gamma_i]}(p_{\rm T}, K_{\rm R}) = &\int_{p_{\rm T}^2}^{Q^2} \frac{\mathrm{d}q^2}{q^2}\left[A_{c\bar{c}}(\alpha_s(K_{\rm R}\, q), K_{\rm R})\ln\frac{Q^2}{q^2}\right. \\
&\left.+\left(\tilde{B}_{c\bar{c}}(\alpha_s(K_{\rm R}\, q), K_{\rm R}) - A_{c\bar{c}}(\alpha_s(K_{\rm R}\, q), K_{\rm R})\ln K_{\rm Q}^2\right)\right] \\
&+\int_{Q^2}^{m_{Q\bar{Q}}^2} \frac{\mathrm{d}q^2}{q^2}\left[A_{c\bar{c}}(\alpha_s(K_{\rm R}\, q), K_{\rm R})\ln\frac{Q^2}{q^2}\right. \\
&\left.+\left(\tilde{B}_{c\bar{c}}(\alpha_s(K_{\rm R}\, q), K_{\rm R}) - A_{c\bar{c}}(\alpha_s(K_{\rm R}\, q), K_{\rm R})\ln K_{\rm Q}^2\right)\right]\,.
\end{aligned} \tag{4.7}$$

Subsequently, for later convenience, we expand the second integral in the r.h.s. of eq. (4.7) to second order in powers of $\alpha_s(K_{\rm R}/K_{\rm Q}\, p_{\rm T})$, and absorb the terms proportional to $\ln\frac{Q}{p_{\rm T}}$ into the first integral neglecting subleading corrections (specifically into the $\tilde{B}_{c\bar{c}}^{(2)}$ coefficient), namely

$$\tilde{B}_{c\bar{c}}^{(2)}(K_{\rm R}, K_{\rm Q}) \equiv \tilde{B}_{c\bar{c}}^{(2)}(K_{\rm R}) - \pi\beta_0 \ln K_{\rm Q}^2\left(A_{c\bar{c}}^{(1)}\ln K_{\rm Q}^2 - 2\tilde{B}_{c\bar{c}}^{(1)}\right)\,, \tag{4.8}$$

[6] Since the following formulas are reported here for the first time we stress that they apply also to the case of colour-singlet production.

JHEP04(2022)079

while the non-logarithmic terms are expanded out of the exponential and absorbed into the $H_{c\bar{c}}$ hard factor. Consistently, we then change the scales of the strong coupling and parton densities in the hard factor $\tilde{H}_{c\bar{c}}$ and parton distribution functions in the luminosity factor (3.31) as follows:

$$\mu_{\rm R} = K_{\rm R}\, p_{\rm T} \to \mu_{\rm R} = \frac{K_{\rm R}}{K_{\rm Q}} p_{\rm T}\,, \quad \mu_{\rm F} = K_{\rm F}\, p_{\rm T} \to \mu_{\rm F} = \frac{K_{\rm F}}{K_{\rm Q}} p_{\rm T}\,. \tag{4.9}$$

The above procedure results in the following scale dependence in the coefficients $\tilde{H}^{(i)}_{c\bar{c}}$ and $\tilde{C}_{ij}$

$$H^{(1)}_{c\bar{c}}(K_{\rm R}, K_{\rm Q}) \equiv H^{(1)}_{c\bar{c}}(K_{\rm R}) + \left(-\frac{A^{(1)}_{c\bar{c}}}{2} \ln K^2_{\rm Q} + \tilde{B}^{(1)}_{c\bar{c}}\right) \ln K^2_{\rm Q}\,, \tag{4.10}$$

$$\begin{aligned}
\tilde{H}^{(2)}_{c\bar{c}}(K_{\rm R}, K_{\rm Q}) \equiv{}& \tilde{H}^{(2)}_{c\bar{c}}(K_{\rm R}) + \frac{(A^{(1)}_{c\bar{c}})^2}{8} \ln^4 K^2_{\rm Q} - \left(\frac{A^{(1)}_{c\bar{c}} \tilde{B}^{(1)}_{c\bar{c}}}{2} + \pi\beta_0 \frac{A^{(1)}_{c\bar{c}}}{3}\right) \ln^3 K^2_{\rm Q} \\
&+ \left(-\frac{A^{(2)}_{c\bar{c}}(K_{\rm R})}{2} + \frac{(\tilde{B}^{(1)}_{c\bar{c}})^2}{2} + \pi\beta_0 \tilde{B}^{(1)}_{c\bar{c}} - n_B \pi\beta_0 A^{(1)}_{c\bar{c}} \ln \frac{(\mu^{(0)}_{\rm R})^2}{m^2_{Q\bar{Q}}}\right) \ln^2 K^2_{\rm Q} \\
&+ \left(\tilde{B}^{(2)}_{c\bar{c}}(K_{\rm R}) + 2 n_B \pi\beta_0 \tilde{B}^{(1)}_{c\bar{c}} \ln \frac{(\mu^{(0)}_{\rm R})^2}{m^2_{Q\bar{Q}}}\right) \ln K^2_{\rm Q} \\
&+ \left(\tilde{B}^{(1)}_{c\bar{c}} \ln K^2_{\rm Q} - \frac{A^{(1)}_{c\bar{c}}}{2} \ln^2 K^2_{\rm Q} - 2\pi\beta_0 \ln K^2_{\rm Q}\right) H^{(1)}_{c\bar{c}}\,,
\end{aligned} \tag{4.11}$$

and

$$C^{(1)}_{ij}(z, K_{\rm F}, K_{\rm Q}) \equiv C^{(1)}_{ij}(z, K_{\rm F}/K_{\rm Q})\,, \tag{4.12}$$

$$\tilde{C}^{(2)}_{ij}(z, K_{\rm F}, K_{\rm R}, K_{\rm Q}) \equiv \tilde{C}^{(2)}_{ij}(z, K_{\rm F}/K_{\rm Q}, K_{\rm R}/K_{\rm Q})\,. \tag{4.13}$$

4.3 Profiled logarithms and scale setting at large $p_{\rm T}$

In order to actually turn off all resummation effects at $p_{\rm T} \sim Q$ we introduce a (new version of the) *modified* logarithm by means of the replacement

$$\ln \frac{Q}{p_{\rm T}} \to L \tag{4.14}$$

with

$$L \equiv \begin{cases} \ln \dfrac{Q}{p_{\rm T}} & \text{if} \quad p_{\rm T} \le \dfrac{Q}{2}\,, \\ \ln\left(a_0 + a_1 \dfrac{p_{\rm T}}{Q} + a_2 \left(\dfrac{p_{\rm T}}{Q}\right)^2\right) & \text{if} \quad \dfrac{Q}{2} < p_{\rm T} \le Q\,, \\ 0 & \text{if} \quad p_{\rm T} > Q\,, \end{cases} \tag{4.15}$$

where $a_0 = 5$, $a_1 = -8$, $a_2 = 4$. The coefficients are chosen in such a way that L and its derivative with respect to $p_{\rm T}$ are continuous at $Q/2$ and that they both vanish at Q. The above parameterisation ensures that the resummation is exactly turned off for $p_{\rm T} \ge Q$, at variance with the modified logarithm adopted in ref. [12] which only vanishes asymptotically for $p_{\rm T} \gg Q$. Following ref. [12], the replacement in eq. (4.14) can be implemented with the following simple procedure:

JHEP04(2022)079

- We rewrite the scale setting in eq. (4.9) as

$$\mu_{\rm R} = K_{\rm R}\, m_{Q\bar{Q}}\, e^{-L}\,, \qquad \mu_{\rm F} = K_{\rm F}\, m_{Q\bar{Q}}\, e^{-L}\,. \tag{4.16}$$

  At small $p_{\rm T}$ this reduces to eq. (4.9) (we recall that $K_{\rm Q} = Q/m_{Q\bar{Q}}$), while at large $p_{\rm T}$ the scales tend to $K_{\rm R}\, m_{Q\bar{Q}}$ and $K_{\rm F}\, m_{Q\bar{Q}}$, respectively.

- We rewrite the lower integration bound of the first integral in the Sudakov (4.1) (the integrand is unchanged) as

$$p_{\rm T} \to Q e^{-L}. \tag{4.17}$$

- We multiply $D_{c\bar{c}}^{[\gamma_i],(\geq 3)}$ in eq. (3.32) by the following Jacobian factor:

$$D_{c\bar{c}}^{[\gamma_i],(\geq 3)} \to \mathcal{J}_Q D_{c\bar{c}}^{[\gamma_i],(\geq 3)};\ \mathcal{J}_Q \equiv -p_{\rm T}\frac{{\rm d}L}{{\rm d}p_{\rm T}} = \begin{cases} 1 & \text{if} \quad p_{\rm T} \leq \dfrac{Q}{2}\,, \\ -p_{\rm T}\dfrac{2a_2 p_{\rm T} + a_1 Q}{a_0 Q^2 + a_1 Q p_{\rm T} + a_2 p_{\rm T}^2} & \text{if} \quad \dfrac{Q}{2} < p_{\rm T} \leq Q\,, \\ 0 & \text{if} \quad p_{\rm T} > Q\,. \end{cases} \tag{4.18}$$

In order to avoid the Landau singularity in the calculation of the Sudakov radiator and in the evolution of parton densities, we implement the freezing procedure of ref. [12] with a freezing scale $Q_0 = 2\,\text{GeV}$. This is easily implemented by further modifying the scales in eq. (4.16) as follows

$$\mu_{\rm R} = K_{\rm R}\, m_{Q\bar{Q}} \left(e^{-L} + \frac{Q_0}{Q}\, g(p_{\rm T})\right), \qquad \mu_{\rm F} = K_{\rm F}\, m_{Q\bar{Q}} \left(e^{-L} + \frac{Q_0}{Q}\, g(p_{\rm T})\right), \tag{4.19}$$

where $g(p_{\rm T})$ is a damping function. A suitable choice (albeit one has some freedom) is [12]

$$g(p_{\rm T}) = \frac{1}{1 + \frac{Q}{Q_0} e^{-L}}\,. \tag{4.20}$$

This prescription is also consistently adopted in the Sudakov radiator $\tilde{S}(p_{\rm T})$ (4.7), at the integrand level. The integration is then still performed numerically. Analogously to what has been discussed for the modified logarithms in eq. (4.18), the choice in eq. (4.19) requires the introduction of an additional factor $\mathcal{J}_{Q_0}$

$$\mathcal{J}_{Q_0} \equiv \frac{{\rm d}\ln\left(Q/\mu_{\rm F}\right)}{{\rm d}L} = Q\, e^{-L} \frac{1 - g^2(p_{\rm T})}{Q\, e^{-L} + Q_0\, g(p_{\rm T})}\,, \tag{4.21}$$

which multiplies *only* the derivative of the luminosity [12] in the definition of $D_{c\bar{c}}^{[\gamma_i],(\geq 3)}$ (3.33). We stress that the freezing only affects running coupling effects, and hence does not modify the double logarithmic structure of eq. (3.32) and the phase-space integration is performed down to vanishing $p_{\rm T}$ including all power corrections at the desired accuracy. Therefore, the scale Q_0 does not play the role of a slicing parameter in the MiNNLO$_{\rm PS}$ calculation.

A final important remark is that in all formulae defined in this section we allow for the scale factors $K_{\rm R}$ and $K_{\rm F}$ to be set dynamically on an event-by-event basis. That is, we can choose to perform the computation with reference renormalisation and factorisation

JHEP04(2022)079

scales at large $p_{\rm T}$ different from a multiple of the top-quark pair invariant mass $m_{Q\bar{Q}} = m_{t\bar{t}}$, while their setting at small $p_{\rm T}$ has to remain of order $p_{\rm T}$ for consistency of the MiNNLO$_{\rm PS}$ procedure, as detailed before. This has the advantage of allowing different scale settings in phase space regions characterised by a large $p_{\rm T}$, which better describe the momentum transfer in the hard scattering. Suitable candidates are for instance scales proportional to

$$H_T^{t\bar{t}} = m_T^t + m_T^{\bar{t}}\,, \quad H_T^{t\bar{t}+\,\text{jets}} = m_T^t + m_T^{\bar{t}} + \sum_{i\notin t} p_{T,i}\,, \tag{4.22}$$

with $m_T^i = \sqrt{m_i^2 + p_{Ti}^2}$ being the transverse mass of particle i.[7] In particular, such settings may be used for the fixed-order part of the calculation by selecting from the inputs of the MiNNLO$_{\rm PS}$ $t\bar{t}$ code `fixedscale 0` and by choosing different values of the parameter `largeptscales`. Moreover, by setting the parameter `whichscale` in the input file such scale setting can be chosen for the powers of the coupling constant of the Born squared amplitude, denoted by $\mu_{\rm R}^{(0)}$ in the equations given in this section. In the phenomenological studies shown below, we use $\mu_{\rm R}^{(0)} = K_{\rm R}\, H_T^{t\bar{t}}/4$ (`whichscale 4`) for the scale of the two Born powers of the strong coupling, while not changing the setting of the other scales (keeping `fixedscale 0` and `largeptscales 0`).

4.4 Top-quark decays and spin correlations

In this section we discuss the inclusion of the top-quark decays and of spin correlations between the decay products. Several event generators can achieve NLO accuracy for top-quark pair production in both production and decay, with the exact inclusion of off-shell (including non-resonant contributions) and spin correlation effects [91, 93–97].

In fixed-order calculations up to NNLO QCD, the inclusion of top-quark decays and spin correlations has been presented in refs. [69, 70] in the narrow-width approximation and in the double-resonant channel only. Including such effects at this perturbative order in event generators is currently still an open problem. In our study we simply consider the inclusion of off-shell effects and spin correlations for the double-resonant channels at the leading order. This is motivated by the observation that the effect of spin correlations in several important top-decay observables (such as the azimuthal correlation between the two charged leptons in the fully leptonic decay channel) is well described at this perturbative order provided one includes NNLO QCD corrections to the production of the top-quark pair (see e.g. ref. [69]).

Our implementation of the top-quark decays follows the approach of ref. [132] that is already implemented in the generator of ref. [133] for the production of a top-quark pair and a light jet, which we used as a starting point to build the MiNLO$'$ and MiNNLO$_{\rm PS}$ generators presented in this work. In the results presented in the next section we consider top quarks and W bosons to be on-shell, but we give the user the possibility to include off-shell effects according to the same algorithm used in the Powheg-hvq process [90], which we describe in detail in appendix B. In the algorithm described in the articles mentioned above,

[7] A detailed discussion about suitable scale settings in top-quark pair production is reported in refs. [67, 130, 131].

JHEP04(2022)079

solely the double-resonant contributions to the decayed matrix elements are used in the reweighting. This simple procedure includes the top-quark decays at LO in the FJ and FJJ configurations. Since in the limit of small p_{T} the entire decay process factorises from the structure of QCD radiation, this procedure ensures a LO treatment of the top-quark decays (including spin correlations) also at the level of fully inclusive observables (i.e. those related to the final state F). In the remainder of this paper we will refer to this implementation of the top-quark decays as the *native* implementation.

In order to validate the native implementation of the top-quark decays and spin correlations, we have produced corresponding results using the well-tested and well-established MadSpin code [134]. Those results have been obtained by passing on-shell $t\bar{t}$ events at NNLO+PS to MadSpin. While both approaches rely on the same basic concept, their implementation and the choices made may differ in some details. In particular, we have produced MadSpin results where in the decayed matrix elements the top quarks are off-shell. Moreover, MadSpin always includes off-shell effects for the W bosons in the top-quark decays, while in the native implementation they are on-shell when the top-quarks are kept on-shell, as stated above. Therefore, the comparison of the native implementation to the MadSpin results allows us to quantify the differences (and uncertainties) that may be expected from the approximation adopted for the top-quark decays. In particular, such comparison allows us to assess whether those differences, although they are not expected to be described by scale-variation uncertainties, could exceed the quoted perturbative uncertainties.

In figure 1 we show three observables in `setup-leptonic`, i.e. in the fully leptonic top-decay mode, and three observables in `setup-semi-leptonic`, i.e. in the semi-leptonic top-decay mode (see section 5.1 for details on the setup). We compare MiNNLO$_{\mathrm{PS}}$ predictions with the native implementation of the top-quark decays in blue and solid against MiNNLO$_{\mathrm{PS}}$ predictions with the top-quark decays included through MadSpin including off-shell effects in brown and dashed. By and large, both implementations lead to results that are very close, regardless of whether or not off-shell top-quark effects are included, in several instances even barely different disregarding statistical fluctuations. In some cases, like the $p_{T,\ell}$ spectrum, there can be differences ranging up to 10%, which are not unexpected due the different approximations made for the top-quark decays, but in all cases those are fully covered by the quoted scale-uncertainty bands. We have tested a large number of distributions in either of these two top-decay modes, arriving to similar conclusions for all of them.

5 Phenomenological results

In this section, we present phenomenological results for top-quark pair production at NNLO+PS with and without decays of the top quarks. After introducing our setup in section 5.1, we perform a comprehensive comparison against LHC data: in section 5.2 we compare MiNNLO$_{\mathrm{PS}}$ predictions for on-shell top quarks against CMS data extrapolated to the inclusive $t\bar{t}$ phase space. We then continue by considering top-quark decays including spin correlations and we compare novel MiNNLO$_{\mathrm{PS}}$ predictions against data from both ATLAS and CMS in various top-decay channels, including fully leptonic (section 5.3), semi-leptonic (section 5.4) and hadronic (section 5.5) top-quark decays.

JHEP04(2022)079

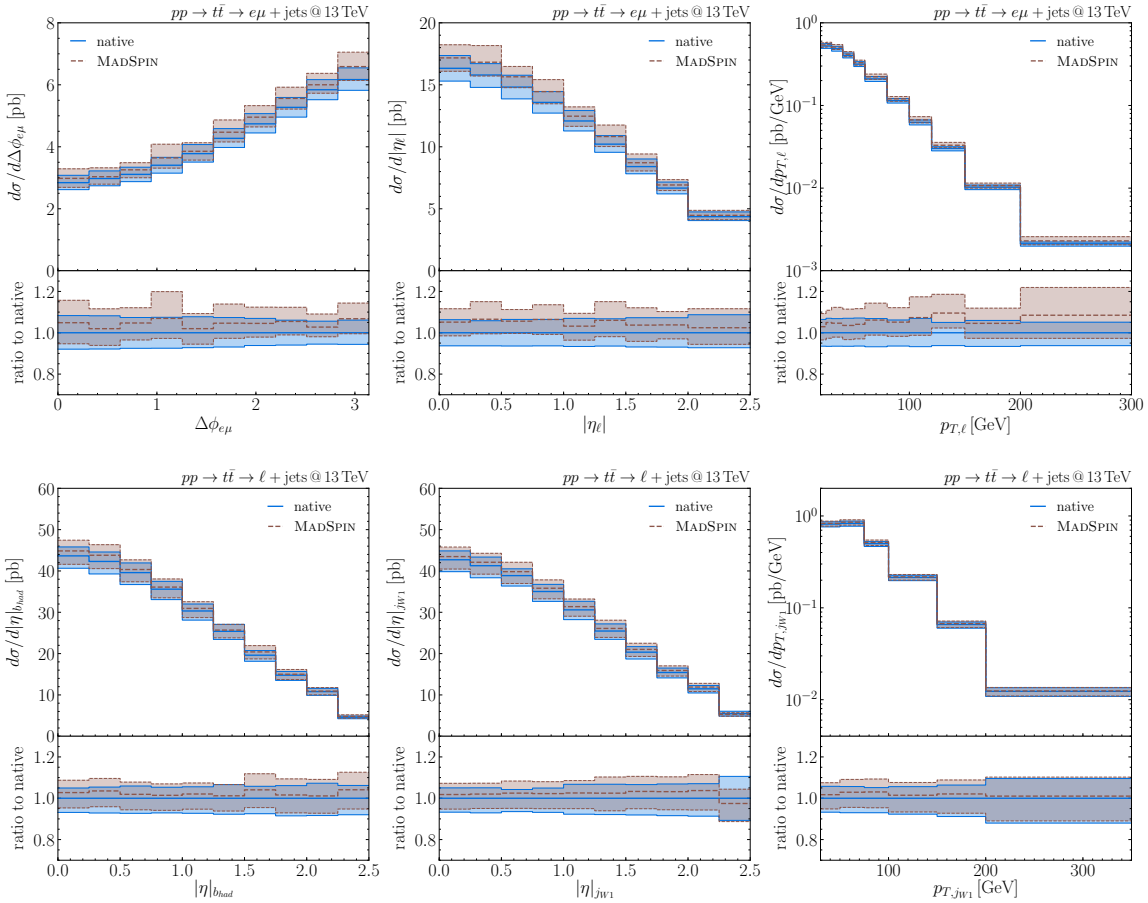

Figure 1. Comparison of MiNNLO$_{\text{PS}}$ predictions with native implementation of the top-quark decays with on-shell top quarks and W bosons (blue, solid) against that of MadSpin with off-shell top quarks and W bosons (brown, dashed) in `setup-leptonic` (upper plots) and `setup-semi-leptonic` (lower plots). See section 5.1 for details on the setup.

5.1 Input parameters and fiducial cuts

We present results for proton-proton collisions at the LHC with a centre-of-mass energy of 13 TeV. The top-quark pole mass is set to $m_t = 173.3\,\text{GeV}$. In the top-quark decays both the top quarks and the W bosons are treated in the narrow-width approximation (see section 4.4 for details), i.e. $\Gamma_t = \Gamma_W = 0\,\text{GeV}$ is used, while assuming branching ratios for each charged lepton $\ell \in \{e, \mu, \tau\}$ of $\text{BR}(t \to b\,\ell\nu_\ell) = 0.108$ and to all quarks $\text{BR}(t \to b\,q\bar{q}') = 0.676$. For the electroweak (EW) parameters, which are relevant for the top-quark decays, we employ the G_μ scheme. Thus, the EW coupling is evaluated as $\alpha_{G_\mu} = \sqrt{2}/\pi G_\mu m_W^2 \sin^2\theta_W$ and the EW mixing angle as $\cos^2\theta_W = m_W^2/m_Z^2$. The EW inputs are set to $G_F = 1.16637 \times 10^{-5}\,\text{GeV}^{-2}$, $m_W = 80.399\,\text{GeV}$, $m_Z = 91.1876\,\text{GeV}$. We consider five massless quark flavours using the corresponding NNLO set of the NNPDF31 [135] with $\alpha_s = 0.118$ via the LHAPDF interface [136] for all our predictions. In MiNLO′ and MiNNLO$_{\text{PS}}$ the PDFs are read by LHAPDF, but their evolution is performed internally through HOPPET [137] together with all convolutions as described in ref. [11].

JHEP04(2022)079

The renormalisation and factorisation scale setting within MiNLO′ and MiNNLOPS has been described in detail in section 4.3. In particular we use eq. (4.19) with $Q_0 = 2\,\text{GeV}$ and $K_\text{R} = K_\text{F} = 1$ for the central scales. To more appropriately describe the momentum transfer in the hard scattering, the renormalisation scale for the two powers of the strong coupling constant entering the Born cross section is set to $\mu_\text{R}^{(0)} = K_\text{R}\, H_T^{t\bar{t}}/4$, with $H_T^{t\bar{t}}$ defined in eq. (4.22). The value of K_R here corresponds to that used for the renormalisation scale within MiNLO′ and MiNNLOPS in eq. (4.19) with $m_{Q\bar{Q}} = m_{t\bar{t}}$, so that the scale within all strong couplings is varied simultaneously. The scale of the modified logarithm in eq. (4.15) that turns off the resummation effects in phase-space regions characterised by large transverse momentum of the top-quark pair is set to $Q = m_{t\bar{t}}/2$. In our phenomenological study we also compare to fixed-order NNLO results (obtained from the implementation of refs. [66, 67] within the Matrix framework [138]), where the scales are set correspondingly as $\mu_\text{R} = K_\text{R}\, m_{t\bar{t}}$, $\mu_\text{F} = K_\text{F}\, m_{t\bar{t}}$, and $\mu_\text{R}^{(0)} = K_\text{R}\, H_T^{t\bar{t}}/4$. Scale uncertainties in all cases are estimated by varying K_R and K_F by a factor of two in each direction, while keeping the minimal and maximal values within the constraint $1/2 \leq K_\text{R}/K_\text{F} \leq 2$.

All showered results have been obtained with Pythia8 [108] with the Monash 2013 tune [139] (specifically `py8tune 14` in the input card) and using the dipole recoil prescription (specifically `SpaceShower:dipoleRecoil = 1` setting of Pythia8). For the inclusive $t\bar{t}$ results, where no top-quark decay is included, we have kept the shower purely at parton level turning off all additional effects. By contrast, for the fiducial results in the phase-space of the top-quark decay products we have included hadronisation, multi-parton interactions as well as QED showering effects. For the final states where these effects are particularly important, like the fully hadronic top-decay mode, we have checked explicitly that using a different tune, in particular the A14 ATLAS tune [140] (specifically `py8tune 21` in the input card), leads to very similar results.

We have considered various setups of fiducial cuts for the different decay modes of the top quarks. For brevity, we simply refer to the relevant experimental studies, where the respective fiducial cuts have been specified in detail. In particular, we show results for a fully inclusive setup in the $t\bar{t}$ phase space of the on-shell top quarks that is dubbed `setup-inclusive` from now on, for the fully leptonic setup of ref. [46] dubbed `setup-leptonic`, for the semi-leptonic setup of ref. [53] dubbed `setup-semi-leptonic`, and for the hadronic setup of ref. [48] dubbed `setup-hadronic`.

5.2 Comparison to data extrapolated to the inclusive $t\bar{t}$ phase space

We start our presentation of phenomenological results by considering distributions in the inclusive $t\bar{t}$ phase space. In figure 2 we show MiNNLOPS (blue, solid), MiNLO′ (black, dotted) and fixed-order NNLO (red, dashed) predictions compared to data from CMS [53] (black points with errors) that has been extrapolated from semi-leptonic top-quark decays to the inclusive $t\bar{t}$ phase space. The first five distributions shown in that figure, which include the rapidity ($y_{t\bar{t}}$), invariant mass ($m_{t\bar{t}}$), and transverse-momentum ($p_{T,t\bar{t}}$) of the $t\bar{t}$ system as well as the rapidity (y_{t_lep}) and transverse momentum (p_{T,t_lep}) of the leptonically decaying top quark, have been considered already in our original publication in ref. [41]. We update that comparison here using the newest settings, in terms of scales etc., considered in this paper.

JHEP04(2022)079

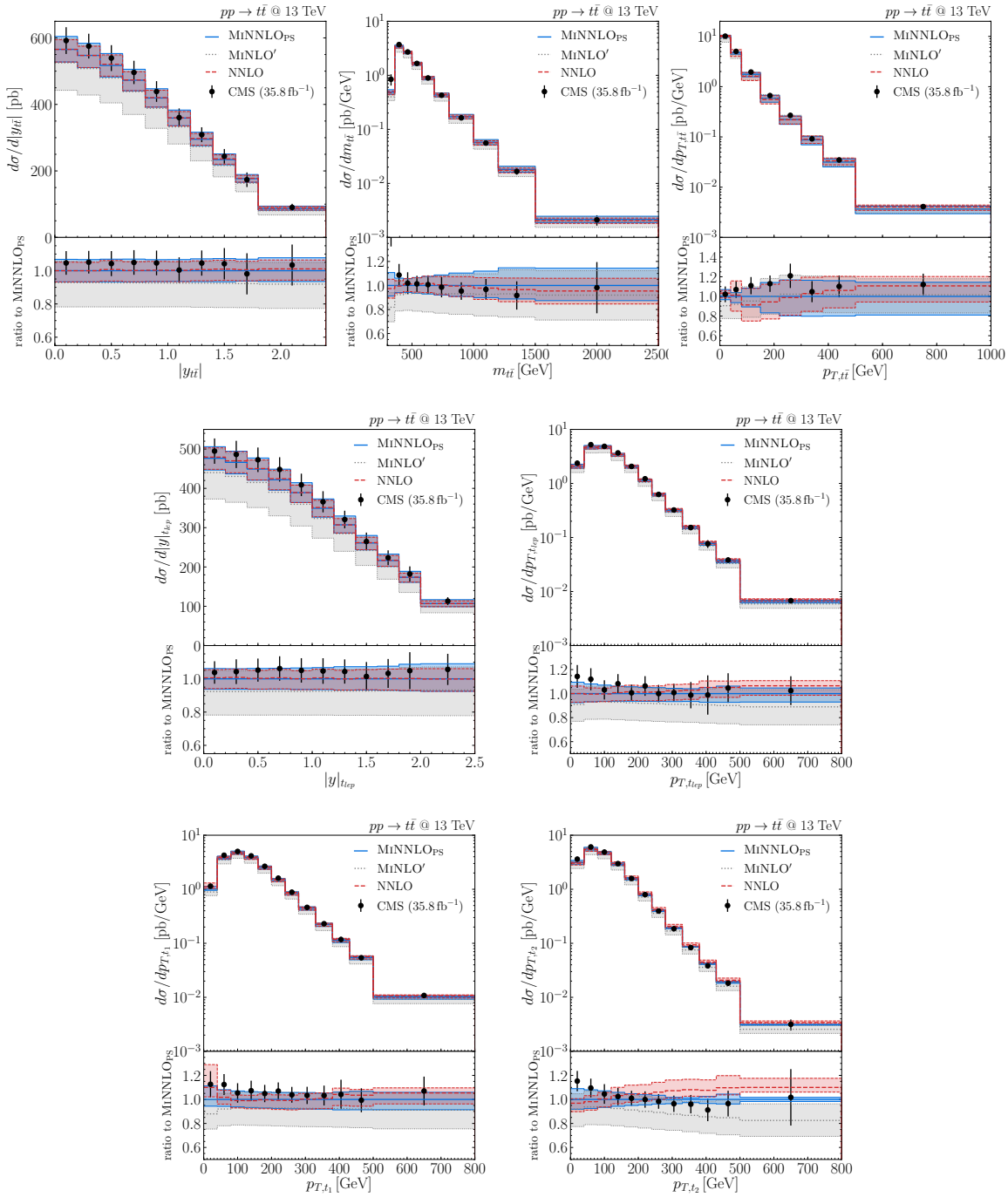

Figure 2. Comparison of MiNNLO$_{\rm PS}$ (blue, solid), MiNLO′ (black, dashed), and NNLO QCD (red, dashed) predictions with CMS data [53] (black points with errors) in `setup-inclusive`.

JHEP04(2022)079

We find excellent agreement between MiNNLO$_{\rm PS}$ and fixed-order NNLO predictions for the rapidity distributions, both for the central predictions and for the scale-uncertainty bands. For the other kinematical distributions some differences between MiNNLO$_{\rm PS}$ and NNLO results can be observed, especially in terms of shape, which however are largely covered by the respective scale uncertainties. With respect to MiNLO$'$ the MiNNLO$_{\rm PS}$ corrections lead to a significant increase at the level of +10% and a substantial reduction of the scale uncertainties by more than a factor of two. The agreement of MiNNLO$_{\rm PS}$ predictions with data is quite remarkable. Only in the very first bin of the $m_{t\bar{t}}$ distribution the data deviates beyond the quoted uncertainties from the MiNNLO$_{\rm PS}$ result. Indeed, the $m_{t\bar{t}}$ region close to the $2\,m_t$ threshold is strongly affected by finite width effects of the top quarks, which are not included due to the on-shell approximation of the top quarks that is employed here. Moreover, non-relativistic effects [84–86] and QED corrections through multiple-photon radiation play an important role at $m_{t\bar{t}}$ values around the $2\,m_t$ threshold, which have to be accounted for at the level of the leptonic final states and not for the inclusive $t\bar{t}$ final state. This clearly shows that such extrapolations come with various uncertainties and why comparisons in the fiducial phase space of the top-quark decay products are advantageous. Finally, it is interesting to notice that for the shape of the $p_{T,t\bar{t}}$ distribution we observe a better description of the data for MiNNLO$_{\rm PS}$ than at fixed-order NNLO. This is not unexpected since the fixed-order result suffers from large logarithmic contributions in the limit $p_{T,t\bar{t}} \to 0$, which are resummed by the parton shower in the MiNNLO$_{\rm PS}$ calculation. We observe that the last $p_{T,t\bar{t}}$ bin shows a mild difference between MiNNLO$_{\rm PS}$ and the NNLO result. We have verified that this difference is entirely due to the effect of the parton shower that, because of the large momentum transfer in the hard process, can radiate at moderately large transverse momentum scales, hence still having an impact around $p_{T,t\bar{t}} \sim 500\,\text{GeV}$.

The last two observables in figure 2, namely the transverse momentum of the leading (p_{T,t_1}) and subleading (p_{T,t_2}) top quark, have not been shown in ref. [41]. These are actually quite interesting as both are somewhat pathological at fixed order [67, 141]: the first distribution is affected by large logarithmic contributions at small p_{T,t_1}, while the second one is affected by large logarithmic contributions for $p_{T,t_2} \gtrsim m_t$, due to their sensitivity to soft-gluon emissions. Therefore, the matching to the parton shower becomes particularly important. We observe that the shapes of the p_{T,t_1} distribution are only slightly different between MiNNLO$_{\rm PS}$ and fixed-order NNLO predictions and both results are in agreement with the experimental data within uncertainties. By contrast, substantial shape effects can be observed for the p_{T,t_2} distribution when comparing the MiNNLO$_{\rm PS}$ and fixed-order NNLO curves. Here, the parton-shower matched MiNNLO$_{\rm PS}$ prediction yields a substantially improved description of the data. This is not unexpected for the reasons discussed before and shows once more the relevance of matching with the parton shower.

5.3 Comparison to data in the fully leptonic top-decay mode

We continue by considering MiNNLO$_{\rm PS}$ predictions in comparison to data for various distributions in the phase space of the top-decay products. For simplicity, we only show the MiNLO$'$ results as a reference prediction in the following.

JHEP04(2022)079

We start with the decay channel where both top quarks decay leptonically, requiring one electron and one muon in the final signature. Figure 3 shows a selection of various distributions that have been measured by ATLAS at 13 TeV in ref. [46] (black points with errors) in comparison to MiNNLO$_{\rm PS}$ (blue, solid) and MiNLO$'$ (black, dotted) predictions. In the results considered here, the electrons and muons may also stem from top-quark decays to τ leptons and their subsequent leptonic decays. Corresponding plots for all other observables considered in the measurement of ref. [46] with and without τ decays to electrons and muons can be found in appendix C.1 and appendix C.2, respectively.

The first two observables in figure 3 are the transverse-momentum spectrum of the two leptons ($p_{T,\ell}$), binned at each event for both the electron and the muon, and the invariant mass of the electron-muon pair ($m_{e\mu}$). We find good agreement within the respective uncertainties between MiNNLO$_{\rm PS}$ predictions and data in all bins of the $p_{T,\ell}$ distribution. In particular the $p_{T,\ell}$ shape is very well described, while there is a slight off-set in the normalisation, with all data points being at the upper edge of the MiNNLO$_{\rm PS}$ uncertainty band. This is not unexpected, as the MiNNLO$_{\rm PS}$ predictions do not include corrections beyond NNLO+PS, such as the additional resummation of threshold logarithms [88], that may slightly increase the normalisation. Also for the $m_{e\mu}$ distribution we find that MiNNLO$_{\rm PS}$ predictions describe the data well, with larger differences only in the first two bins in $m_{e\mu}$. These differences can be traced back to two possible effects missing here. The first one is that the top-quarks are treated in the on-shell approximation. Since this leads to an underestimate of the cross section for $m_{t\bar{t}} \gtrsim 2\, m_t$, as observed in the previous section, this might induce an effect also at low $m_{e\mu}$. Moreover, in this region QED/EW corrections through multiple photon emissions are relevant. While we include those through the QED shower, the approximation of the QED shower might not yield a complete description of such effects.

The lower two plots in figure 3 show double differential distributions. In particular the rapidity of the two leptons (η_ℓ), binned each event for both the electron and the muon, and the azimuthal difference between the electron and the muon ($\Delta\phi_{e\mu}$) are shown in slices of $m_{e\mu}$ in the following order: inclusive, $m_{e\mu} < 80\,\text{GeV}$, $80\,\text{GeV} < m_{e\mu} < 120\,\text{GeV}$, $120\,\text{GeV} < m_{e\mu} < 200\,\text{GeV}$, and $200\,\text{GeV} < m_{e\mu} < 500\,\text{GeV}$. For the η_ℓ distribution we observe a rather similar agreement between MiNNLO$_{\rm PS}$ predictions and data as for the $p_{T,\ell}$ distribution: the shapes are described very well and the data is at the upper edge of the uncertainty band, but overall still compatible. The same is found inclusively and in essentially all bins of $m_{e\mu}$. For $m_{e\mu} < 80\,\text{GeV}$ the differences become slightly larger at forward rapidities, which could have the same origin as the difference observed at low $m_{e\mu}$. What is interesting to observe from the main frame is the fact that for the bins with larger $m_{e\mu}$ the leptons become successively more forward. In fact in the highest $m_{e\mu}$ bin there is even a small dip at central rapidity.

The $\Delta\phi_{e\mu}$ distribution is quite an important observable, as it is directly sensitive to spin correlations in the top-quark decays. It therefore allows us to test our implementation in comparison to data. By and large, we find good agreement in $\Delta\phi_{e\mu}$ between MiNNLO$_{\rm PS}$ predictions and data in all slices of $m_{e\mu}$. Only in the region where the electron and the muon are close in the azimuthal angle slight differences in shape appear. Nevertheless, given

JHEP04(2022)079

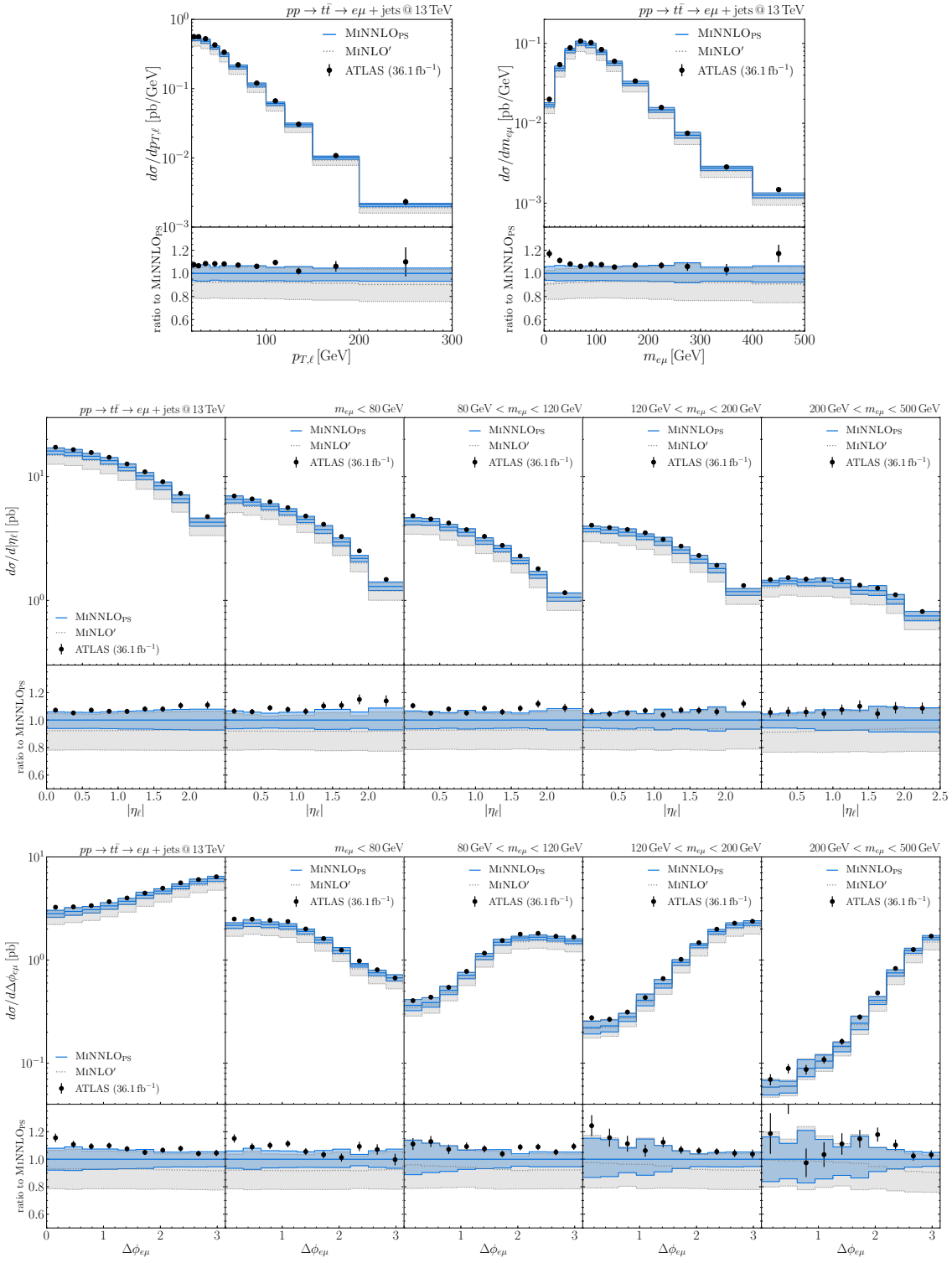

Figure 3. Comparison of MiNNLO$_{\text{PS}}$ (blue, solid) and MiNLO′ (black, dashed) predictions with ATLAS data [46] (black points with errors) in `setup-leptonic`, including decays of τ leptons.

JHEP04(2022)079

the fact that spin correlations in the top-quark decays have been included only through an approximation at tree-level, the observed agreement is quite remarkable. Another interesting feature can be observed in the main frame of the $\Delta\phi_{e\mu}$ distributions. For $m_{e\mu} < 80\text{GeV}$ the shape of the distribution is reversed with respect to the other slices in $m_{e\mu}$. This feature can be understood by pure kinematic considerations. The peak of the invariant mass distribution of the pair is at about 90 GeV (top right plot of figure 3). The inclusive distribution (bottom left plot) favours configurations where the two leptons are back to back. Instead, as one requires the invariant mass to be smaller, one forces the leptons to be closer in angle. When the invariant mass is large, then once again the favoured kinematics is the one where the two leptons are back to back.

For all observables in figure 3 we find that the corrections induced by MiNNLO$_{\text{PS}}$ with respect to MiNLO$'$ are at the order of 10% and generally quite flat in phase space. The only case where some differences in shape between MiNNLO$_{\text{PS}}$ and MiNLO$'$ can be appreciated are the $\Delta\phi_{e\mu}$ distributions at high $m_{e\mu}$. As far as scale uncertainties are concerned, the MiNNLO$_{\text{PS}}$ predictions feature significantly smaller uncertainty bands than those of MiNLO$'$, with a reduction of roughly a factor of two. We remark again that we have considered a large number of observables, comparing MiNNLO$_{\text{PS}}$, MiNLO$'$ and ATLAS data in `setup-leptonic`, and similar conclusions as those pointed out for the distributions shown in this section are found for all of them, as the reader can appreciate from the additional figures in appendix C.1 and appendix C.2.

5.4 Comparison to data in the semi-leptonic top-decay mode

We now turn to results for semi-leptonic top-quark decays, where one of the W bosons stemming from the top quark decays to leptons and the other to hadrons. Figure 4 shows a selection of various distributions measured by CMS at 13 TeV in ref. [53] (black points with errors) compared to MiNNLO$_{\text{PS}}$ (blue, solid) and MiNLO$'$ (black, dotted) predictions. Other distributions measured in this analysis can be found in appendix C.3.

We start with the rapidity ($y_{t\bar{t}}$), invariant mass ($m_{t\bar{t}}$), and transverse momentum ($p_{T,t\bar{t}}$) distributions of the two reconstructed top quarks. As for the corresponding distributions extrapolated to the inclusive $t\bar{t}$ phase space studied in figure 2 of section 5.2, the agreement with data is very good for the MiNNLO$_{\text{PS}}$ predictions, with none of the data points deviating beyond the quoted uncertainties. It is interesting to notice that, contrary to figure 2, also the first bin in the $m_{t\bar{t}}$ distribution is well described by MiNNLO$_{\text{PS}}$. This indicates that QED effects on the leptonic final states included through the QED shower here, which could not be applied in section 5.2, may indeed be important in that region. Moreover, this shows the importance of performing such comparison directly in the fiducial phase space of the top-quark decay products. Note, however, that there is still a slight difference in terms of shape between the MiNNLO$_{\text{PS}}$ curve and the data points at low $m_{t\bar{t}}$ that is likely due to the missing finite width effects in the applied on-shell approximation of the top quarks.

The other plots shown in figure 4 are the rapidity and transverse-momentum distributions of the leading jet coming from the hadronic W decay ($\eta_{j_{W1}}$ and $p_{T,j_{W1}}$), of the bottom-flavoured jet coming from the hadronically decaying top quark ($\eta_{b_{\text{had}}}$ and $p_{T,b_{\text{had}}}$)

JHEP04(2022)079

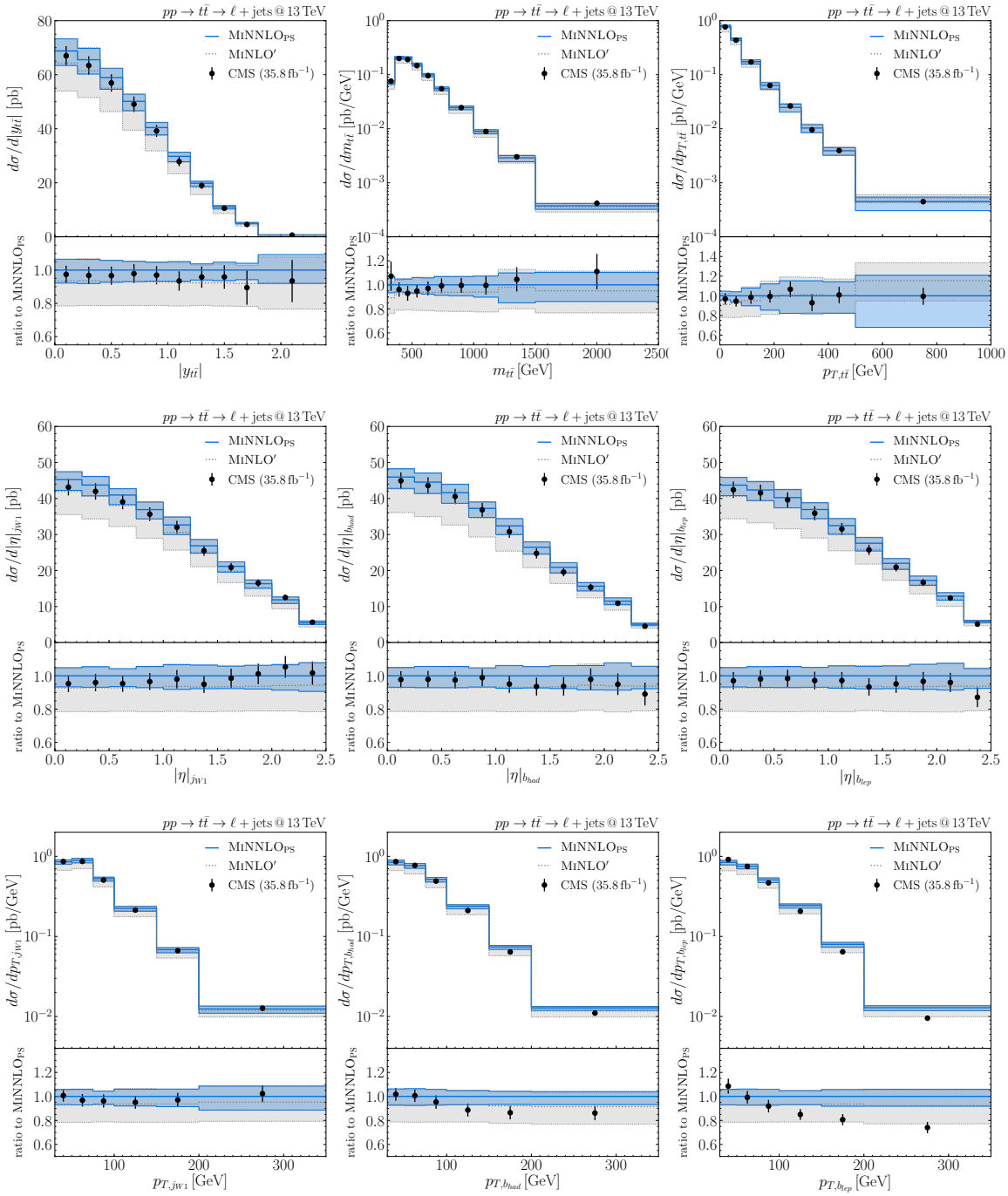

Figure 4. Comparison of MiNNLO$_{\text{PS}}$ (blue, solid) and MiNLO′ (black, dashed) predictions with CMS data [53] (black points with errors) in `setup-semi-leptonic`.

JHEP04(2022)079

and of the bottom-flavoured jet coming from the leptonically decaying top quark ($\eta_{b_{\rm lep}}$ and $p_{T,b_{\rm lep}}$). MiNNLO$_{\rm PS}$ predictions and data agree perfectly for all rapidity distributions, both in terms of shape and in terms of normalisation. As far as the transverse-momentum spectra are concerned, the same level of agreement as for the observables just discussed is found also for $p_{T,j_{W1}}$. Also for the $p_{T,b_{\rm had}}$ distribution MiNNLO$_{\rm PS}$ provides a reasonable description of data with slight shape differences towards large $p_{T,b_{\rm had}}$. Among all the distributions we have considered throughout this paper, it is only $p_{T,b_{\rm lep}}$ that shows a significant deviation of the data with respect to our MiNNLO$_{\rm PS}$ prediction: there is a clear difference in the shape, such that towards large $p_{T,b_{\rm lep}}$ the discrepancy between MiNNLO$_{\rm PS}$ and data increases. Given that the MiNNLO$_{\rm PS}$ prediction describes the measured $p_{T,b_{\rm had}}$ spectrum reasonably well it is surprising that such discrepancy is found for the $p_{T,b_{\rm lep}}$ spectrum, since one would expect the latter actually to be cleaner both in terms of its theoretical modeling and in terms of its measurement. At the moment, we cannot provide any deeper explanation for the observed behaviour and it will be interesting to see whether this trend persists in future measurements in the semi-leptonic top-decay mode.

5.5 Comparison to data in the fully hadronic top-decay mode

Finally, we have also considered the fully hadronic decay mode of the top quarks. In this case the measurements are plagued by relatively large experimental uncertainties due to the substantial QCD backgrounds. In figure 5 we present a selection of various distributions measured by ATLAS at 13 TeV in ref. [48] (black points with errors) compared to MiNNLO$_{\rm PS}$ (blue, solid) and MiNLO$'$ (black, dotted) predictions. Other distributions measured in this analysis can be found in appendix C.4.

The first observable shown in figure 5 is the cross section as a function of the number of jets $N_{\rm jets}$. Since we consider hadronically decaying top quarks only there are already six partons in the tree-level process, including the two bottom quarks. Therefore MiNNLO$_{\rm PS}$ predictions are NNLO+PS accurate for $N_{\rm jets} = 6$, NLO+PS accurate for $N_{\rm jets} = 7$, LO+PS accurate for $N_{\rm jets} = 8$, and all multiplicities $N_{\rm jets} \geq 9$ are described purely by the parton shower. Indeed, the MiNNLO$_{\rm PS}$ scale uncertainties increase towards larger jet multiplicities. Similarly, the corrections induced by MiNNLO$_{\rm PS}$ with respect to MiNLO$'$ and the ensuing reduction of the scale uncertainties become successively more significant for smaller jet multiplicities. Taking into account the decreased accuracy at higher multiplicities, MiNNLO$_{\rm PS}$ is doing a good job in describing the data for the different jet multiplicities. In particular the first NNLO-accurate $N_{\rm jets} = 6$ bin is in excellent agreement.

The second plot in figure 5 shows the distribution in $H_T^{t\bar{t}}$, as defined in eq. (4.22). Since this observables determines our preferred scale choice for $\mu_{\rm R}^{(0)}$, the scale of the two powers of the strong coupling constant entering the Born cross section, it is reassuring to see that the agreement with data for this observable is excellent, both in terms of shape and in terms of normalisation. Moreover, as one can see, the MiNLO$'$ calculation predicts a quite different shape compared to MiNNLO$_{\rm PS}$, leading to a worse agreement in the tail of the $H_T^{t\bar{t}}$ distribution.

The third observable shown in figure 5 is the cross section as a function of the ratio ($R_{W\,t}^{\rm leading}$) of the transverse momentum of the W boson originating from the leading top

JHEP04(2022)079

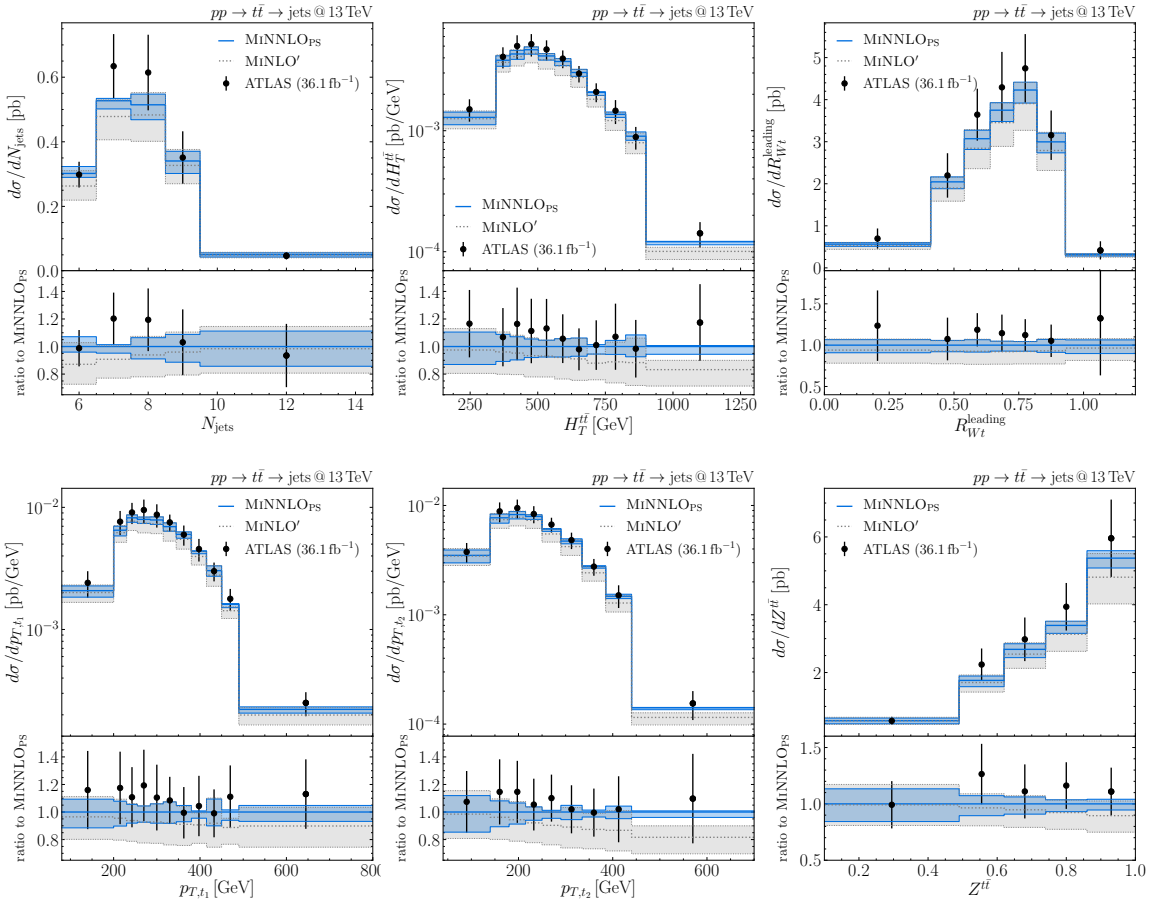

Figure 5. Comparison of MiNNLO$_{\rm PS}$ (blue, solid) and MiNLO′ (black, dashed) predictions with ATLAS data [48] (black points with errors) in `setup-hadronic`.

quark with respect to the transverse momentum of the leading top quark. As can be seen, the cross section peaks around the value where the W boson takes 75% of the top-quark transverse momentum, while it is rather unlikely that the W boson has a transverse momentum which is larger than that of its parent (leading) top quark, or less than half of it. Also here MiNNLO$_{\rm PS}$ predictions are in good agreement with the data. It is reassuring to see especially the shape to be extremely well described, given that the definition of this ratio originates entirely from the hadronic top-quark decays that are included only at tree level in our calculation. In fact, ref. [48] has defined and measured various such ratios and we have found our MiNNLO$_{\rm PS}$ predictions to be in excellent agreement with the data in all cases, as can be seen from the additional observables provided in appendix C.4.

The last three observables in figure 5 concern the transverse momenta of the top quarks. More precisely the one of the leading (p_{T,t_1}) and the subleading (p_{T,t_2}) top quark is shown as well as the ratio of the latter to the former ($Z^{t\bar{t}} = p_{T,t_2}/p_{T,t_1}$). As discussed before, these observables cannot be described appropriately by fixed-order calculations as they are subject to large logarithmic corrections due to soft-gluon effects. By contrast, our MiNNLO$_{\rm PS}$

JHEP04(2022)079

calculation is perfectly able to describe the shapes and normalisation of all three measured distributions in all bins within the quoted uncertainties. In particular for p_{T,t_2} we find that the agreement is better than compared to the MiNLO′ result, which features quite a different shape than MiNNLO$_{\rm PS}$ towards large p_{T,t_2}. The distribution in $Z^{t\bar{t}}$ peaks around one, which is not unexpected since the top quarks are back-to-back at LO. The distribution for $Z^{t\bar{t}} < 1$ is filled only upon inclusion of addition real QCD emissions starting from NLO, which is also indicated by the enlarged uncertainties towards small $Z^{t\bar{t}}$.

6 Summary

The experimental precision of LHC measurements is challenging the accuracy of theoretical predictions, which need to keep up with the steadily decreasing uncertainties of the measured observables. In this context, the accuracy of full-fledged Monte Carlo event generation tools is particularly important, and it becomes indispensable to advance the description of LHC interactions through the inclusion of perturbative information at highest-possible order.

In this paper, we have presented a novel formulation of the MiNNLO$_{\rm PS}$ method to achieve the matching of NNLO QCD corrections to parton showers for processes with a pair of heavy quarks in the final state. The goal was to keep the various positive features of the MiNNLO$_{\rm PS}$ approach, while making it applicable to a new class of collider processes. In particular, MiNNLO$_{\rm PS}$ preserves the (LL) accuracy of any parton shower ordered in the transverse momentum, it does not introduce any new scale or slicing parameter to separate between different jet multiplicities, and it directly includes the NNLO corrections on-the-fly in the event generation. The latter two render the implementation particularly efficient as no large (non-local) cancellations appear and no post-processing of the events is required.

The new formulation of MiNNLO$_{\rm PS}$ for a heavy quark pair is based on the observation that the transverse-momentum resummation formula of the pair, despite being considerably more complicated, can be rewritten in a form very similar to that for a colour singlet to the accuracy we are interested in. After achieving this, the NNLO matching to the parton shower can be obtained with steps analogous to those of the MiNNLO$_{\rm PS}$ procedure for colour singlets. A detailed derivation of the final matching formula has been provided and all technical and computational aspects have been discussed, including the renormalisation, factorisation and resummation scale dependence, introduction of a new modified logarithm and its profiling, as well as the respective scale settings.

We have applied the formalism to the production of a top-quark pair, one of the most relevant and best studied processes at LHC. The decay of the (on-shell) top-quarks has been consistently included via the tree-level amplitudes, fully accounting for spin correlations of the top quarks and W bosons in the decay chain. A comprehensive phenomenological study of our MiNNLO$_{\rm PS}$ predictions has been performed in comparison to a fixed-order NNLO calculation for on-shell top-quark pair production without decay, to our less accurate MiNLO′ results, and to experimental data in all relevant top-decay modes. For the case of on-shell top-quarks without their decays we found excellent agreement of MiNNLO$_{\rm PS}$ for fully inclusive observables with the fixed-order NNLO predictions, while observables sensitive to soft-gluon effects demonstrated the advantages of the MiNNLO$_{\rm PS}$ matching to

JHEP04(2022)079

the parton shower, with (the expected) improved agreement with data (extrapolated to the inclusive $t\bar{t}$ phase space) compared to fixed order. When comparing to less accurate MiNLO′ results we find that the MiNNLO$_{\rm PS}$ procedure induces corrections of typically $\mathcal{O}(+10\%)$ that are generally, but for a few exceptions, quite flat in phase space, as well as substantially smaller scale uncertainties, typically by a factor of two or more. We note that also the MiNLO′ prediction stems from a genuinely new calculation emerging from the developed formalism. Compared to standard NLO+PS calculations the improvements can be expected to be even more prominent.

As far as the top-quark decays are concerned, we have compared two different approaches to include the tree-level decays of the top quarks, both through the native implementation in the $t\bar{t}$+jet calculation and through MadSpin. We have shown the ensuing results to be in good agreement, fully covered by the residual scale uncertainties. We have then considered a significant number of observables in the leptonic, semi-leptonic and hadronic top-decay modes using the native implementation and compared MiNNLO$_{\rm PS}$ predictions with LHC data. Additional results were reported in the appendices. In conclusion, MiNNLO$_{\rm PS}$ describes data in all three top-decay modes remarkably well, also for observables sensitive to the top-quark decays and the respective spin correlations. Among all results we have found tension with data only in a single observable, namely for the transverse-momentum spectrum of the bottom-flavoured jet from the leptonically decaying top quark in the semi-leptonic top decay mode, whose source we can not identify at the moment.

We reckon that this calculation will be very useful especially for the experimental analyses based on top-quark final states at the LHC. Our MiNNLO$_{\rm PS}$ $t\bar{t}$ generator is implemented in the Powheg-Box-V2 framework. It is publicly available and can be downloaded within Powheg-Box-V2 as any standard (NLO+PS) process as instructed on the corresponding webpage http://powhegbox.mib.infn.it/.

Acknowledgments

We are grateful to Simone Amoroso for several fruitful discussions, for help with setting up the top-quark decays through MadSpin, and for his constructive comments on the manuscript. We also would like to thank Rikkert Frederix for help with requiring on-shell top quarks within MadSpin, and Massimiliano Grazzini for comments on the manuscript. This research was supported in part by the National Science Foundation under Grant No. NSF PHY-1748958 in the context of the KITP programme "New Physics from Precision at High Energies". P.N. acknowledges support from Fondazione Cariplo and Regione Lombardia, grant 2017-2070, and from INFN.

JHEP04(2022)079

A Resummation ingredients

We provide here the necessary ingredients for implementing the MiNNLO$_{\rm PS}$ method for top-quark pair production following eq. (3.32), that is, the explicit results for γ_i and $\mathcal{C}_{c\bar{c}}^{[\gamma_i]}$.

Instead of considering γ_i with $i = 1, \ldots, n_c$ we will use the alternative notation $\gamma_{(k,l)}$ with $k, l = 1, \ldots, \sqrt{n_c}$. We will accordingly consider $\mathcal{C}_{c\bar{c}}^{[\gamma_{(k,l)}]}$. Using this notation, we can write the following compact expressions:

$$\gamma_{(k,l)} \equiv \gamma_{(k,l)}^{c\bar{c}} = 2\left[\lambda_k^{c\bar{c}} + (\lambda_l^{c\bar{c}})^*\right], \tag{A.1}$$

$$\mathcal{C}_{c\bar{c}}^{[\gamma_{(k,l)}]} = \bar{\mathbf{C}}_{(l,k)}^{c\bar{c}} \bar{\mathbf{H}}_{(k,l)}^{c\bar{c}}. \tag{A.2}$$

In the above equations, we denoted by $\lambda_k^{c\bar{c}}$ the k-th eigenvalue of the one-loop soft anomalous dimension, working in a colour basis given by the matrix $\mathbf{C}^{c\bar{c}}$ and where the matrix $\mathbf{H}^{c\bar{c}}$ is given by the colour-decomposed LO hard-scattering amplitude. The matrices $\bar{\mathbf{C}}^{c\bar{c}}$ and $\bar{\mathbf{H}}^{c\bar{c}}$ are obtained from $\mathbf{C}^{c\bar{c}}$ and $\mathbf{H}^{c\bar{c}}$ by performing a rotation to the basis in which $\mathbf{\Gamma}_t^{(1)}$ is diagonal.

Explicit results for the colour matrices and eigenvalues needed to compute eqs. (A.1) and (A.2) can be found in ref. [129]. For the sake of completeness, they are given below. The colour matrices $\mathbf{C}^{c\bar{c}}$ for the quark- and gluon-initiated channels can be chosen in the following way,

$$\mathbf{C}^{q\bar{q}} = \frac{C_A}{2}\begin{pmatrix} 2C_A & 0 \\ 0 & C_F \end{pmatrix}, \quad \mathbf{C}^{gg} = C_F \begin{pmatrix} 2C_A^2 & 0 & 0 \\ 0 & C_A^2 & 0 \\ 0 & 0 & C_A^2 - 4 \end{pmatrix}. \tag{A.3}$$

The two eigenvalues of $\mathbf{\Gamma}_t^{(1)}$ in the quark-initiated channel are given by

$$\lambda_1^{q\bar{q}} = \frac{1}{2}\left(C_A(\Gamma_s + \Gamma_t) + \sqrt{C_A^2(\Gamma_t - \Gamma_s)^2 + 4\Gamma_s\Gamma_t}\right) + \Gamma_{\rm I}^{q\bar{q}}, \tag{A.4}$$

$$\lambda_2^{q\bar{q}} = \frac{1}{2}\left(C_A(\Gamma_s + \Gamma_t) - \sqrt{C_A^2(\Gamma_t - \Gamma_s)^2 + 4\Gamma_s\Gamma_t}\right) + \Gamma_{\rm I}^{q\bar{q}}, \tag{A.5}$$

while the three eigenvalues corresponding to the gluon-initiated channel can be written in the following way:

$$\lambda_1^{gg} = \frac{1}{6}\left[X^{1/3} + Y + 2(A_{11} + 2A_{22})\right] + \Gamma_{\rm I}^{gg}, \tag{A.6}$$

$$\lambda_2^{gg} = \frac{1}{12}\left[-X^{1/3} - Y + \sqrt{3}i(X^{1/3} - Y) + 4(A_{11} + 2A_{22})\right] + \Gamma_{\rm I}^{gg}, \tag{A.7}$$

$$\lambda_3^{gg} = \frac{1}{12}\left[-X^{1/3} - Y - \sqrt{3}i(X^{1/3} - Y) + 4(A_{11} + 2A_{22})\right] + \Gamma_{\rm I}^{gg}, \tag{A.8}$$

JHEP04(2022)079

where we have defined the following quantities

$$\Gamma_t = -\frac{1}{4}\ln\left(\frac{p_1\cdot p_3\, p_2\cdot p_4}{p_1\cdot p_4\, p_2\cdot p_3}\right), \tag{A.9}$$

$$\Gamma_s = -\frac{1}{4}\left[\frac{1}{2v}\ln\left(\frac{1+v}{1-v}\right) - i\pi\left(\frac{1}{v}+1\right) - \ln\left(\frac{4p_1\cdot p_4\, p_2\cdot p_3}{s\, m_t^2}\right)\right], \tag{A.10}$$

$$\Gamma_{\rm I}^{q\bar{q}} = -\frac{C_F}{2}\left(1 - \frac{1}{2v}\left[\ln\left(\frac{1+v}{1-v}\right) - 2i\pi\right] - \ln\left(\frac{p_1\cdot p_3\, p_2\cdot p_4}{p_1\cdot p_4\, p_2\cdot p_3}\right)\right), \tag{A.11}$$

$$\Gamma_{\rm I}^{gg} = -\frac{C_F}{2}\left(1 - \frac{1}{2v}\left[\ln\left(\frac{1+v}{1-v}\right) - 2i\pi\right]\right) + \frac{C_A+C_F}{4}\ln\left(\frac{p_1\cdot p_3\, p_2\cdot p_4}{p_1\cdot p_4\, p_2\cdot p_3}\right), \tag{A.12}$$

and the following variables specific to the gluon channel,

$$\begin{aligned} X = {} & -18A_{12}^2(C_A^2-8)(A_{11}-A_{22}) + 8(A_{11}-A_{22})^3, \\ & + \Big\{4(A_{11}-A_{22})^2\left[4(A_{11}-A_{22})^2 - 9A_{12}^2(C_A^2-8)\right]^2, \\ & - \left[4(A_{11}-A_{22})^2 + 3A_{12}^2(C_A^2+4)\right]^3\Big\}^{1/2}, \end{aligned} \tag{A.13}$$

$$Y = \left[4(A_{11}-A_{22})^2 + 3A_{12}^2(C_A^2+4)\right]X^{-1/3}, \tag{A.14}$$

$$A_{11} = \Gamma_t(C_A+C_F), \tag{A.15}$$

$$A_{22} = \Gamma_t(C_F + C_A/2) + \Gamma_s C_A, \tag{A.16}$$

$$A_{12} = -\Gamma_t. \tag{A.17}$$

In the present colour basis, the LO matrix $\mathbf{H}^{c\bar{c}}$ takes the following form

$$\mathbf{H}^{q\bar{q}} = \frac{2}{C_A C_F}\begin{pmatrix}0&0\\0&1\end{pmatrix}, \quad \mathbf{H}^{gg} = \frac{1}{C_F[C_A^2(1+r^2)-2]}\begin{pmatrix}1/C_A^2 & r/C_A & 1/C_A\\ r/C_A & r^2 & r\\ 1/C_A & r & 1\end{pmatrix}, \tag{A.18}$$

with $r = (t-u)/s$. Finally, $\bar{\mathbf{C}}^{c\bar{c}}$ and $\bar{\mathbf{H}}^{c\bar{c}}$ are obtained by applying the following change of basis,

$$\bar{\mathbf{C}}^{c\bar{c}} = (\mathbf{R}^{c\bar{c}})^\dagger \mathbf{C}^{c\bar{c}}\,\mathbf{R}^{c\bar{c}}, \quad \bar{\mathbf{H}}^{c\bar{c}} = (\mathbf{R}^{c\bar{c}})^{-1}\mathbf{H}^{c\bar{c}}\,((\mathbf{R}^{c\bar{c}})^{-1})^\dagger \tag{A.19}$$

where the rotation matrices to go into the basis in which $\mathbf{\Gamma}_t^{(1)}$ is diagonal are given by

$$\mathbf{R}^{q\bar{q}} = \begin{pmatrix}\frac{1}{2\Gamma_t}\left[\lambda_2^{q\bar{q}} - \Gamma_{\rm I}^{q\bar{q}} - 2C_F\Gamma_t\right] & \frac{1}{2\Gamma_t}\left[\lambda_1^{q\bar{q}} - \Gamma_{\rm I}^{q\bar{q}} - 2C_F\Gamma_t\right]\\ 1 & 1\end{pmatrix}, \tag{A.20}$$

for the quark-antiquark channel, and

$$\mathbf{R}^{gg} = \begin{pmatrix}\frac{A_{12}}{\lambda_1^{gg}-\Gamma_{\rm I}^{gg}-A_{11}} & \frac{A_{12}}{\lambda_2^{gg}-\Gamma_{\rm I}^{gg}-A_{11}} & \frac{A_{12}}{\lambda_3^{gg}-\Gamma_{\rm I}^{gg}-A_{11}}\\ 1 & 1 & 1\\ \frac{C_A A_{12}/2}{\lambda_1^{gg}-\Gamma_{\rm I}^{gg}-A_{22}} & \frac{C_A A_{12}/2}{\lambda_2^{gg}-\Gamma_{\rm I}^{gg}-A_{22}} & \frac{C_A A_{12}/2}{\lambda_3^{gg}-\Gamma_{\rm I}^{gg}-A_{22}}\end{pmatrix}, \tag{A.21}$$

for the gluon-initiated channel.

JHEP04(2022)079

B Generation of virtualities in top-quark decays

We now discuss how we generate off-shell effects (when the option `zerowidth 0` is used) in $t\bar{t}$ decays. We stress that more accurate treatments of finite-width effects of the top quarks in generators are available at NLO accuracy [91, 93–97]. In the following, we discuss the implementation of a minimal prescription already adopted in refs. [89, 90] that we use in the context of our MiNNLO$_{\rm PS}$ calculation.

For clarity, in the following we indicate with Q and $\bar{Q}$ the t and $\bar{t}$ quarks. The way the virtualities are chosen will be described later. We start by describing the mapping from the kinematics configurations with on-shell $t\bar{t}$ quarks in the final state to the configuration where the $t\bar{t}$ have virtualities M_Q and $M_{\bar{Q}}$. Quantities before/after the mapping will be written in lower/upper case. We will consider two reference frames: the partonic centre-of-mass (CM) frame (i.e. the rest frame of the incoming partons), denoted with $S_{\rm CM}$, and the centre-of-mass frame of the $Q\bar{Q}$ system denoted by $S_{Q\bar{Q}}$. Frame dependent quantities in the $S_{Q\bar{Q}}$ frame will be accompanied by a prime, to avoid confusion. We proceed as follows:

- We start from the $S_{\rm CM}$ frame. We boost the heavy quark and antiquark system to their rest frame $S_{Q\bar{Q}}$, with the boost velocity

$$\vec{\beta} = -\frac{\vec{p}_Q + \vec{p}_{\bar{Q}}}{p_Q^0 + p_{\bar{Q}}^0}\,, \tag{B.1}$$

  where $p_{Q/\bar{Q}}$ denote the heavy-quark four-momenta, and $\vec{p}_{Q/\bar{Q}}$ and $p^0_{Q/\bar{Q}}$ are their vector components and energies in the $S_{\rm CM}$ frame.

- In the $S_{Q\bar{Q}}$ frame, we change the energy of the quark and antiquark maintaining their three-momenta fixed in such a way that, denoting with $P_{Q/\bar{Q}}$ the four-momenta after the mapping, we have

$$P_Q^2 = M_Q^2, \qquad P_{\bar{Q}}^2 = M_{\bar{Q}}^2, \qquad \vec{P}'_{Q/\bar{Q}} = \vec{p}'_{Q/\bar{Q}}\,, \tag{B.2}$$

  where $M_{Q/\bar{Q}}$ are the generated virtualities of the heavy quarks, which may be different from $m_{Q/\bar{Q}}$, and $\vec{P}'_{Q/\bar{Q}}$ and $\vec{p}'_{Q/\bar{Q}}$ are the three-momenta of the corresponding four-vectors evaluated in the $S_{Q\bar{Q}}$ frame.

- The momenta P_Q and $P_{\bar{Q}}$ are boosted back to the $S_{\rm CM}$ frame with boost velocity

$$\vec{\beta}' = \frac{\vec{p}_Q + \vec{p}_{\bar{Q}}}{\sqrt{(P_Q + P_{\bar{Q}})^2 + (\vec{p}_Q + \vec{p}_{\bar{Q}})^2}}\,. \tag{B.3}$$

  We thus have, in the $S_{\rm CM}$ frame, $\vec{p}_Q + \vec{p}_{\bar{Q}} = \vec{P}_Q + \vec{P}_{\bar{Q}}$, but in general $\vec{p}_{Q/\bar{Q}} \neq \vec{P}_{Q/\bar{Q}}$.

- The four-momenta of any associated light partons are left unchanged by this procedure. Thus, calling $e_{\rm CM}$ and $E_{\rm CM}$ the total initial partonic energy in the $S_{\rm CM}$ frame before and after the mapping procedure, we have

$$E_{\rm CM} = e_{\rm CM} + E_{Q\bar{Q}} - e_{Q\bar{Q}}\,, \tag{B.4}$$

JHEP04(2022)079

while the total three-momentum in the $S_{\rm CM}$ frame remains zero. Thus, the rapidity of the partonic CM frame is not changed by our procedure. Denoting with $x_{1/2}$ and $X_{1/2}$ the incoming parton momentum fractions before and after the mapping, we must have $X_1/X_2 = x_1/x_2$, and

$$X_{1/2} = x_{1/2} \times \frac{E_{\rm CM}}{e_{\rm CM}}\,. \tag{B.5}$$

The above procedure provides the off-shell $t\bar{t}$ kinematics for given virtualities (invariant masses) $M_{Q/\bar{Q}}$ of the top quarks starting from on-shell $t\bar{t}$ momenta. The values of $M_{Q/\bar{Q}}$ for each event are generated according to a Breit-Wigner distribution

$$M^2 = m^2 + \Gamma m \tan\left(\frac{r\pi}{2}\right)\,, \tag{B.6}$$

where r is a random number uniformly distributed between -1 and 1. This formula is used not only to generate $M_{Q/\bar{Q}}$, it is also used to generate the virtualities of the $W^\pm$ bosons M_{W^+/W^-}, using the top and W-boson masses and widths. The generated values are subject to the following restrictions:

- Values of $M^2_{Q/\bar{Q}} < m_W^2$ or $M^2_{Q/\bar{Q}} > 2m_t^2$ are rejected.
- Values of the virtualities that prevent the construction of a consistent decay chain are rejected.

Finally, the weight of the event is multiplied by the following correction factor, accounting for the enlarged off-shell phase space, changed kinematics, PDFs, etc.:

$$\begin{aligned} w_c = {} & \frac{E_{\rm CM}}{e_{\rm CM}} \times \frac{\sqrt{m_Q^2 + |\vec{p}\,'_Q|^2}}{\sqrt{M_Q^2 + |\vec{p}\,'_Q|^2}} \times \frac{\sqrt{m_{\bar{Q}}^2 + |\vec{p}\,'_{\bar{Q}}|^2}}{\sqrt{M_{\bar{Q}}^2 + |\vec{p}\,'_{\bar{Q}}|^2}} \times \frac{e_{Q\bar{Q}} M_{Q\bar{Q}}}{E_{Q\bar{Q}} m_{Q\bar{Q}}} \\ & \times \frac{f_1(X_1)}{f_1(x_1)} \times \frac{f_2(X_2)}{f_2(x_2)} \\ & \times \frac{\frac{|\vec{K}_b|}{M_Q^2}}{\frac{|\vec{k}_b|}{m_Q^2}} \times \frac{\frac{|\vec{K}_{\bar{b}}|}{M_{\bar{Q}}^2}}{\frac{|\vec{k}_{\bar{b}}|}{m_{\bar{Q}}^2}} \times \frac{\frac{|\vec{K}_{l^+}|}{M_{W^+}^2}}{\frac{|\vec{k}_{l^+}|}{m_{W^+}^2}} \times \frac{\frac{|\vec{K}_{l^-}|}{M_{W^-}^2}}{\frac{|\vec{k}_{l^-}|}{m_{W^-}^2}}\,, \end{aligned} \tag{B.7}$$

where $|\vec{p}\,'_Q| = |\vec{p}\,'_{\bar{Q}}|$ by definition, and $\vec{k}$ and $\vec{K}$ denote the three-momentum of a decay product in the *resonance* rest frame (i.e. both for top and W decays). The second line corrects for the fact that the parton luminosities are evaluated at different momentum fractions in the off-shell $t\bar{t}$ kinematics.

JHEP04(2022)079

It is obtained by writing the full phase space as

$$\begin{aligned}\int \mathrm{d}\Phi &= \int \mathrm{d}y_{\mathrm{CM}}\mathrm{d}\tau_X \mathrm{d}^4 P_{Q\bar{Q}}\mathrm{d}\Phi_k \delta^4(X_1 p_1 + X_2 p_2 - P_{Q\bar{Q}} - k) \\ &\quad \times \int \frac{\mathrm{d}^3\vec{P}'_Q}{P^{0\prime}_Q}\frac{\mathrm{d}^3\vec{P}'_{\bar{Q}}}{P^{0\prime}_{\bar{Q}}}\delta^4(P_Q + P_{\bar{Q}} - P_{Q\bar{Q}}) \\ &= \int \mathrm{d}y_{\mathrm{CM}}\mathrm{d}\tau_X \mathrm{d}^3 P_{Q\bar{Q}}\mathrm{d}\Phi_k \delta^3(-\vec{P}_{Q\bar{Q}} - \vec{k})\delta(X_1 p_1^0 + X_2 p_2^0 - P^0_{Q\bar{Q}} - k^0) \\ &\quad \times \mathrm{d}P^0_{Q\bar{Q}}\mathrm{d}M^2_{Q\bar{Q}}\delta(P^2_{Q\bar{Q}} - M^2_{Q\bar{Q}}) \int \frac{\mathrm{d}^3\vec{P}'_Q}{P^{0\prime}_Q P^{0\prime}_{\bar{Q}}}\delta(P'^0_Q + P'^0_{\bar{Q}} - M_{Q\bar{Q}}) \\ &= \int \mathrm{d}y_{\mathrm{CM}}\frac{2\sqrt{\tau_X}\mathrm{d}y_{\mathrm{CM}}}{2E_{\mathrm{beam}}}\mathrm{d}\Phi_k \frac{M_{Q\bar{Q}}}{P^0_{Q\bar{Q}}}\int \frac{\mathrm{d}^3\vec{P}'_Q}{P^{0\prime}_Q P^{0\prime}_{\bar{Q}}}, \end{aligned} \tag{B.8}$$

where all frame-dependent quantities in the outer integral (including $p^0_{1/2}$) are evaluated in the S_{CM} frame, while those in the inner integral are evaluated in the $S_{Q\bar{Q}}$ frame. We have used

$$\begin{aligned} X_1 &= \exp(y_{\mathrm{CM}})\sqrt{\tau_X}\,, & X_2 &= \exp(-y_{\mathrm{CM}})\sqrt{\tau_X}\,, \\ p_1^0 &= E_{\mathrm{beam}}\exp(-y_{\mathrm{CM}})\,, & p_2^0 &= E_{\mathrm{beam}}\exp(y_{\mathrm{CM}})\,, \end{aligned} \tag{B.9}$$

where $\tau_X = X_1 X_2$ and y_{CM} is the rapidity of the partonic CM system. The phase space for the light partons in the final state is represented by $\mathrm{d}\Phi_k$. It is clear that the only difference with respect to the phase space at fixed masses is given by the factor

$$\frac{\sqrt{\tau_X}}{\sqrt{\tau_x}} \times \frac{\frac{M_{Q\bar{Q}}}{P^0_{Q\bar{Q}}}}{\frac{m_{Q\bar{Q}}}{p^0_{Q\bar{Q}}}} \times \frac{\frac{1}{P^{0\prime}_Q P^{0\prime}_{\bar{Q}}}}{\frac{1}{p^{0\prime}_Q p^{0\prime}_{\bar{Q}}}} = \frac{E_{\mathrm{CM}}}{e_{\mathrm{CM}}} \times \frac{p^0_{Q\bar{Q}} M_{Q\bar{Q}}}{P^0_{Q\bar{Q}} m_{Q\bar{Q}}} \times \frac{p^{0\prime}_Q p^{0\prime}_{\bar{Q}}}{P^{0\prime}_Q P^{0\prime}_{\bar{Q}}}\,. \tag{B.10}$$

As far as the correction factors to the resonant decays are concerned, they are included through the third line in eq. (B.7). The phase space together with the normalisation of the width is given by $\frac{|\vec{k}|}{M^2}$. Thus a factor

$$\frac{\frac{|\vec{K}|}{M^2}}{\frac{|\vec{k}|}{m^2}} \tag{B.11}$$

is provided for each decaying resonance.

For the correction factor in eq. (B.7) an upper bound is determined, which is implemented using a standard hit-and-miss technique. In our implementation, the hit-and-miss technique is used for each on-shell event that is produced. Strictly speaking, it would be more correct to regenerate the on-shell event in case of a miss. Whether the improved accuracy would be worth the loss of efficiency is a matter yet to be studied.

C Additional comparisons to data

In this appendix we show the comparison of MiNNLO$_{\mathrm{PS}}$ and MiNLO$'$ predictions to data for additional observables. Since similar comments to those made about the plots shown in the main text generally apply here as well, we refrain from commenting on these results any further.

JHEP04(2022)079

C.1 Fully leptonic top-decay mode including τ decays to electrons/muons

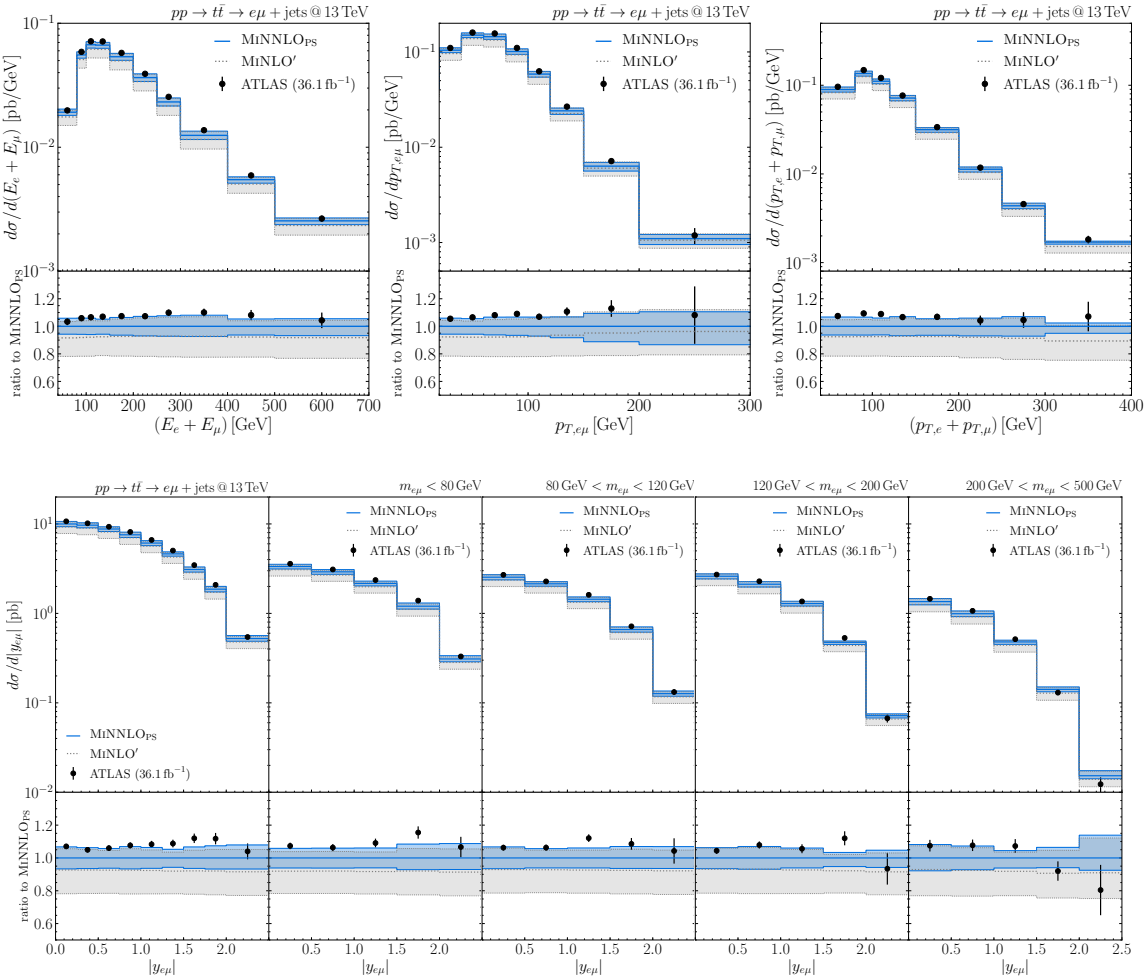

Figure 6. Comparison of MiNNLO$_{\text{PS}}$ (blue, solid) and MiNLO′ (black, dashed) predictions with ATLAS data [46] (black points with errors) in `setup-leptonic`, including decays of τ leptons.

JHEP04(2022)079

C.2 Fully leptonic top-decay mode excluding τ decays to electrons/muons

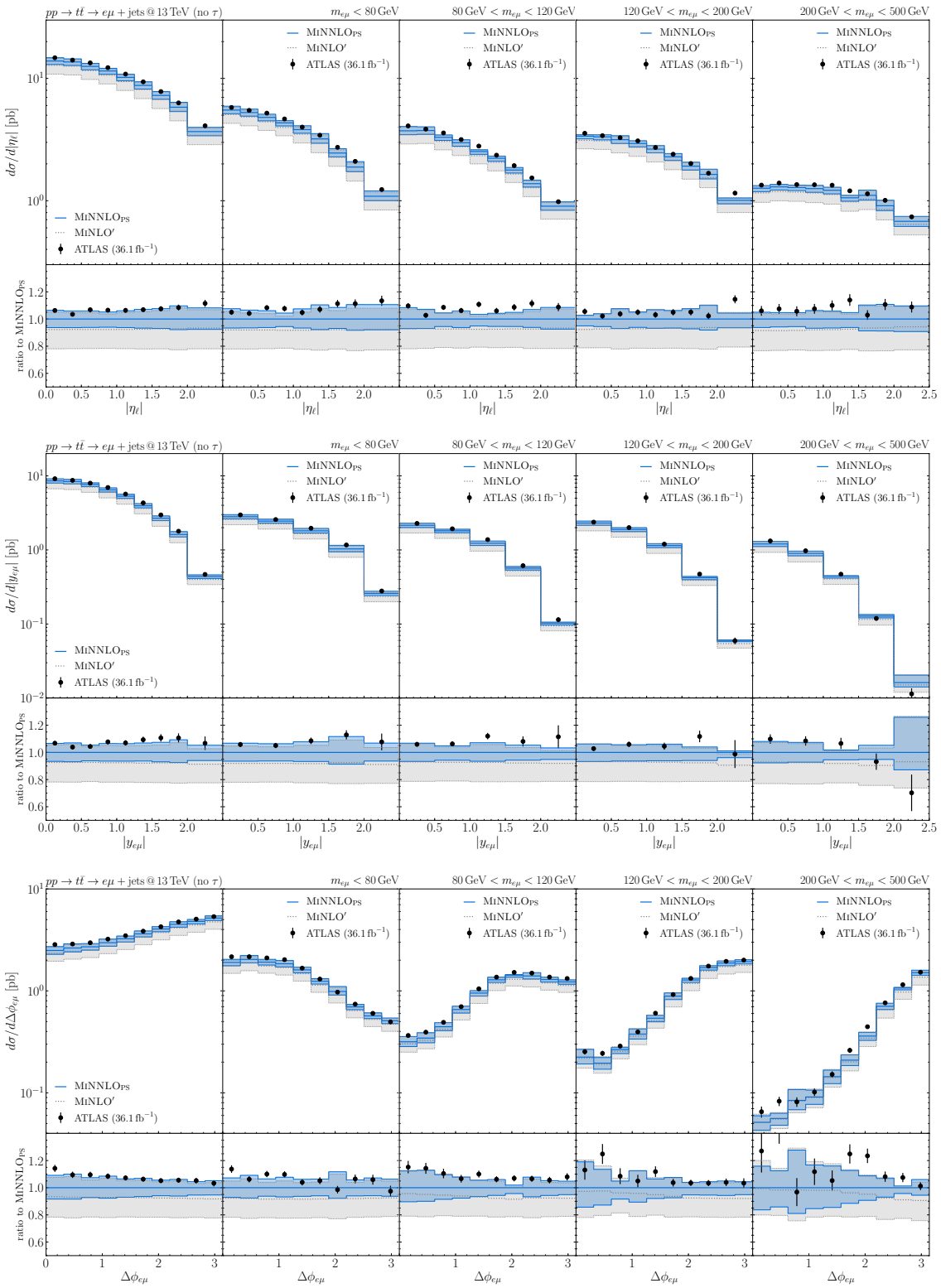

Figure 7. Comparison of MiNNLO$_{\text{PS}}$ (blue, solid) and MiNLO′ (black, dashed) predictions with ATLAS data [46] (black points with errors) in `setup-leptonic`, excluding decays of τ leptons.

JHEP04(2022)079

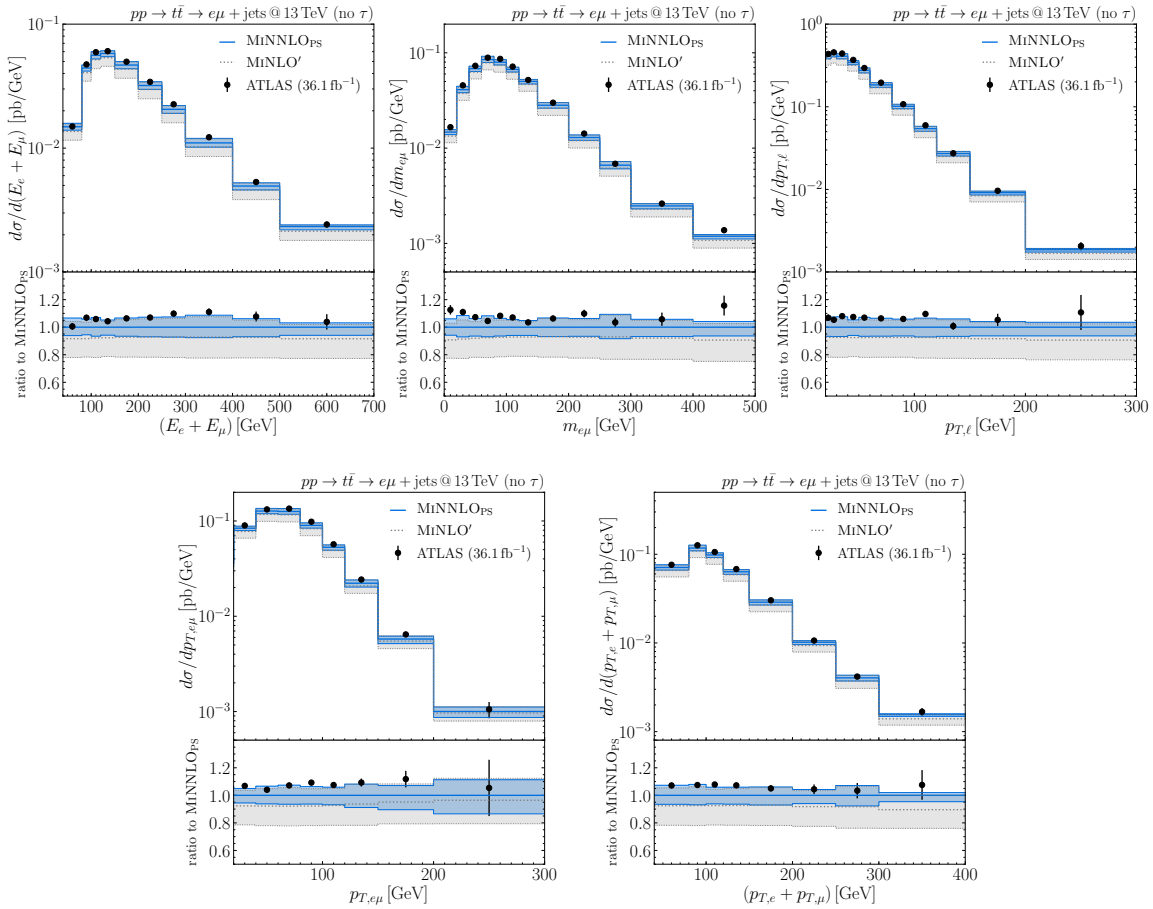

Figure 8. Comparison of MiNNLO$_{\text{PS}}$ (blue, solid) and MiNLO′ (black, dashed) predictions with ATLAS data [46] (black points with errors) in `setup-leptonic`, excluding decays of τ leptons.

JHEP04(2022)079

C.3 Semi-leptonic top-quark decay mode

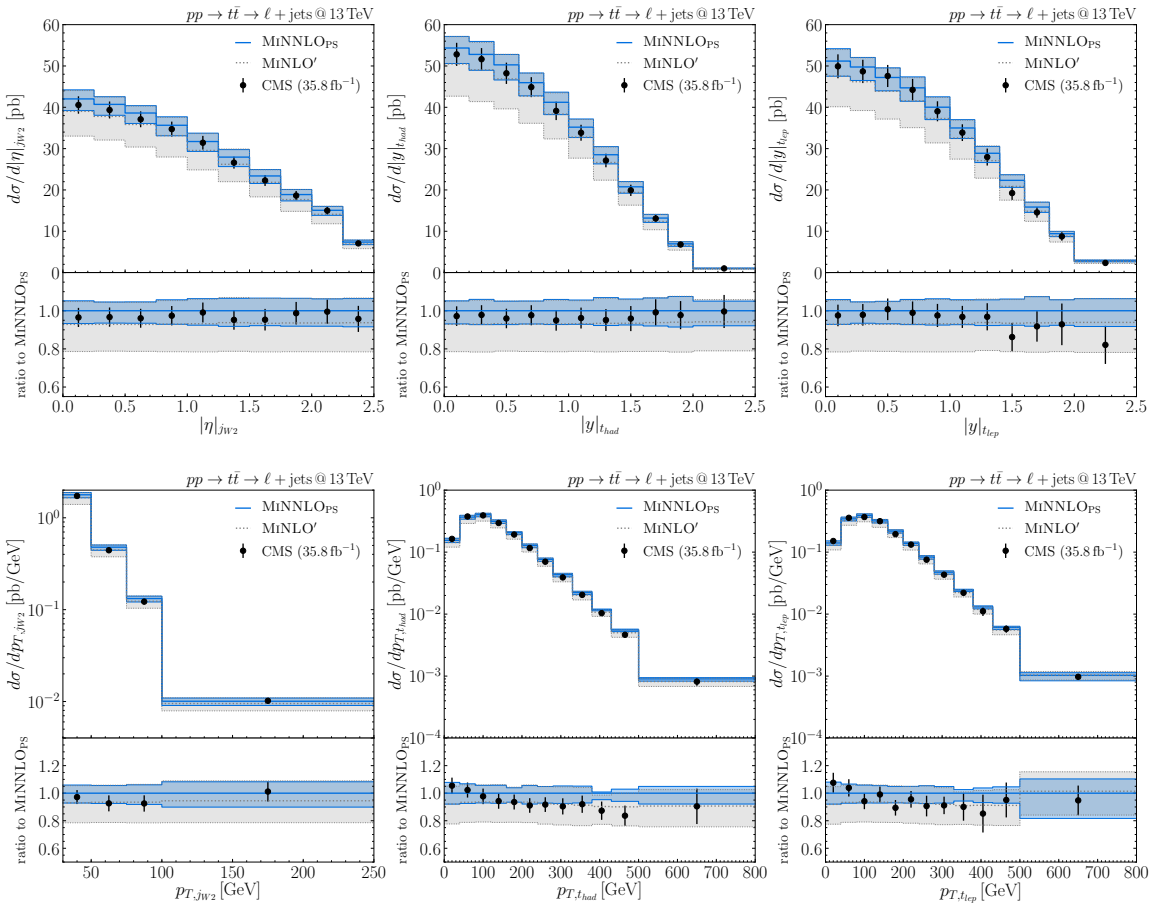

Figure 9. Comparison of MiNNLO$_{\text{PS}}$ (blue, solid) and MiNLO′ (black, dashed) predictions with CMS data [53] (black points with errors) in `setup-semi-leptonic`.

JHEP04(2022)079

C.4 Fully hadronic top-quark decay mode

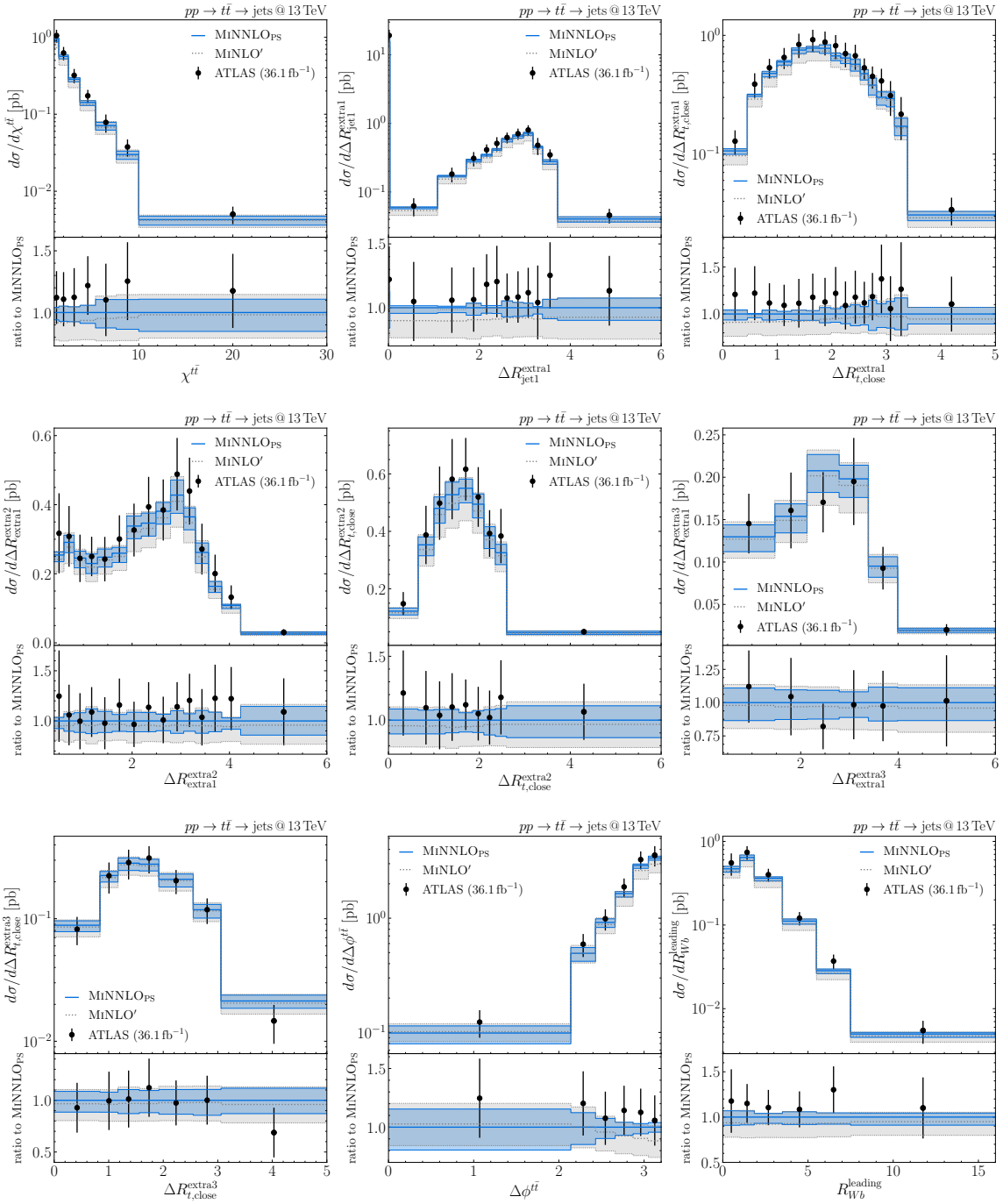

Figure 10. Comparison of MiNNLO$_{\mathrm{PS}}$ (blue, solid) and MiNLO′ (black, dashed) predictions with ATLAS data [48] (black points with errors) in `setup-hadronic`.

JHEP04(2022)079

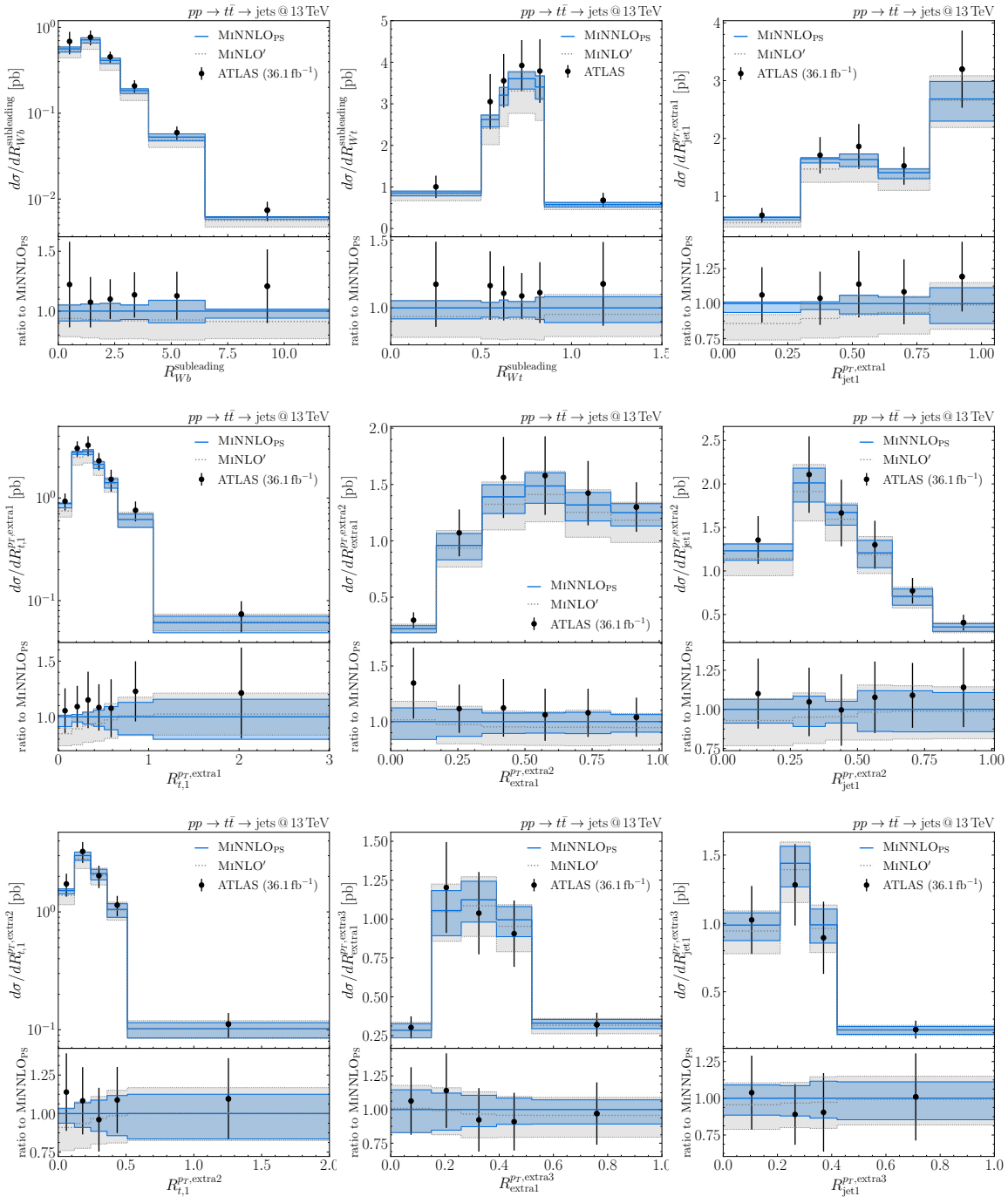

Figure 11. Comparison of MiNNLO$_{\mathrm{PS}}$ (blue, solid) and MiNLO′ (black, dashed) predictions with ATLAS data [48] (black points with errors) in `setup-hadronic`.

JHEP04(2022)079

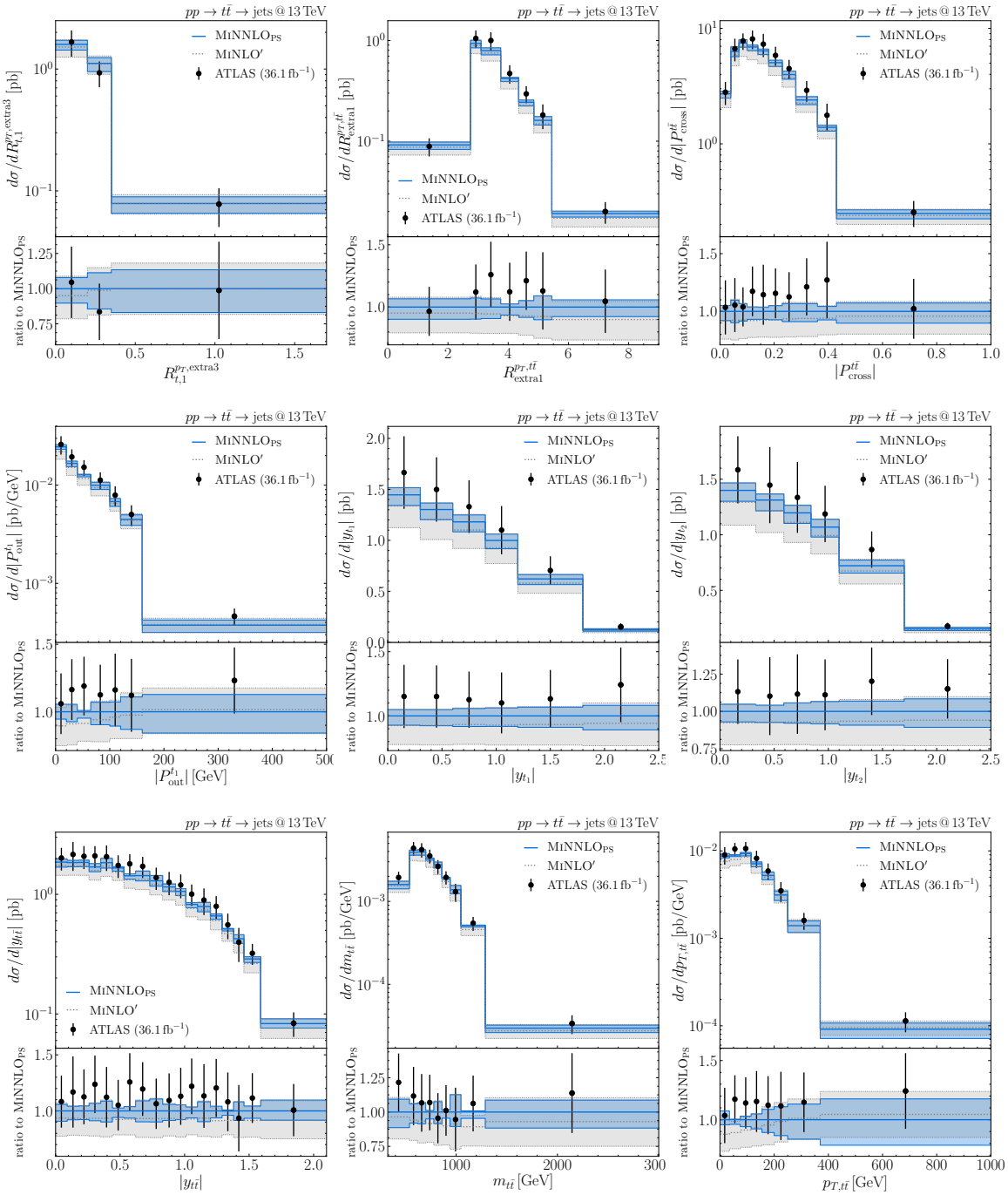

Figure 12. Comparison of MiNNLO$_{\rm PS}$ (blue, solid) and MiNLO′ (black, dashed) predictions with ATLAS data [48] (black points with errors) in `setup-hadronic`.

JHEP04(2022)079

References

[1] S. Frixione and B.R. Webber, *Matching NLO QCD computations and parton shower simulations*, *JHEP* **06** (2002) 029 [hep-ph/0204244] [INSPIRE].

[2] P. Nason, *A New method for combining NLO QCD with shower Monte Carlo algorithms*, *JHEP* **11** (2004) 040 [hep-ph/0409146] [INSPIRE].

[3] S. Jadach, W. Płaczek, S. Sapeta, A. Siódmok and M. Skrzypek, *Matching NLO QCD with parton shower in Monte Carlo scheme — the KrkNLO method*, *JHEP* **10** (2015) 052 [arXiv:1503.06849] [INSPIRE].

[4] P. Nason and G.P. Salam, *Multiplicative-accumulative matching of NLO calculations with parton showers*, *JHEP* **01** (2022) 067 [arXiv:2111.03553] [INSPIRE].

[5] K. Hamilton, P. Nason, C. Oleari and G. Zanderighi, *Merging H/W/Z + 0 and 1 jet at NLO with no merging scale: a path to parton shower + NNLO matching*, *JHEP* **05** (2013) 082 [arXiv:1212.4504] [INSPIRE].

[6] K. Hamilton, P. Nason, E. Re and G. Zanderighi, *NNLOPS simulation of Higgs boson production*, *JHEP* **10** (2013) 222 [arXiv:1309.0017] [INSPIRE].

[7] S. Alioli, C.W. Bauer, C. Berggren, F.J. Tackmann, J.R. Walsh and S. Zuberi, *Matching Fully Differential NNLO Calculations and Parton Showers*, *JHEP* **06** (2014) 089 [arXiv:1311.0286] [INSPIRE].

[8] S. Alioli, C.W. Bauer, C. Berggren, F.J. Tackmann and J.R. Walsh, *Drell-Yan production at NNLL'+NNLO matched to parton showers*, *Phys. Rev. D* **92** (2015) 094020 [arXiv:1508.01475] [INSPIRE].

[9] S. Alioli et al., *Matching NNLO predictions to parton showers using N^3LL color-singlet transverse momentum resummation in geneva*, *Phys. Rev. D* **104** (2021) 094020 [arXiv:2102.08390] [INSPIRE].

[10] S. Höche, Y. Li and S. Prestel, *Drell-Yan lepton pair production at NNLO QCD with parton showers*, *Phys. Rev. D* **91** (2015) 074015 [arXiv:1405.3607] [INSPIRE].

[11] P.F. Monni, P. Nason, E. Re, M. Wiesemann and G. Zanderighi, *MiNNLO$_{PS}$: a new method to match NNLO QCD to parton showers*, *JHEP* **05** (2020) 143 [arXiv:1908.06987] [INSPIRE].

[12] P.F. Monni, E. Re and M. Wiesemann, *MiNNLO$_{PS}$: optimizing $2 \to 1$ hadronic processes*, *Eur. Phys. J. C* **80** (2020) 1075 [arXiv:2006.04133] [INSPIRE].

[13] J.M. Campbell, S. Höche, H.T. Li, C.T. Preuss and P. Skands, *Towards NNLO+PS Matching with Sector Showers*, arXiv:2108.07133 [INSPIRE].

[14] S. Höche, F. Krauss and S. Prestel, *Implementing NLO DGLAP evolution in Parton Showers*, *JHEP* **10** (2017) 093 [arXiv:1705.00982] [INSPIRE].

[15] F. Dulat, S. Höche and S. Prestel, *Leading-Color Fully Differential Two-Loop Soft Corrections to QCD Dipole Showers*, *Phys. Rev. D* **98** (2018) 074013 [arXiv:1805.03757] [INSPIRE].

JHEP04(2022)079

[16] M. Dasgupta, F.A. Dreyer, K. Hamilton, P.F. Monni and G.P. Salam, *Logarithmic accuracy of parton showers: a fixed-order study*, *JHEP* **09** (2018) 033 [*Erratum ibid.* **03** (2020) 083] [arXiv:1805.09327] [INSPIRE].

[17] G. Bewick, S. Ferrario Ravasio, P. Richardson and M.H. Seymour, *Logarithmic accuracy of angular-ordered parton showers*, *JHEP* **04** (2020) 019 [arXiv:1904.11866] [INSPIRE].

[18] M. Dasgupta, F.A. Dreyer, K. Hamilton, P.F. Monni, G.P. Salam and G. Soyez, *Parton showers beyond leading logarithmic accuracy*, *Phys. Rev. Lett.* **125** (2020) 052002 [arXiv:2002.11114] [INSPIRE].

[19] J.R. Forshaw, J. Holguin and S. Plätzer, *Building a consistent parton shower*, *JHEP* **09** (2020) 014 [arXiv:2003.06400] [INSPIRE].

[20] K. Hamilton, R. Medves, G.P. Salam, L. Scyboz and G. Soyez, *Colour and logarithmic accuracy in final-state parton showers*, *JHEP* **03** (2021) 041 [arXiv:2011.10054] [INSPIRE].

[21] L. Gellersen, S. Höche and S. Prestel, *Disentangling soft and collinear effects in QCD parton showers*, arXiv:2110.05964 [INSPIRE].

[22] A. Karlberg, E. Re and G. Zanderighi, *NNLOPS accurate Drell-Yan production*, *JHEP* **09** (2014) 134 [arXiv:1407.2940] [INSPIRE].

[23] R. Frederix and K. Hamilton, *Extending the MINLO method*, *JHEP* **05** (2016) 042 [arXiv:1512.02663] [INSPIRE].

[24] W. Astill, W. Bizon, E. Re and G. Zanderighi, *NNLOPS accurate associated HW production*, *JHEP* **06** (2016) 154 [arXiv:1603.01620] [INSPIRE].

[25] W. Astill, W. Bizoń, E. Re and G. Zanderighi, *NNLOPS accurate associated HZ production with $H \to b\bar{b}$ decay at NLO*, *JHEP* **11** (2018) 157 [arXiv:1804.08141] [INSPIRE].

[26] E. Re, M. Wiesemann and G. Zanderighi, *NNLOPS accurate predictions for W^+W^- production*, *JHEP* **12** (2018) 121 [arXiv:1805.09857] [INSPIRE].

[27] W. Bizoń, E. Re and G. Zanderighi, *NNLOPS description of the $H \to b\bar{b}$ decay with MiNLO*, *JHEP* **06** (2020) 006 [arXiv:1912.09982] [INSPIRE].

[28] S. Alioli, A. Broggio, S. Kallweit, M.A. Lim and L. Rottoli, *Higgsstrahlung at NNLL'+NNLO matched to parton showers in GENEVA*, *Phys. Rev. D* **100** (2019) 096016 [arXiv:1909.02026] [INSPIRE].

[29] S. Alioli et al., *Resummed predictions for hadronic Higgs boson decays*, *JHEP* **04** (2021) 254 [arXiv:2009.13533] [INSPIRE].

[30] S. Alioli et al., *Precise predictions for photon pair production matched to parton showers in GENEVA*, *JHEP* **04** (2021) 041 [arXiv:2010.10498] [INSPIRE].

[31] S. Alioli et al., *Next-to-next-to-leading order event generation for Z boson pair production matched to parton shower*, *Phys. Lett. B* **818** (2021) 136380 [arXiv:2103.01214] [INSPIRE].

[32] T. Cridge, M.A. Lim and R. Nagar, *$W\gamma$ production at NNLO+PS accuracy in Geneva*, *Phys. Lett. B* **826** (2022) 136918 [arXiv:2105.13214] [INSPIRE].

[33] S. Höche, Y. Li and S. Prestel, *Higgs-boson production through gluon fusion at NNLO QCD with parton showers*, *Phys. Rev. D* **90** (2014) 054011 [arXiv:1407.3773] [INSPIRE].

[34] S. Höche, S. Kuttimalai and Y. Li, *Hadronic Final States in DIS at NNLO QCD with Parton Showers*, *Phys. Rev. D* **98** (2018) 114013 [arXiv:1809.04192] [INSPIRE].

JHEP04(2022)079

[35] D. Lombardi, M. Wiesemann and G. Zanderighi, *Advancing MiNNLO$_{PS}$ to diboson processes: $Z\gamma$ production at NNLO+PS*, *JHEP* **06** (2021) 095 [arXiv:2010.10478] [INSPIRE].

[36] D. Lombardi, M. Wiesemann and G. Zanderighi, *W^+W^- production at NNLO+PS with MINNLO$_{PS}$*, *JHEP* **11** (2021) 230 [arXiv:2103.12077] [INSPIRE].

[37] L. Buonocore, G. Koole, D. Lombardi, L. Rottoli, M. Wiesemann and G. Zanderighi, *ZZ production at nNNLO+PS with MiNNLO$_{PS}$*, *JHEP* **01** (2022) 072 [arXiv:2108.05337] [INSPIRE].

[38] D. Lombardi, M. Wiesemann and G. Zanderighi, *Anomalous couplings in $Z\gamma$ events at NNLO+PS and improving $\nu\bar{\nu}\gamma$ backgrounds in dark-matter searches*, *Phys. Lett. B* **824** (2022) 136846 [arXiv:2108.11315] [INSPIRE].

[39] S. Zanoli, M. Chiesa, E. Re, M. Wiesemann and G. Zanderighi, *Next-to-next-to-leading order event generation for VH production with $H \to b\bar{b}$ decay*, arXiv:2112.04168 [INSPIRE].

[40] Y. Hu, C. Sun, X.-M. Shen and J. Gao, *Hadronic decays of Higgs boson at NNLO matched with parton shower*, *JHEP* **08** (2021) 122 [arXiv:2101.08916] [INSPIRE].

[41] J. Mazzitelli, P.F. Monni, P. Nason, E. Re, M. Wiesemann and G. Zanderighi, *Next-to-Next-to-Leading Order Event Generation for Top-Quark Pair Production*, *Phys. Rev. Lett.* **127** (2021) 062001 [arXiv:2012.14267] [INSPIRE].

[42] LHC Higgs Cross Section Working Group collaboration, *Handbook of LHC Higgs Cross Sections: 4. Deciphering the Nature of the Higgs Sector*, arXiv:1610.07922 [INSPIRE].

[43] I. Brivio et al., *O new physics, where art thou? A global search in the top sector*, *JHEP* **02** (2020) 131 [arXiv:1910.03606] [INSPIRE].

[44] J. Ellis, M. Madigan, K. Mimasu, V. Sanz and T. You, *Top, Higgs, Diboson and Electroweak Fit to the Standard Model Effective Field Theory*, *JHEP* **04** (2021) 279 [arXiv:2012.02779] [INSPIRE].

[45] ATLAS collaboration, *Measurements of top-quark pair differential and double-differential cross-sections in the ℓ+jets channel with pp collisions at $\sqrt{s} = 13$ TeV using the ATLAS detector*, *Eur. Phys. J. C* **79** (2019) 1028 [*Erratum ibid.* **80** (2020) 1092] [arXiv:1908.07305] [INSPIRE].

[46] ATLAS collaboration, *Measurement of the $t\bar{t}$ production cross-section and lepton differential distributions in $e\mu$ dilepton events from pp collisions at $\sqrt{s} = 13$ TeV with the ATLAS detector*, *Eur. Phys. J. C* **80** (2020) 528 [arXiv:1910.08819] [INSPIRE].

[47] ATLAS collaboration, *Measurement of the $t\bar{t}$ production cross-section in the lepton+jets channel at $\sqrt{s} = 13$ TeV with the ATLAS experiment*, *Phys. Lett. B* **810** (2020) 135797 [arXiv:2006.13076] [INSPIRE].

[48] ATLAS collaboration, *Measurements of top-quark pair single- and double-differential cross-sections in the all-hadronic channel in pp collisions at $\sqrt{s} = 13$ TeV using the ATLAS detector*, *JHEP* **01** (2021) 033 [arXiv:2006.09274] [INSPIRE].

[49] CMS collaboration, *Measurement of the $t\bar{t}$ production cross section using events in the $e\mu$ final state in pp collisions at $\sqrt{s} = 13$ TeV*, *Eur. Phys. J. C* **77** (2017) 172 [arXiv:1611.04040] [INSPIRE].

[50] CMS collaboration, *Measurement of the $t\bar{t}$ production cross section using events with one lepton and at least one jet in pp collisions at $\sqrt{s} = 13$ TeV*, *JHEP* **09** (2017) 051 [arXiv:1701.06228] [INSPIRE].

JHEP04(2022)079

[51] CMS collaboration, *Measurements of $\mathrm{t\bar{t}}$ differential cross sections in proton-proton collisions at $\sqrt{s} = 13$ TeV using events containing two leptons*, *JHEP* **02** (2019) 149 [arXiv:1811.06625] [INSPIRE].

[52] CMS collaboration, *Measurements of differential cross sections of top quark pair production as a function of kinematic event variables in proton-proton collisions at $\sqrt{s} = 13$ TeV*, *JHEP* **06** (2018) 002 [arXiv:1803.03991] [INSPIRE].

[53] CMS collaboration, *Measurement of differential cross sections for the production of top quark pairs and of additional jets in lepton+jets events from pp collisions at $\sqrt{s} = 13$ TeV*, *Phys. Rev. D* **97** (2018) 112003 [arXiv:1803.08856] [INSPIRE].

[54] CMS collaboration, *Measurement of normalized differential $\mathrm{t\bar{t}}$ cross sections in the dilepton channel from pp collisions at $\sqrt{s} = 13$ TeV*, *JHEP* **04** (2018) 060 [arXiv:1708.07638] [INSPIRE].

[55] CMS collaboration, *Determination of the Top-Quark Pole Mass and Strong Coupling Constant from the $t\bar{t}$ Production Cross Section in pp Collisions at $\sqrt{s} = 7$ TeV*, *Phys. Lett. B* **728** (2014) 496 [*Erratum ibid.* **738** (2014) 526] [arXiv:1307.1907] [INSPIRE].

[56] T. Klijnsma, S. Bethke, G. Dissertori and G.P. Salam, *Determination of the strong coupling constant $\alpha_s(m_Z)$ from measurements of the total cross section for top-antitop quark production*, *Eur. Phys. J. C* **77** (2017) 778 [arXiv:1708.07495] [INSPIRE].

[57] CMS collaboration, *Measurement of $\mathrm{t\bar{t}}$ normalised multi-differential cross sections in pp collisions at $\sqrt{s} = 13$ TeV, and simultaneous determination of the strong coupling strength, top quark pole mass, and parton distribution functions*, *Eur. Phys. J. C* **80** (2020) 658 [arXiv:1904.05237] [INSPIRE].

[58] ATLAS collaboration, *Measurement of the top-quark mass in $t\bar{t} + 1$-jet events collected with the ATLAS detector in pp collisions at $\sqrt{s} = 8$ TeV*, *JHEP* **11** (2019) 150 [arXiv:1905.02302] [INSPIRE].

[59] A.M. Cooper-Sarkar, M. Czakon, M.A. Lim, A. Mitov and A.S. Papanastasiou, *Simultaneous extraction of α_s and m_t from LHC $t\bar{t}$ differential distributions*, arXiv:2010.04171 [INSPIRE].

[60] P. Bärnreuther, M. Czakon and A. Mitov, *Percent Level Precision Physics at the Tevatron: First Genuine NNLO QCD Corrections to $q\bar{q} \to t\bar{t} + X$*, *Phys. Rev. Lett.* **109** (2012) 132001 [arXiv:1204.5201] [INSPIRE].

[61] M. Czakon and A. Mitov, *NNLO corrections to top-pair production at hadron colliders: the all-fermionic scattering channels*, *JHEP* **12** (2012) 054 [arXiv:1207.0236] [INSPIRE].

[62] M. Czakon and A. Mitov, *NNLO corrections to top pair production at hadron colliders: the quark-gluon reaction*, *JHEP* **01** (2013) 080 [arXiv:1210.6832] [INSPIRE].

[63] M. Czakon, P. Fiedler and A. Mitov, *Total Top-Quark Pair-Production Cross Section at Hadron Colliders Through $O(\alpha_S^4)$*, *Phys. Rev. Lett.* **110** (2013) 252004 [arXiv:1303.6254] [INSPIRE].

[64] M. Czakon, D. Heymes and A. Mitov, *High-precision differential predictions for top-quark pairs at the LHC*, *Phys. Rev. Lett.* **116** (2016) 082003 [arXiv:1511.00549] [INSPIRE].

[65] M. Czakon, P. Fiedler, D. Heymes and A. Mitov, *NNLO QCD predictions for fully-differential top-quark pair production at the Tevatron*, *JHEP* **05** (2016) 034 [arXiv:1601.05375] [INSPIRE].

JHEP04(2022)079

[66] S. Catani, S. Devoto, M. Grazzini, S. Kallweit, J. Mazzitelli and H. Sargsyan, *Top-quark pair hadroproduction at next-to-next-to-leading order in QCD*, *Phys. Rev. D* **99** (2019) 051501 [arXiv:1901.04005] [INSPIRE].

[67] S. Catani, S. Devoto, M. Grazzini, S. Kallweit and J. Mazzitelli, *Top-quark pair production at the LHC: Fully differential QCD predictions at NNLO*, *JHEP* **07** (2019) 100 [arXiv:1906.06535] [INSPIRE].

[68] S. Catani, S. Devoto, M. Grazzini, S. Kallweit and J. Mazzitelli, *Top-quark pair hadroproduction at NNLO: differential predictions with the $\overline{MS}$ mass*, *JHEP* **08** (2020) 027 [arXiv:2005.00557] [INSPIRE].

[69] A. Behring, M. Czakon, A. Mitov, A.S. Papanastasiou and R. Poncelet, *Higher order corrections to spin correlations in top quark pair production at the LHC*, *Phys. Rev. Lett.* **123** (2019) 082001 [arXiv:1901.05407] [INSPIRE].

[70] M. Czakon, A. Mitov and R. Poncelet, *NNLO QCD corrections to leptonic observables in top-quark pair production and decay*, *JHEP* **05** (2021) 212 [arXiv:2008.11133] [INSPIRE].

[71] G. Bevilacqua, M. Czakon, A. van Hameren, C.G. Papadopoulos and M. Worek, *Complete off-shell effects in top quark pair hadroproduction with leptonic decay at next-to-leading order*, *JHEP* **02** (2011) 083 [arXiv:1012.4230] [INSPIRE].

[72] A. Denner, S. Dittmaier, S. Kallweit and S. Pozzorini, *NLO QCD corrections to off-shell top-antitop production with leptonic decays at hadron colliders*, *JHEP* **10** (2012) 110 [arXiv:1207.5018] [INSPIRE].

[73] G. Bevilacqua, H.B. Hartanto, M. Kraus and M. Worek, *Top Quark Pair Production in Association with a Jet with Next-to-Leading-Order QCD Off-Shell Effects at the Large Hadron Collider*, *Phys. Rev. Lett.* **116** (2016) 052003 [arXiv:1509.09242] [INSPIRE].

[74] G. Bevilacqua, H.B. Hartanto, M. Kraus and M. Worek, *Off-shell Top Quarks with One Jet at the LHC: A comprehensive analysis at NLO QCD*, *JHEP* **11** (2016) 098 [arXiv:1609.01659] [INSPIRE].

[75] W. Beenakker, A. Denner, W. Hollik, R. Mertig, T. Sack and D. Wackeroth, *Electroweak one loop contributions to top pair production in hadron colliders*, *Nucl. Phys. B* **411** (1994) 343 [INSPIRE].

[76] W. Bernreuther, M. Fücker and Z.G. Si, *Mixed QCD and weak corrections to top quark pair production at hadron colliders*, *Phys. Lett. B* **633** (2006) 54 [*Erratum ibid.* **644** (2007) 386] [hep-ph/0508091] [INSPIRE].

[77] J.H. Kühn, A. Scharf and P. Uwer, *Electroweak effects in top-quark pair production at hadron colliders*, *Eur. Phys. J. C* **51** (2007) 37 [hep-ph/0610335] [INSPIRE].

[78] A. Denner and M. Pellen, *NLO electroweak corrections to off-shell top-antitop production with leptonic decays at the LHC*, *JHEP* **08** (2016) 155 [arXiv:1607.05571] [INSPIRE].

[79] M. Czakon, D. Heymes, A. Mitov, D. Pagani, I. Tsinikos and M. Zaro, *Top-pair production at the LHC through NNLO QCD and NLO EW*, *JHEP* **10** (2017) 186 [arXiv:1705.04105] [INSPIRE].

[80] H.X. Zhu, C.S. Li, H.T. Li, D.Y. Shao and L.L. Yang, *Transverse-momentum resummation for top-quark pairs at hadron colliders*, *Phys. Rev. Lett.* **110** (2013) 082001 [arXiv:1208.5774] [INSPIRE].

JHEP04(2022)079

[81] H.T. Li, C.S. Li, D.Y. Shao, L.L. Yang and H.X. Zhu, *Top quark pair production at small transverse momentum in hadronic collisions*, *Phys. Rev. D* **88** (2013) 074004 [arXiv:1307.2464] [INSPIRE].

[82] S. Catani, M. Grazzini and A. Torre, *Transverse-momentum resummation for heavy-quark hadroproduction*, *Nucl. Phys. B* **890** (2014) 518 [arXiv:1408.4564] [INSPIRE].

[83] S. Catani, M. Grazzini and H. Sargsyan, *Transverse-momentum resummation for top-quark pair production at the LHC*, *JHEP* **11** (2018) 061 [arXiv:1806.01601] [INSPIRE].

[84] M. Beneke, P. Falgari, S. Klein and C. Schwinn, *Hadronic top-quark pair production with NNLL threshold resummation*, *Nucl. Phys. B* **855** (2012) 695 [arXiv:1109.1536] [INSPIRE].

[85] M. Beneke et al., *Inclusive Top-Pair Production Phenomenology with TOPIXS*, *JHEP* **07** (2012) 194 [arXiv:1206.2454] [INSPIRE].

[86] W.-L. Ju, G. Wang, X. Wang, X. Xu, Y. Xu and L.L. Yang, *Top quark pair production near threshold: single/double distributions and mass determination*, *JHEP* **06** (2020) 158 [arXiv:2004.03088] [INSPIRE].

[87] S. Alioli, A. Broggio and M.A. Lim, *Zero-jettiness resummation for top-quark pair production at the LHC*, *JHEP* **01** (2022) 066 [arXiv:2111.03632] [INSPIRE].

[88] M.L. Czakon et al., *Top quark pair production at complete NLO accuracy with NNLO+NNLL' corrections in QCD*, *Chin. Phys. C* **44** (2020) 083104 [arXiv:1901.08281] [INSPIRE].

[89] S. Frixione, P. Nason and B.R. Webber, *Matching NLO QCD and parton showers in heavy flavor production*, *JHEP* **08** (2003) 007 [hep-ph/0305252] [INSPIRE].

[90] S. Frixione, P. Nason and G. Ridolfi, *A Positive-weight next-to-leading-order Monte Carlo for heavy flavour hadroproduction*, *JHEP* **09** (2007) 126 [arXiv:0707.3088] [INSPIRE].

[91] R. Frederix and S. Frixione, *Merging meets matching in MC@NLO*, *JHEP* **12** (2012) 061 [arXiv:1209.6215] [INSPIRE].

[92] J.M. Campbell, R.K. Ellis, P. Nason and E. Re, *Top-Pair Production and Decay at NLO Matched with Parton Showers*, *JHEP* **04** (2015) 114 [arXiv:1412.1828] [INSPIRE].

[93] S. Hoeche, F. Krauss, P. Maierhoefer, S. Pozzorini, M. Schonherr and F. Siegert, *Next-to-leading order QCD predictions for top-quark pair production with up to two jets merged with a parton shower*, *Phys. Lett. B* **748** (2015) 74 [arXiv:1402.6293] [INSPIRE].

[94] K. Cormier, S. Plätzer, C. Reuschle, P. Richardson and S. Webster, *Parton showers and matching uncertainties in top quark pair production with HERWIG 7*, *Eur. Phys. J. C* **79** (2019) 915 [arXiv:1810.06493] [INSPIRE].

[95] T. Ježo and P. Nason, *On the Treatment of Resonances in Next-to-Leading Order Calculations Matched to a Parton Shower*, *JHEP* **12** (2015) 065 [arXiv:1509.09071] [INSPIRE].

[96] T. Ježo, J.M. Lindert, P. Nason, C. Oleari and S. Pozzorini, *An NLO+PS generator for $t\bar{t}$ and Wt production and decay including non-resonant and interference effects*, *Eur. Phys. J. C* **76** (2016) 691 [arXiv:1607.04538] [INSPIRE].

[97] R. Frederix, S. Frixione, A.S. Papanastasiou, S. Prestel and P. Torrielli, *Off-shell single-top production at NLO matched to parton showers*, *JHEP* **06** (2016) 027 [arXiv:1603.01178] [INSPIRE].

[98] P. Nason, *The Top Mass in Hadronic Collisions*, in *From My Vast Repertoire. . . : Guido Altarelli's Legacy*, A. Levy, S. Forte and G. Ridolfi eds., pp. 123–151 (2019) [DOI] [arXiv:1712.02796] [INSPIRE].

JHEP04(2022)079

[99] A.H. Hoang, *What is the Top Quark Mass?*, *Ann. Rev. Nucl. Part. Sci.* **70** (2020) 225 [arXiv:2004.12915] [INSPIRE].

[100] M. Beneke, P. Marquard, P. Nason and M. Steinhauser, *On the ultimate uncertainty of the top quark pole mass*, *Phys. Lett. B* **775** (2017) 63 [arXiv:1605.03609] [INSPIRE].

[101] A.H. Hoang, C. Lepenik and M. Preisser, *On the Light Massive Flavor Dependence of the Large Order Asymptotic Behavior and the Ambiguity of the Pole Mass*, *JHEP* **09** (2017) 099 [arXiv:1706.08526] [INSPIRE].

[102] A.H. Hoang, S. Plätzer and D. Samitz, *On the Cutoff Dependence of the Quark Mass Parameter in Angular Ordered Parton Showers*, *JHEP* **10** (2018) 200 [arXiv:1807.06617] [INSPIRE].

[103] S. Ferrario Ravasio, P. Nason and C. Oleari, *All-orders behaviour and renormalons in top-mass observables*, *JHEP* **01** (2019) 203 [arXiv:1810.10931] [INSPIRE].

[104] S. Catani, B.R. Webber and G. Marchesini, *QCD coherent branching and semiinclusive processes at large x*, *Nucl. Phys. B* **349** (1991) 635 [INSPIRE].

[105] S. Frixione, P. Nason and C. Oleari, *Matching NLO QCD computations with Parton Shower simulations: the POWHEG method*, *JHEP* **11** (2007) 070 [arXiv:0709.2092] [INSPIRE].

[106] S. Alioli, P. Nason, C. Oleari and E. Re, *A general framework for implementing NLO calculations in shower Monte Carlo programs: the POWHEG BOX*, *JHEP* **06** (2010) 043 [arXiv:1002.2581] [INSPIRE].

[107] K. Hamilton, P. Nason and G. Zanderighi, *MINLO: Multi-Scale Improved NLO*, *JHEP* **10** (2012) 155 [arXiv:1206.3572] [INSPIRE].

[108] T. Sjöstrand et al., *An introduction to PYTHIA 8.2*, *Comput. Phys. Commun.* **191** (2015) 159 [arXiv:1410.3012] [INSPIRE].

[109] M. Bahr et al., *HERWIG++ Physics and Manual*, *Eur. Phys. J. C* **58** (2008) 639 [arXiv:0803.0883] [INSPIRE].

[110] S. Catani and M.H. Seymour, *A General algorithm for calculating jet cross-sections in NLO QCD*, *Nucl. Phys. B* **485** (1997) 291 [*Erratum ibid.* **510** (1998) 503] [hep-ph/9605323] [INSPIRE].

[111] S. Catani and M. Grazzini, *QCD transverse-momentum resummation in gluon fusion processes*, *Nucl. Phys. B* **845** (2011) 297 [arXiv:1011.3918] [INSPIRE].

[112] S. Catani, L. Cieri, D. de Florian, G. Ferrera and M. Grazzini, *Universality of transverse-momentum resummation and hard factors at the NNLO*, *Nucl. Phys. B* **881** (2014) 414 [arXiv:1311.1654] [INSPIRE].

[113] S. Catani, S. Devoto, M. Grazzini and J. Mazzitelli, *Soft parton contribution to heavy quark production at low transverse momentum*, in preparation.

[114] S. Catani and M. Grazzini, *An NNLO subtraction formalism in hadron collisions and its application to Higgs boson production at the LHC*, *Phys. Rev. Lett.* **98** (2007) 222002 [hep-ph/0703012] [INSPIRE].

[115] S. Catani, S. Devoto, M. Grazzini, S. Kallweit and J. Mazzitelli, *Bottom-quark production at hadron colliders: fully differential predictions in NNLO QCD*, *JHEP* **03** (2021) 029 [arXiv:2010.11906] [INSPIRE].

[116] P.F. Monni, E. Re and P. Torrielli, *Higgs Transverse-Momentum Resummation in Direct Space*, *Phys. Rev. Lett.* **116** (2016) 242001 [arXiv:1604.02191] [INSPIRE].

JHEP04(2022)079

[117] W. Bizon, P.F. Monni, E. Re, L. Rottoli and P. Torrielli, *Momentum-space resummation for transverse observables and the Higgs $p_\perp$ at $N^3LL+NNLO$*, *JHEP* **02** (2018) 108 [arXiv:1705.09127] [INSPIRE].

[118] M. Czakon, *Tops from Light Quarks: Full Mass Dependence at Two-Loops in QCD*, *Phys. Lett. B* **664** (2008) 307 [arXiv:0803.1400] [INSPIRE].

[119] S. Catani and M. Grazzini, *Higgs Boson Production at Hadron Colliders: Hard-Collinear Coefficients at the NNLO*, *Eur. Phys. J. C* **72** (2012) 2013 [*Erratum ibid.* **72** (2012) 2132] [arXiv:1106.4652] [INSPIRE].

[120] M. Czakon and A. Mitov, *Top++: A Program for the Calculation of the Top-Pair Cross-Section at Hadron Colliders*, *Comput. Phys. Commun.* **185** (2014) 2930 [arXiv:1112.5675] [INSPIRE].

[121] S. Catani, L. Cieri, D. de Florian, G. Ferrera and M. Grazzini, *Vector boson production at hadron colliders: hard-collinear coefficients at the NNLO*, *Eur. Phys. J. C* **72** (2012) 2195 [arXiv:1209.0158] [INSPIRE].

[122] T. Gehrmann, T. Lubbert and L.L. Yang, *Transverse parton distribution functions at next-to-next-to-leading order: the quark-to-quark case*, *Phys. Rev. Lett.* **109** (2012) 242003 [arXiv:1209.0682] [INSPIRE].

[123] P. Bärnreuther, M. Czakon and P. Fiedler, *Virtual amplitudes and threshold behaviour of hadronic top-quark pair-production cross sections*, *JHEP* **02** (2014) 078 [arXiv:1312.6279] [INSPIRE].

[124] T. Gehrmann, T. Luebbert and L.L. Yang, *Calculation of the transverse parton distribution functions at next-to-next-to-leading order*, *JHEP* **06** (2014) 155 [arXiv:1403.6451] [INSPIRE].

[125] M.G. Echevarria, I. Scimemi and A. Vladimirov, *Unpolarized Transverse Momentum Dependent Parton Distribution and Fragmentation Functions at next-to-next-to-leading order*, *JHEP* **09** (2016) 004 [arXiv:1604.07869] [INSPIRE].

[126] R. Angeles-Martinez, M. Czakon and S. Sapeta, *NNLO soft function for top quark pair production at small transverse momentum*, *JHEP* **10** (2018) 201 [arXiv:1809.01459] [INSPIRE].

[127] M.-X. Luo, T.-Z. Yang, H.X. Zhu and Y.J. Zhu, *Transverse Parton Distribution and Fragmentation Functions at NNLO: the Gluon Case*, *JHEP* **01** (2020) 040 [arXiv:1909.13820] [INSPIRE].

[128] M.-X. Luo, X. Wang, X. Xu, L.L. Yang, T.-Z. Yang and H.X. Zhu, *Transverse Parton Distribution and Fragmentation Functions at NNLO: the Quark Case*, *JHEP* **10** (2019) 083 [arXiv:1908.03831] [INSPIRE].

[129] H. Sargsyan, *Heavy-Quark Pair Production at Hadron Collider: Transverse-Momentum Resummation, NNLO Corrections and Azimuthal Asymmetries*, Ph.D. Thesis, University of Zurich (2017) [DOI] [INSPIRE].

[130] M. Czakon, D. Heymes and A. Mitov, *Dynamical scales for multi-TeV top-pair production at the LHC*, *JHEP* **04** (2017) 071 [arXiv:1606.03350] [INSPIRE].

[131] F. Caola, F.A. Dreyer, R.W. McDonald and G.P. Salam, *Framing energetic top-quark pair production at the LHC*, *JHEP* **07** (2021) 040 [arXiv:2101.06068] [INSPIRE].

JHEP04(2022)079

[132] S. Frixione, E. Laenen, P. Motylinski and B.R. Webber, *Angular correlations of lepton pairs from vector boson and top quark decays in Monte Carlo simulations*, *JHEP* **04** (2007) 081 [hep-ph/0702198] [INSPIRE].

[133] S. Alioli, S.-O. Moch and P. Uwer, *Hadronic top-quark pair-production with one jet and parton showering*, *JHEP* **01** (2012) 137 [arXiv:1110.5251] [INSPIRE].

[134] P. Artoisenet, R. Frederix, O. Mattelaer and R. Rietkerk, *Automatic spin-entangled decays of heavy resonances in Monte Carlo simulations*, *JHEP* **03** (2013) 015 [arXiv:1212.3460] [INSPIRE].

[135] NNPDF collaboration, *Parton distributions from high-precision collider data*, *Eur. Phys. J. C* **77** (2017) 663 [arXiv:1706.00428] [INSPIRE].

[136] A. Buckley et al., *LHAPDF6: parton density access in the LHC precision era*, *Eur. Phys. J. C* **75** (2015) 132 [arXiv:1412.7420] [INSPIRE].

[137] G.P. Salam and J. Rojo, *A Higher Order Perturbative Parton Evolution Toolkit (HOPPET)*, *Comput. Phys. Commun.* **180** (2009) 120 [arXiv:0804.3755] [INSPIRE].

[138] M. Grazzini, S. Kallweit and M. Wiesemann, *Fully differential NNLO computations with MATRIX*, *Eur. Phys. J. C* **78** (2018) 537 [arXiv:1711.06631] [INSPIRE].

[139] P. Skands, S. Carrazza and J. Rojo, *Tuning PYTHIA 8.1: the Monash 2013 Tune*, *Eur. Phys. J. C* **74** (2014) 3024 [arXiv:1404.5630] [INSPIRE].

[140] ATLAS collaboration, *ATLAS PYTHIA 8 tunes to 7 TeV data*, ATL-PHYS-PUB-2014-021 (2014).

[141] M.L. Czakon et al., *NNLO versus NLO multi-jet merging for top-pair production including electroweak corrections*, in *11th International Workshop on Top Quark Physics*, (2019) [arXiv:1901.04442] [INSPIRE].

JHEP04(2022)079